Spreading and transport properties of quantum walks
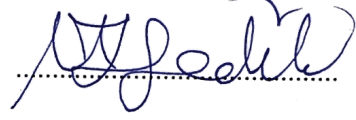
by

İskender Yalçınkaya

Submitted to the Graduate School of Engineering and Natural Sciences
in partial fulfillment of
the requirements for the degree of
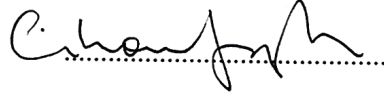Doctor of Philosophy

Sabancı University
Spring 2016

SPREADING AND TRANSPORT PROPERTIES OF QUANTUM WALKS
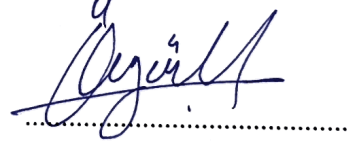
APPROVED BY

Prof. Dr. Zafer Gedik
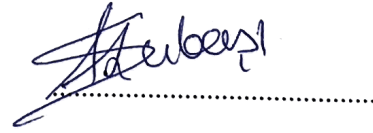
(Thesis Supervisor)

Prof. Dr. Cihan Saçlıoğlu

Asst. Prof. Kamer Kaya

Prof. Dr. Özgür Esat Müstecaplıoğlu

Assoc. Prof. Dr. Levent Subaşı

DATE OF APPROVAL   10/08/2016

Spreading and transport properties of quantum walks

İskender Yalçınkaya

Physics, Doctor of Philosophy Thesis, 2016

Thesis Supervisor: Prof. Dr. Zafer Gedik

Abstract

Quantum computing aims to harness and exploit the quantum mechanical phenomena such as superposition, entanglement and contextuality in order to encode and process information. In this context, quantum walks, which has been suggested as the quantum counterpart of classical random walks, is an emerging topic in quantum computing that provides powerful techniques for developing new quantum algorithms, quantum simulation and quantum state transfer. This thesis intends to investigate the properties of quantum walks which may potentially promote further work in such techniques in quantum computation.

We first propose a novel method for transferring arbitrary unknown qubit state between two points in space with quantum walk architecture. We determine the cases providing perfect state transfers over both finite and infinite lattices with different boundary conditions and we introduce recovery operators assisting the transfer process. Next, by modeling the incoherent and coherent transport with classical random walks and quantum walks, respectively, we calculate the transport efficiencies over an explosive percolation lattice. We show that the minimal correlation between discrete clusters leads to maximal localizations which originating from random scatterings. These localization effects, however, are rather small when compared to the supportive effect of the abrupt growth of the largest cluster on transport efficiency, which eventually allows us to obtain more efficient transports in case of minimal correlations. We support our results with further calculations on whether the eigenstates of the systems we study are localized or not. Lastly, we turn our attention to the spreading dynamics and the coin-position entanglement for two-dimensional quantum walks under an artificial magnetic fields by introducing Peierls phases to the system. In particular, we show that the spreading of the quantum walk is diffusive rather than ballistic when the ratio of the magnetic flux through unit cell - where the walk takes place - to the flux quantum is an irrational number. On the contrary, the walk recovers its original ballistic behavior when this ratio is chosen to be a rational number. Furthermore, we demonstrate that coin-position entanglement is nearly maximum under an artificial magnetic field, even for large number of steps.

KUANTUM YÜRÜYÜŞLERİNİN YAYILIM VE TAŞINIM ÖZELLİKLERİ

İskender Yalçınkaya

Fizik, Doktora Tezi, 2016

Tez Danışmanı: Prof. Dr. Zafer Gedik

Özet

Kuantum hesaplamanın temel amacı bilginin kodlanmasında ve işlenmesinde kuantum mekaniğinin süperpozisyon, dolaşıklık ve bağlamsallık gibi özelliklerinden faydalanmaktır. Klasik rastgele yürüyüşlerin kuantum karşılığı olarak ortaya atılan kuantum yürüyüşleri, yeni kuantum algoritmaları oluşturma, kuantum benzetimi ve kuantum hal aktarımı konularında etkili teknikler sunması bakımından, kuantum hesaplamanın yoğun olarak ilgi gören konularından biri haline gelmiştir. Bu çalışmanın amacı, bahsedilen bu teknikleri geliştirip daha ileriye taşıyabilecek kuantum yürüyüşü özelliklerinin araştırılmasıdır.

İlk olarak kuantum yürüyüşlerini kullanarak, bilinmeyen bir kübit halini uzayda iki nokta arasında aktarmak için özgün bir yöntem geliştirdik. Sonlu ve sonsuz örgüler üzerinde farklı sınır koşulları kullanarak mükemmel hal aktarımına olanak sağlayan durumları belirledik ve aktarım sürecine yardımcı olan kurtarma işleçlerini tanımladık. Ardından, eşevresiz ve eşevreli taşınımları sırasıyla klasik rastgele yürüyüş ve kuantum yürüyüşü ile modelleyerek, patlayıcı bir perkolasyon örgüsü üzerindeki taşınım verimlerini hesapladık. Ayrık topaklar arasındaki asgari bir ilintinin, örgü üzerinde rastgele saçılma kaynaklı azami yerelleşmelere neden olduğunu gösterdik. Buna rağmen, gerçekleşen bu yerelleşmelerin taşınım verimine olumsuz etkisi, aniden büyüyen en büyük topağın katkısı yanında çok küçük kaldığından, sonuç olarak asgari ilintilerle standart perkolasyona kıyasla daha verimli taşınımlar elde ettik. Sonuçlarımızı, incelediğimiz sistemlerin özhallerinin yerel veya yaygın olma durumlarını hesaplayarak destekledik. Son olarak, kuantum yürüyüşü için Peierls fazlarına benzer fazlar tanımlayarak, yapay manyetik alan etkisi altındaki iki boyutta kuantum yürüyüşlerinin yayılım özelliklerini ve para-konum dolaşıklığını inceledik. Bilhassa, yürüyüşün gerçekleştiği örgünün birim hücresinden geçen manyetik akının akı kuantumuna oranı bir irrasyonel sayı ise kuantum yürüyüşünün doğal balistik yayılma davranışı yerine difüzif bir davranış sergilediğini gösterdik. Bu oranın bir rasyonel sayı olması durumunda ise yürüyüşün özgün balistik yayılma karakteristiğine sahip olduğunu gördük. Ayrıca yapay manyetik alanların varlığında, büyük adım sayılarında bile konum ve para uzayının neredeyse azami dolaşık kaldığını gösterdik.

ACKNOWLEDGEMENTS

... does throw dice and walks nice.

Contents

List of Figures

List of Tables

Chapter 1

INTRODUCTION

1.1 Motivation

One may follow the traces of quantum walks back to Feynman's checkerboard model in 1940s [1] for a free relativistic spin 1/2 particle moving in one-dimension. In order to find out the kernel of the path integral, Feynman himself summed over all possible paths in the discretized space-time, which can be visualized by a particle walking randomly on a checkerboard. In spite of its undeniable analogy with this very early work, the name 'Quantum random walk' was actually coined by Aharonov et al. [2] after nearly five decades for the model they introduced as a quantum counterpart of the classical random walk. This new quantum model became prominent with its larger average path length, and hence, quadratically higher spreading rate than of its classical counterpart [3, 4]. Few years later, Farhi and Guttmann introduced their model [5], today known as the continuous-time quantum walk, which is a quantum computation technique to reach the nth level of a decision tree faster than a Markov process.

After these pioneering works, it has been understood that quantum walks are very useful for developing new efficient quantum algorithms [6], e.g., for solving the element distinctness problem [7] and for finding a marked element from a set [8]. It was shown that the number of steps required for reaching a specified vertex of an n-dimensional hypercube with quantum walks is polynomial in n [9], whereas it is exponential in the classical counterpart. On the other hand, quantum walks provide a model for universal quantum computation [10, 11] and supply a fertile framework for simulating other quantum systems such as topological phases [12], Anderson localization [13, 14], nonlinear δ-kicked quantum systems [15], the breakdown of an electric-field driven system [16], excitonic energy transfer through the photosynthetic light-harvesting complexes [17] and the creation of entanglement in bipartite systems [18]. Furthermore, quantum walks are promising resources for quantum state transfer over various graphs and spin chains [19–23].

Today, quantum walks are realized experimentally in various physical systems [18, 24–29]. Particularly, the latest developments in the realization of both quantum walks and artificial gauge fields by ultracold atomic systems pave the way for further achievements in quantum simulations and quantum state transfer studies.

1.2   Overview

The second chapter provides the compulsory mathematical tools and concepts for this thesis. We present the postulates of quantum mechanics for isolated systems both in vector and density matrix formalism. Following the introduction of qubits and and their representation on Bloch sphere, we overview discrete-time quantum walks thoroughly including the entanglement properties and the effect of decoherence.

In the third chapter, we focus on the transfer of qubit states with the quantum walk architecture. In particular, we propose a novel method to transfer any unknown qubit state perfectly between two discrete points in space by using discrete-time quantum walks. We find out the transfer conditions both in finite and infinite position spaces by enhancing the dynamics of the walk via additional quantum operators. We also investigate the conditions which result in state revivals and periodicity.

The fourth chapter we investigate coherent transport over a finite square lattice in which the growth of bond percolation clusters are subjected to an Achlioptas type selection process, i.e., whether a bond will be placed or not depends on the sizes of clusters it may potentially connect. Different than the standard percolation where the growth of discrete clusters are completely random, clusters in this case grow in correlation with one another. We show that certain values of correlation strength, if chosen in a way to suppress the growth of the largest cluster which actually results in an explosive growth later on, may lead to more efficient transports than in the case of standard percolation, provided that certain fraction of total possible bonds are present in the lattice. In this case transport efficiency obeys a power law in the vicinity of bond fraction where effective transport begins. It turns out that the higher correlation strengths may also reduce the efficiency as well. We also compare our results with those of the incoherent transport and examine the spreading of eigenstates of corresponding structures. We demonstrate that structural differences of discrete clusters due to different correlations result in different localization properties.

In the fifth chapter, we investigate the spreading properties of discrete-time quantum walks under an artificial magnetic field. We introduce the Peierls substitution into the quantum walk formalism in order to imitate the phases acquired by a charged particle

moving in a square lattice under perpendicular uniform magnetic field. We classify the spreading rates as ballistic or diffusive in terms of magnetic flux through unit cell. We particularly study the cases in which the ratio of magnetic flux to the flux quantum is an irrational number. We demonstrate the localization properties of quantum walk under magnetic field. Lastly, we study the effect of magnetic field on the entanglement between the coin and position spaces and associate these results with the localization effects.

In the last chapter we summarize our objectives and results obtained in this thesis.

Chapter 2

FUNDAMENTAL CONCEPTS

The purpose of this introductory chapter is to convey the basic concepts and mathematical machinery required for the description of quantum systems and relevantly, quantum walks. We will start by introducing the postulates describing the time evolution of isolated quantum systems. Then, we will present the density matrix formalism of quantum mechanics which also covers the open system dynamics. Using these basics, we will then be able to define the discrete- and continuous-time quantum walks for both closed and open quantum systems. The notation used throughout this thesis will also be specified here. This chapter should be considered as a naive presentation of the subject; a *sine qua non* for understanding the following chapters. The interested reader may refer to [4, 30–35] for comprehensive overviews.

2.1   Postulates of quantum mechanics

At the end of the nineteenth century, accumulation of new experimental data which undeniably contradicts the predictions of the present theory - today known as classical physics - forced scientists to develop not just a modified version of the theory but a completely new one for the description of microscopic phenomena. Indeed, quantum mechanics, together with the relativity theories, guided the human conception of nature towards a framework where it is well understood that daily human experiences are inadequate *per se* in describing natural phenomena. During the first half of the twentieth century, quantum mechanics has completely been developed by many scientists and it still provides a solid mathematical structure for new physical theories. Although there are many monumental introductory and advanced level textbooks on quantum mechanics now [36–42], we will introduce it here once more for the sake of the completeness of this thesis. However, we will limit the scope of this chapter only to the building blocks of the theory, the part that is crucial for describing quantum walks and their dynamics.

2.1.1 Isolated quantum systems

An isolated quantum system does not exchange any information by no means, i.e., mass and/or energy, with its environment by definition. In other words, it evolves completely independent of its surrounding. Such systems are characterized by the five postulates indicated below:

Postulate 1. STATE : An isolated quantum system is completely described by a unit vector called state that exists in a d-dimensional Hilbert space $\mathcal{H}^d$.

The Hilbert space is an abstract vector space of complex numbers $\mathbb{C}$, in which a vector is denoted by a *ket* $|\psi\rangle$. It has the following properties:

i. Let $|\psi\rangle$ and $|\psi'\rangle$ correspond to different states of a quantum system. A *linear combination* $a|\psi\rangle + b|\psi'\rangle$ is also a state of the system, where $a, b \in \mathbb{C}$.

ii. An *inner product* is defined such that there is a map from each ordered pair of vectors to complex numbers, $\langle\psi|\psi'\rangle \to \mathbb{C}$. The state $\langle\psi|$, called *bra*, is an element of the vector space $\mathcal{H}^*$ which is dual to $\mathcal{H}$. The inner product is *positive semidefinite* $\langle\psi|\psi\rangle \geqslant 0$ (equality holds for $|\psi\rangle = 0$), *linear* $\langle\psi''|(a|\psi\rangle + b|\psi'\rangle) = a\langle\psi''|\psi\rangle + b\langle\psi''|\psi'\rangle$ and *skew symmetric* $\langle\psi|\psi'\rangle = \langle\psi'|\psi\rangle^*$. Two states $|\psi\rangle$ and $|\psi'\rangle$ are *orthogonal* if $\langle\psi|\psi'\rangle = 0$.

iii. The quantity $|\psi| = \langle\psi|\psi\rangle^{1/2}$ is the *norm* of the state $|\psi\rangle$. A *unit*, or *normalized* vector is a vector with unit norm, $|\psi| = 1$. Since a quantum state is postulated to be a unit vector, an overall phase has no physical significance, $|e^{i\theta}|\psi\rangle| = |\psi\rangle$. In general, we can say that a quantum state is only associated with a 'direction' in the space. Therefore, by convention, a unit vector is chosen to be the representative of the class $\{c_1|\psi\rangle, c_2|\psi\rangle, \dots\}$ in which vectors differ only by a nonzero complex scalar. The validity of such selection is ensured by the fact that each vector corresponds to the same physical state.

iv. The *dimension* is the maximum number of linearly independent vectors that can be defined within the vector space. Each state $|\psi\rangle$ and its dual $\langle\psi|$ can be written as a linear combination of d linearly independent vectors in a d-dimensional Hilbert space as,

$$|\psi\rangle = \sum_{i=1}^{d} c_i|i\rangle, \qquad \langle\psi| = \sum_{i=1}^{d} c_i^*\langle i| \qquad (2.1)$$

where $c_i \in \mathbb{C}$ are the *components* and the set of vectors $|i\rangle$ constitute a *basis* for the Hilbert space $\mathcal{H}^d$. Now, the addition and scalar multiplication can be expressed in terms of these components as

$$|\psi\rangle + |\psi'\rangle = \sum_{i=1}^{d} (c_i + c_{i'})|i\rangle \quad \text{and} \quad a|\psi\rangle = \sum_{i=1}^{d} ac_i|i\rangle, \tag{2.2}$$

respectively, where $a \in \mathbb{C}$. Since the jth component can be obtained by $\langle j|\psi\rangle$, we can write any state in the form

$$|\psi\rangle = \sum_{i=1}^{d} |i\rangle\langle i|\psi\rangle \equiv \left(\sum_{i=1}^{d} |i\rangle\langle i| \right) |\psi\rangle. \tag{2.3}$$

The expression $\sum_{i=1}^{d} |i\rangle\langle i| = I$ is the *completeness relation* corresponding to the summation of the *outer products* of basis vectors. The operator I here is the identity operator.

v. A linearly independent basis can be converted -e.g., by using Gram-Schmidt process - to an *orthonormal basis* satisfying $\langle i|j\rangle = \delta_{ij}$. Thus, inner products can be expressed in terms of the components as

$$\langle\psi|\psi'\rangle = \sum_{ij} c'_i c_j^* \langle j|i\rangle = \sum_{i=1}^{d} c'_i c_i^*. \tag{2.4}$$

At this point, let us clarify an important issue explicitly. A vector space should not change as we change our perspective, or rather formally, it is invariant under rotations. Once we choose an orthonormal basis, we can rotate it to obtain another one and this way, infinitely many orthonormal bases can be defined in a given vector space. Now, it is useful to choose one of these - say, in our initial arbitrary perspective for the vector space - and 'label' it in a special way. The formalism we have built up to now naturally allows us to do such labeling. Assume we chose an orthonormal basis. We know that any vector can be represented in the form (2.3). In order to see the form of any basis vector $|j\rangle$ in terms of others, we simply replace $|\psi\rangle$ by $|j\rangle$ in (2.3) which yields

$$|j\rangle = \sum_{i=1}^{d} |i\rangle\langle i|j\rangle = \sum_{i=1}^{d} \delta_{ij}|i\rangle. \tag{2.5}$$

Now, it is clear that the components of the jth basis vector are all zero except the jth term which is set to one by definition. Therefore, it is convenient to represent a basis vector as a column vector $|j\rangle \leftrightarrow (0, \ldots 0, 1, 0 \ldots 0)^T$ where the jth element

6

is equal to one. A quantum state can be represented by column and row vectors (or state vectors, in general) in this basis as,

$$|\psi\rangle \leftrightarrow (c_1, c_2, \ldots, c_d)^T, \qquad \langle\psi| \leftrightarrow (c_1^*, c_2^*, \ldots, c_d^*), \qquad (2.6)$$

where c_i are the components of the vector. We will use the symbol "$\leftrightarrow$" while representing a state in this *natural basis* throughout the thesis. This *natural basis* is the one that we will use throughout the thesis with $\leftrightarrow$ symbol. The scalar multiplication, addition, inner product and outer product of vectors in $\mathcal{H}^d$ can be written in vector form as

$$a|\psi\rangle \leftrightarrow (ac_1, ac_2, \ldots, ac_d)^T, \qquad (2.7)$$

$$|\psi\rangle + |\psi'\rangle \leftrightarrow (c_1 + c_1', c_2 + c_2', \ldots, c_d + c_d')^T, \qquad (2.8)$$

$$\langle\psi|\psi'\rangle \leftrightarrow c_1^* c_1' + c_2^* c_2' + \ldots + c_d^* c_d', \qquad (2.9)$$

$$|\psi\rangle\langle\psi'| \leftrightarrow \begin{bmatrix} c_1 c_1'^* & c_1 c_2'^* & \ldots & c_1 c_d'^* \\ c_2 c_1'^* & c_2 c_2'^* & \ldots & c_2 c_d'^* \\ \vdots & \vdots & \ddots & \vdots \\ c_d c_1'^* & c_d c_2'^* & \ldots & c_d c_d'^* \end{bmatrix}. \qquad (2.10)$$

We also note that the convention $|\psi| = 1$ results in the normalization of the probability distribution $\sum_i |c_i|^2 = 1$ since $|c_i|^2$ gives the probability of being in the state $|i\rangle$.

Postulate 2. OBSERVABLE : Measurable quantities, namely, the observables of a quantum system are associated with Hermitian operators.

In general, an *operator* X is a linear map from vectors to vectors: $|\psi\rangle \to X|\psi\rangle$ and $X(a|\psi\rangle + b|\psi'\rangle) = aX|\psi\rangle + bX|\psi'\rangle$. For a given orthonormal basis, an operator can be specified by its components $\langle i|X|j\rangle = X_{ij}$ which specifies a $d \times d$ square matrix:

$$X \leftrightarrow \begin{bmatrix} X_{11} & X_{12} & \ldots & X_{1d} \\ X_{21} & X_{22} & \ldots & X_{2d} \\ \vdots & \vdots & \ddots & \vdots \\ X_{d1} & X_{d2} & \ldots & X_{dd} \end{bmatrix}. \qquad (2.11)$$

A *Hermitian operator*, A, satisfies the property $\langle i|A|j\rangle = \langle j|A|i\rangle^*$ denoted by $A = A^\dagger$ where $A^\dagger$ is the transpose conjugate of A. The eigenvalues of A are real and the eigenvectors -or eigenstates- corresponding to different eigenvalues are orthogonal. Therefore, any state in the Hilbert space $\mathcal{H}^d$ can be written as the linear combination of d eigenstates of an observable.

Postulate 3. DYNAMICS : The time evolution of a state is governed by a unitary operator. If the initial state at time t is $|\psi(t)\rangle$, then the final state at time t' is given as

$$|\psi(t')\rangle = U(t', t)|\psi(t)\rangle. \tag{2.12}$$

Here, $U(t', t)$ is a *unitary* operator which satisfies $U^\dagger = U^{-1}$. Since U corresponds to a 'rotation' in the space, the inner products between vectors are preserved, i.e., the norms remain unchanged. The Schrödinger equation

$$i\hbar \frac{d}{dt}|\psi(t)\rangle = H|\psi(t)\rangle, \tag{2.13}$$

describes the infinitesimal time evolution for $|\psi\rangle$, where H is a Hermitian operator known as the *Hamiltonian* of the quantum system. For a time-independent Hamiltonian, the exact form of $U(t', t)$ is

$$U(t', t) = \exp\left[-\frac{i}{\hbar}H(t - t')\right], \tag{2.14}$$

which is obtained by solving (2.13). Here, the exponential of any operator is defined as

$$\exp(\Omega) \equiv \sum_{n=1}^{\infty} \frac{\Omega^n}{n!}. \tag{2.15}$$

Postulate 4. MEASUREMENT : Measurements on a quantum system are associated with projection operators in the Hilbert space.

A measurement is a process in which an observer acquires information about the quantum state. Before measuring an observable A, the quantum state $|\psi\rangle$ of the system is assumed to be in a linear combination of the eigenstates $|\psi\rangle = \sum_i c_i|a_i\rangle$ of an observable A with eigenvalues a_i. A measurement transforms the state $|\psi\rangle$ into one of the eigenstates of the observable with probability $P(a_i) = |\langle a_i|\psi\rangle|^2 = |c_i|^2$ and the observer learns the value of the corresponding a_i. The mathematical equivalent of this measuring process is a *projection* operator $E_i = |a_i\rangle\langle a_i|$. Therefore, the probability reads as $P(a_i) = \langle\psi|E_i|\psi\rangle$ and the quantum state just after the measurement becomes

$$|\psi'\rangle = \frac{E_i|\psi\rangle}{\sqrt{\langle\psi|E_i|\psi\rangle}}. \tag{2.16}$$

Projection operators satisfy the completeness relation $\sum_i E_i = I$. If there are many systems that are identically prepared in the state $|\psi\rangle$, the *expectation value* of the outcomes - the average of the outcomes - after the measurement E_i reads

$$\langle a_i\rangle \equiv \sum_i a_i P(a_i) = \sum_i a_i\langle\psi|E_i|\psi\rangle = \langle\psi|A|\psi\rangle. \tag{2.17}$$

Postulate 5. COMPOSITE SYSTEMS : The total Hilbert space of a composite system is the tensor product of Hilbert spaces of the individual systems.

We encounter the case of a *composite system* when we try to think of a quantum system by parts. Let us think now that a given system has two parts, A and B, with Hilbert spaces $\mathcal{H}_A$ and $\mathcal{H}_B$, respectively. In this case, the total Hilbert space of the total system is given by the tensor product $\mathcal{H}_T = \mathcal{H}_A \otimes \mathcal{H}_B$. If these parts are prepared in the states $|\psi_A\rangle$ and $|\psi_B\rangle$, the state of the total system becomes $|\psi_T\rangle = |\psi_A\rangle \otimes |\psi_B\rangle \equiv |\psi_A\psi_B\rangle$. Now, the basis for $\mathcal{H}_T$ becomes $|i,j\rangle \equiv |i\rangle_A|j\rangle_B \equiv |\psi_A\rangle|\psi_B\rangle$ an satisfies the orthonormality relation $\langle i,j|k,l\rangle = \delta_{ik}\delta_{jl}$. An operator $X_A \otimes Y_B$ applies X_A on system A and Y_B on system B separately as

$$X_A \otimes Y_B|\psi_A\rangle \otimes |\psi_B\rangle = X_A|\psi_A\rangle \otimes Y_B|\psi_B\rangle. \tag{2.18}$$

In general, for many independent quantum systems numbered as $1, 2, \ldots, n$ in quantum states $|\psi_1\rangle, |\psi_2\rangle, \ldots, |\psi_n\rangle$, the state of the composite system takes the form $|\psi_1\rangle \otimes |\psi_2\rangle \otimes \cdots \otimes |\psi_n\rangle$.

2.1.2 Density matrix formalism

When we try to describe the behavior of a smaller part of a larger system, the postulates introduced in the previous chapter lose their validity, i.e., the states are not unit vectors, time evolution is not unitary and the measurements are not represented by orthogonal projections anymore. The smaller part is called an *open quantum system* S which is in interaction with its exterior, namely the *environment* E. The size of the total system $(S + E)$ is chosen specific to the problem under consideration. Since there exists no perfectly isolated system in nature, the investigation of open system dynamics instead seems to be a more realistic approach and the method used for describing such systems is, by convention, the density matrix formalism.

The state vector for isolated systems represents an infinite ensemble of identically prepared systems. In reality, of course, it is impossible to prepare systems with such perfection. In general, all we know is that the system S is prepared in one of a number of states from the ensemble $\{|\psi_1\rangle, |\psi_2\rangle, \ldots, |\psi_r\rangle\}$ with respective probabilities $\{p_1, p_2, \ldots, p_r\}$. All the states in this ensemble are normalized with no necessity of mutual orthogonality. The probabilities satisfy the condition $\sum_i^r p_i = 1$. The state of the system in this case is represented by the density matrix given as

$$\rho = \sum_i p_i|\psi_i\rangle\langle\psi_i|. \tag{2.19}$$

9

This is a summation of the outer products of the states $|\psi_i\rangle$. If a system is described only by a single state $|\psi\rangle$, then it is a *pure state* and its density matrix is simply $\rho = |\psi\rangle\langle\psi|$. On the other hand, a state which is built out of the pure states of an ensemble as in (2.19), is a *mixed state*. We note that a mixed state is not a linear combination of pure states because such combination would just yield another pure state (see Postulate 1 in the previous chapter). In general, the density matrix satisfies the following properties:

i. It is Hermitian $\rho = \rho^\dagger$ since $(|\psi\rangle\langle\psi|)^\dagger = |\psi\rangle\langle\psi|$.

ii. The sum of its diagonal elements, namely the *trace*, is one, $\text{Tr}(\rho) = 1$.

iii. It is a positive operator, i.e., its eigenvalues are non-negative.

iv. ρ is a pure state, if $\rho^2 = \rho$.

v. It satisfies $\text{Tr}(\rho^2) \leq 1$ where the equality holds if and only if ρ is a pure state.

It is possible to reformulate the postulates of quantum mechanics by using the density matrix formalism. Applying the product rule of derivative to the outer product $|\psi(t)\rangle\langle\psi(t)|$ and using the Schrödinger equation (2.13) along with its conjugate, dynamical evolution of a mixed state takes the form

$$\frac{d}{dt}\rho(t) = \frac{1}{i\hbar}[H, \rho(t)].\tag{2.20}$$

Using (2.19), the time evolution of a mixed state becomes

$$\begin{aligned}
\rho(t') &= \sum_i p_i |\psi_i(t')\rangle\langle\psi_i(t')| \\
&= U(t',t)\left(\sum_i p_i |\psi_i(t)\rangle\langle\psi_i(t)|\right) U^\dagger(t',t) \\
&= U(t',t)\rho(t)U^\dagger(t',t)\tag{2.21}
\end{aligned}$$

If the density matrix of a system is ρ before some measurement M_n, then the probability of obtaining nth outcome is $p(n) = \text{Tr}\left(M_n\rho M_n^\dagger\right)$ and the state of the system after the measurement reads

$$\rho \to \frac{M_n\rho M_n^\dagger}{\text{Tr}(M_n\rho M_n^\dagger)}\tag{2.22}$$

where the measurement operators M_n satisfy the completeness relation $\sum_n M_n^\dagger M_n = I$. We also note that any global phase is automatically eliminated in the density matrix formalism since the density matrix form of any state such as $|\psi\rangle = e^{i\theta}|\phi\rangle$ is $\rho = e^{i\theta}|\phi\rangle\langle\phi|e^{-i\theta} = |\phi\rangle\langle\phi|$.

The reduced density matrix

Any information about a system may be acquired by doing measurements and when it comes to measuring some part of a composite system, it is the *the reduced density matrix* that provides the correct measurement statistics. It is, therefore, a very important tool while describing the composite system dynamics. Assume we have a composite system which consists of two subsystems A and B with respective Hilbert spaces $\mathcal{H}_A$ and $\mathcal{H}_B$. We define the reduced density matrix of the subsystem A as

$$\rho_A \equiv \text{Tr}_B(\rho_{AB}) \tag{2.23}$$

where Tr_B is the *partial trace* operation over the subsystem B. If $|a\rangle$ and $|a'\rangle$ are two arbitrary states of the subsystem A, and $|b\rangle$ and $|b'\rangle$ are two arbitrary states of the subsystem B, then the partial trace operation over B of the composite system AB is defined as

$$\text{Tr}_B(|a\rangle\langle a'| \otimes |b\rangle\langle b'|) = \sum_i (I \otimes \langle i_B|)(|a\rangle\langle a'| \otimes |b\rangle\langle b'|)(I \otimes |i_B\rangle)$$

$$= \sum_i |a\rangle\langle a'| \otimes \langle i_B|b\rangle\langle b'|i_B\rangle$$

$$= |a\rangle\langle a'|\text{Tr}(|b\rangle\langle b'|)$$

$$= |a\rangle\langle a'|\langle b|b'\rangle,$$

where $\{|i_B\rangle\}$ is the orthonormal basis for the space $\mathcal{H}_B$. The reduced density matrix ρ_A of a product form state, such as $\rho_{AB} = \rho_A \otimes \rho_B$, simply equals to the density matrix of A itself since $\rho_A = \text{Tr}_B(\rho_A \otimes \rho_B) = \rho_A\text{Tr}_B(\rho_B) = \rho_A$. We will see in Sec. 2.4.4 that there are also states which cannot be written in product form, called entangled states. Let us give an example of an entangled state and of how we calculate a reduced density matrix of a composite system. Consider the following state given in both vector and density matrix forms as

$$|\psi\rangle_{AB} = \frac{1}{\sqrt{2}}(|0\rangle_A|0\rangle_B + |1\rangle_A|1\rangle_B),$$

$$\rho_{AB} = \frac{1}{2}(|0,0\rangle\langle 0,0| + |0,0\rangle\langle 1,1| + |1,1\rangle\langle 0,0| + |1,1\rangle\langle 1,1|).$$

All the terms in ρ_{AB} can be rewritten in the same manner so that $|0,0\rangle\langle 1,1| = |0\rangle\langle 1| \otimes |0\rangle\langle 1|$. Then, the reduced density matrix of the subsystem A can be found by tracing over the subsystem B:

$$\rho_A = \frac{1}{2}(|0\rangle\langle 0|\langle 0|0\rangle + |0\rangle\langle 1|\langle 0|1\rangle + |1\rangle\langle 0|\langle 1|0\rangle + |1\rangle\langle 1|\langle 1|1\rangle)$$

$$= \frac{1}{2}(|0\rangle\langle 0| + |1\rangle\langle 1|)$$

The expression above is a maximally mixed state of one qubit. In the natural basis $|0\rangle \leftrightarrow (1,0)^T$ and $|1\rangle \leftrightarrow (0,1)^T$, the reduced density ρ_A takes the form

$$\rho_A \leftrightarrow \begin{bmatrix} 1/2 & 0 \\ 0 & 1/2 \end{bmatrix}.$$

2.2 Qubits and their geometric representation

A 'bit' is the smallest unit of data in classical information systems. It can be found in either one of the two states 0 or 1. Today's computers control enormous number of bits to encode and process data. A qubit (QUantum BIT), on the other hand, is defined as the quantum counterpart of a 'bit' in quantum information systems and quantum information processing. Unlike the usual bits, it may also possess the superposition of states 0 and 1. Physically, it is a two-level quantum system, e.g., up and down spin states of an electron or two polarization states of a photon. Mathematically, it is defined by a unit vector in two-dimensional Hilbert space spanned by the natural orthonormal basis $|0\rangle \leftrightarrow (1,0)^T$ and $|1\rangle \leftrightarrow (0,1)^T$. This particular basis is also known as the *computational basis*. One way of representing the state of a qubit is

$$|\psi\rangle = \alpha|0\rangle + \beta|1\rangle, \tag{2.24}$$

where α and β are complex numbers satisfying the completeness relation $|\alpha|^2 + |\beta|^2 = 1$. A measurement on the qubit state results in the state $|0\rangle$ or $|1\rangle$ with probabilities $|\alpha|^2$ and $|\beta|^2$, respectively. In other words, a measurement destroys the quantum coherence irreversibly and chooses only one of the two possible states with some probability. Therefore, it is not possible to obtain the state of a qubit by direct examination. However, such knowledge is not the main interest in many cases. For example, the supremacy of certain quantum algorithms over their classical counterparts arises due to the coherent dynamics governed by unitary operators. In this context, if there exists anything called 'all information' contained in a qubit, it cannot be treated as a measurable quantity and it may only be meaningful in terms of coherent dynamics.

Bloch sphere

It is possible to represent all qubit states using a 3-dimensional unit sphere. We see in (2.24) that a qubit state is parametrized by four real numbers: two coming from α and two from β. However, one parameter can be eliminated since a global phase has no physical significance and another elimination may be done by using the normalization
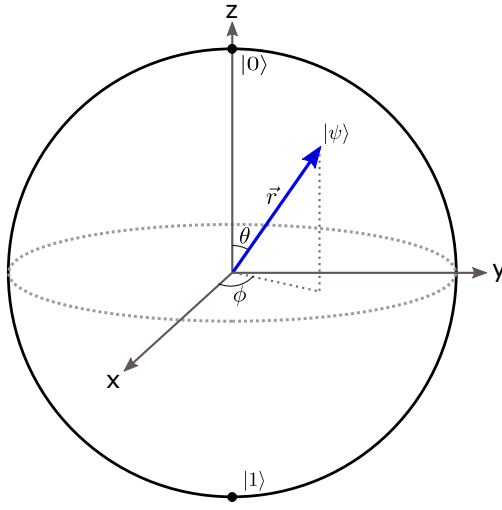
Figure 2.1: The Bloch sphere. A pure qubit state is represented by a Bloch vector $|\vec{r}| = 1$, whereas for the mixed qubit states $|\vec{r}| < 1$. The length of the vector $\vec{r}$ gives the information about how mixed a given state is: The shorter the Bloch vector, the more mixed is the corresponding state.

condition. Therefore, in the end, only two real parameters should be sufficient to describe a qubit state in total. In polar representation, a qubit state in (2.24) reads as

$$|\psi\rangle = r_1|0\rangle + r_2 e^{i(\zeta-\gamma)}|1\rangle \tag{2.25}$$

where we ignore the global phase $e^{i\gamma}$ without any loss of generality. Going back to Cartesian coordinates, we have

$$|\psi\rangle = z|0\rangle + (x+iy)|1\rangle. \tag{2.26}$$

Since the normalization condition $x^2 + y^2 + z^2 = 1$ defines a unit sphere in 3-dimensional space, (2.26) can be represented by the two parameters θ and ϕ in spherical coordinates as

$$|\psi\rangle = \cos\theta|0\rangle + \sin\theta e^{i\phi}|1\rangle \tag{2.27}$$

where $\theta \in [0, \pi]$ and $\phi \in [0, 2\pi]$. Now, note that for $\theta = \pi/2$, we have $|\psi\rangle = e^{i\phi}|1\rangle$ which suggests that it is possible to generate all qubit states within the interval $\theta \in [0, \pi/2]$. In order to check the opposite states on the lower hemisphere for a given (θ, ϕ), we substitute them by $(\pi - \theta, \pi + \phi)$ as in

$$|\phi'\rangle = \cos(\pi-\theta)|0\rangle + \sin(\pi-\theta)e^{i(\pi+\phi)}|1\rangle \tag{2.28}$$

$$= -\cos\theta|0\rangle - \sin\theta e^{i\phi}|1\rangle = -|\psi\rangle. \tag{2.29}$$

This shows us that the states on the lower hemisphere differ only by a phase of -1 from the the ones in the upper hemisphere. Therefore, we can map the points on the upper hemisphere onto the whole sphere by $\theta \to 2\theta$ and the final form of a qubit state in Bloch sphere representation becomes

$$|\psi\rangle = \cos\frac{\theta}{2}|0\rangle + \sin\frac{\theta}{2}e^{i\phi}|1\rangle \tag{2.30}$$

where again, $\theta \in [0, \pi]$ and $\phi \in [0, 2\pi]$. In density matrix form, (2.30) becomes

$$\rho = |\psi\rangle\langle\psi| \leftrightarrow \begin{bmatrix} \cos^2\frac{\theta}{2} & e^{-i\phi}\sin\frac{\theta}{2}\cos\frac{\theta}{2} \\ e^{i\phi}\sin\frac{\theta}{2}\cos\frac{\theta}{2} & \sin^2\frac{\theta}{2} \end{bmatrix} \tag{2.31}$$

$$= \frac{1}{2}\begin{bmatrix} 1+\cos\theta & \cos\phi\sin\theta - i\sin\phi\sin\theta \\ \cos\phi\sin\theta - i\sin\phi\sin\theta & 1-\sin\theta \end{bmatrix} \tag{2.32}$$

Any 2×2 matrix can be written in the basis of matrices $\{I, \sigma_x, \sigma_y, \sigma_z\}$, where σ_k are the *Pauli matrices*

$$\sigma_k = \begin{bmatrix} \delta_{k3} & \delta_{k1} - i\delta_{k2} \\ \delta_{k1} + i\delta_{k2} & -\delta_{k3} \end{bmatrix}, \tag{2.33}$$

with $k = 1, 2$ and 3. Therefore, decomposing (2.32) in this basis yields

$$\rho = \frac{1}{2}(I + \sigma_1\cos\phi\sin\theta + \sigma_2\sin\phi\sin\theta + \sigma_3\cos\theta)$$

$$= \frac{1}{2}(I + \hat{n}.\vec{\sigma}) \tag{2.34}$$

where $\hat{n} = (n_1, n_2, n_3)$ is a 3-dimensional unit vector in spherical coordinates and $\vec{\sigma} = (\sigma_1, \sigma_2, \sigma_3)$. We know that each surface point on the Bloch sphere corresponds to a pure state. Furthermore, we can represent any mixed state ρ by a point inside the Bloch sphere with a vector $\vec{r}$ as in

$$\rho = \frac{1}{2}(I + \vec{r}.\vec{\sigma}) \tag{2.35}$$

where $|r| < 1$. The eigenvalues $\frac{1}{2}(1 \pm |\vec{r}|)$ of ρ are required to be non-negative for it is known that the density matrices are positive semidefinite, and this non-negativity in the end, yields $|\vec{r}| \leqslant 1$. Therefore, while the vectors with $|\vec{r}| = 1$ correspond to pure states, the others with $|\vec{r}| < 1$ correspond to mixed states (see Fig. 2.1).

2.3 Random walk on the line

Probably the simplest example of a random walk is the motion of a particle on a line in which the motion is controlled by the tossing of coin. The particle jumps one step right or one step left as the coin toss results in heads or tails, respectively. A single application of this process defines a step of the walk and the time evolution is determined by successive steps. Since the time evolution is probabilistic, we cannot talk about the exact position of the particle. Instead, we can calculate the probability P of finding the particle at position $n \in \mathbb{Z}$ after some steps t. It is well-known that such probability distributions are Binomial as in the expression

$$P_n(t) = \frac{1}{2^t} \frac{t!}{\left(\frac{t+n}{2}\right)! \left(\frac{t-n}{2}\right)!}, \tag{2.36}$$

valid for $n \leq t$ and even $(n+t)$, and zero otherwise. We see in Fig. 2.2 that the spreading of the distribution is wider for larger number of steps. In order to quantify the spreading of this distribution, the variance

$$\sigma^2(t) = \sum_{i=1}^{R} P_i(t)(n_i - \bar{n})^2 = \langle n^2 \rangle - \langle n \rangle^2 \tag{2.37}$$

can be used, where the summation is taken over the ensemble $\{n_1, n_2, \ldots, n_R\}$ that contains the final positions of the particle for R realizations of the t-step walk. Obviously, Eq. (2.37) provides the information of how wide the probability is distributed over the line. The standard deviation $\sigma = \sqrt{\sigma^2}$ can also be chosen as an equivalent measure for spreading. In the random walk case, the variance can be obtained by using normal distribution approximation of (2.36) for large values of the t as in

$$P_n(t) \simeq \frac{2}{\sqrt{2\pi t}} e^{-\frac{n^2}{2t}} \tag{2.38}$$

where the variance is given by $\sigma^2 = t$. Such spreading dynamics - in which the variance is linearly proportional to the step number (or equivalently, proportional to time) - are called *diffusive*. It is conventional to use this description of spreading dynamics while studying random walks as will be done in the following sections.

2.4 Discrete-time quantum walks

The first proposal of the discrete-time quantum walk [2] was published with the title "*Quantum random walks*" and provided a quantum model outperforming its classical
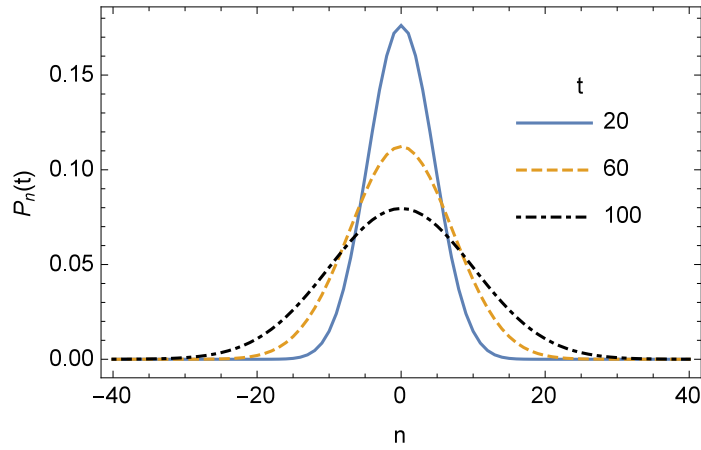
Figure 2.2: Probability distribution of the random walk on the line around $n = 0$ for different step numbers t. Here, only nonzero values of $P_n(t)$ are drawn.

counterpart in terms of spreading rates. Contrary to the wrong impression created by their generic names, the analogy between a random walk and a discrete-time quantum walk is based not on the randomness, but merely on the schematic way in which we apply the step procedure. Honestly, the quantum model of the walk is not as 'random' as the classical random walk in the context of the dynamics as we will see in the following sections.

2.4.1 The model

In the discrete-time quantum walk, the position of the particle is associated with a state vector in the the Hilbert space $\mathcal{H}_p$ of infinite dimension which is spanned by the computational basis $\{|n\rangle : n \in \mathbb{Z}\}$. In order to build an analogy with the classical random walk, the motion of the particle should depend on an external degree of freedom, namely a *quantum coin*. For the case of walk on a line, this quantum coin can be selected as a two-level quantum system whose state lives in a two-dimensional Hilbert space $\mathcal{H}_c^2$ with the computational basis $\{|c\rangle : c = \{0, 1\}\}$. This is actually the well-known qubit state (2.24). Therefore, the composite system called the *walker* is described by the quantum state $|c, n\rangle$ in the Hilbert space $\mathcal{H} = \mathcal{H}_c \otimes \mathcal{H}_p$. The translation of the walker is associated with a unitary *shift operator*

$$S = \sum_{n=-\infty}^{+\infty} (|0\rangle\langle 0| \otimes |n-1\rangle\langle n| + |1\rangle\langle 1| \otimes |n+1\rangle\langle n|) \tag{2.39}$$

which conditionally shifts the position of the walker in either one of the directions depending on the coin state as follows:

$$S|0, n\rangle = |0, n-1\rangle \tag{2.40}$$

16

$$S|1, n\rangle = |0, n+1\rangle \tag{2.41}$$

Here, the choice of which coin state controls which direction is completely arbitrary, i.e., we could have equivalently chosen $|0\rangle$ for $|n\rangle \rightarrow |n+1\rangle$ and $|1\rangle$ for $|n\rangle \rightarrow |n-1\rangle$. For further analogy with the classical random walk, a 'quantum coin' should be tossed before each shift operation. Similarly, this tossing process here is associated with a unitary *coin operator C*. In the original proposal of the discrete-time quantum walk, it was chosen as the Hadamard gate

$$C_H = \frac{1}{\sqrt{2}}(|0\rangle\langle 0| + |0\rangle\langle 1| + |1\rangle\langle 0| - |1\rangle\langle 1|) \leftrightarrow \frac{1}{\sqrt{2}}\begin{bmatrix} 1 & 1 \\ 1 & -1 \end{bmatrix}, \tag{2.42}$$

which transforms each coin basis into an equiprobable superposition of both. The quantum walk utilizing the Hadamard gate is called the *Hadamard walk*. In general, the coin operation can be any unitary operation in SU(2),

$$C_{(gen)} = \begin{bmatrix} \sqrt{\rho} & \sqrt{1-\rho}e^{i\theta} \\ \sqrt{1-\rho}e^{i\phi} & -\sqrt{\rho}e^{i(\theta+\phi)} \end{bmatrix}. \tag{2.43}$$

from which Eq. (2.42) can be obtained by choosing $\rho = 1/2$ and $\theta = \phi = 0$. It can also be seen that ρ and $1-\rho$ are the probabilities for moving left and right, respectively. The parameters θ and ϕ define the most general unitary operator up to a $U(1)$ phase. Now, analog to the classical case, a *step* of the walk is defined by the operator $U = S(C \otimes I)$ which is a composition of the coin and shift operators. Note that the coin operator acts only on the coin space and the shift operator acts on both spaces to move the walker accordingly. Starting from an initial state $|\Psi_0\rangle$ for the walker, a t-step quantum walk is described by

$$|\Psi_t\rangle = \overbrace{U.U \dots U}^{t} = U^t|\Psi_0\rangle \tag{2.44}$$

which is a sequential application of the step operator U to the initial state $|\psi_0\rangle$. Let us examine now a simple two-step walk explicitly that starts with the initial walker state $|\Psi_0\rangle = |0, 0\rangle$:

Step 1: $|\Psi_0\rangle \xrightarrow{C \otimes I} \frac{1}{\sqrt{2}}(|0\rangle + |1\rangle) \otimes |0\rangle$

$\xrightarrow{S} \frac{1}{\sqrt{2}}(|0, -1\rangle + |1, +1\rangle) = |\Psi_1\rangle$

Step 2: $|\Psi_1\rangle \xrightarrow{C \otimes I} \frac{1}{2}[(|0\rangle + |1\rangle) \otimes |-1\rangle + (|0\rangle - |1\rangle) \otimes |+1\rangle]$

$\xrightarrow{S} \frac{1}{2}[|0, -2\rangle + (|0\rangle + |1\rangle) \otimes |0\rangle - |1, +2\rangle] = |\Psi_2\rangle$

We see that after the first step, we find the particle only at positions $n = -1$ or $n = +1$ with the same probability. The second step gets the amplitudes coming from $n = -1$ and $n = +1$ superposed at $n = 0$. This causes the probability at $n = 0$ to be 0.5 while it is 0.25 at other positions. Although we witnessed a constructive interference with the application of the shift operator, there will be destructive interference as well in succeeding steps when the coin operator is applied. For example, at the third step, the coin state associated with the position $n = 0$ will transform as $(|0\rangle + |1\rangle) \xrightarrow{C} 2|0\rangle$ up to some phase due to $|1\rangle - |1\rangle$ annihilation. The reason for this is the negative sign introduced by the Hadamard gate when applied to $|1\rangle$. Consequently, more cancellations are expected to take place in the terms with coin state $|1\rangle$. Starting from the third step, this results in an asymmetrical probability distribution and we expect the probability to accumulate at left since the coin state $|1\rangle$ induces a movement towards right which is displayed in Fig. 2.3(a),(b). Actually, such cancellations are directly related to the initial condition. If we choose the initial state as $|\Psi_0\rangle = |1, 0\rangle$, the cancellations occur for the coin state $|0\rangle$ and we obtain the mirror symmetric distribution shown in Fig. 2.3(c). A symmetrical distribution, however, can be obtained by choosing an initial state of the form

$$|\Psi_0\rangle = \frac{1}{\sqrt{2}}(|0\rangle + i|1\rangle) \otimes |0\rangle. \tag{2.45}$$

Now it is obvious that the extra i in the initial state prevents the $|1\rangle$ terms from being canceled, and thus the resulting distribution gets symmetrical around the starting position as in Fig. 2.3(d). In general, the state of the walker after t steps is the superposition of $|c, n\rangle$ states as seen below

$$|\Psi_t\rangle = \sum_{c,n} a_{n,c}(t)|c, n\rangle \tag{2.46}$$

where $a_{n,c}(t)$ are the amplitudes of the corresponding states. The probability of being found at any position is calculated by summing over the probabilities in the coin space as in

$$P_n(t) = \sum_c |a_{n,c}(t)|^2. \tag{2.47}$$

Similar to classical random walk, $P_n(t) = 0$ if $n + t$ is odd and $P_n(t) \neq 0$ if $n + t$ is even. In Fig. 2.4, we numerically calculate the variance (2.37) in each step to find out the spreading dynamics. We see that the spreading of the discrete-time quantum walk is quadratically faster than of the classical random walk. Although we only provide a result for the initial state $|\psi_0\rangle = \frac{1}{\sqrt{2}}(|0\rangle + i|1\rangle)$ here, similar behaviors can be obtained for other initial states as well.
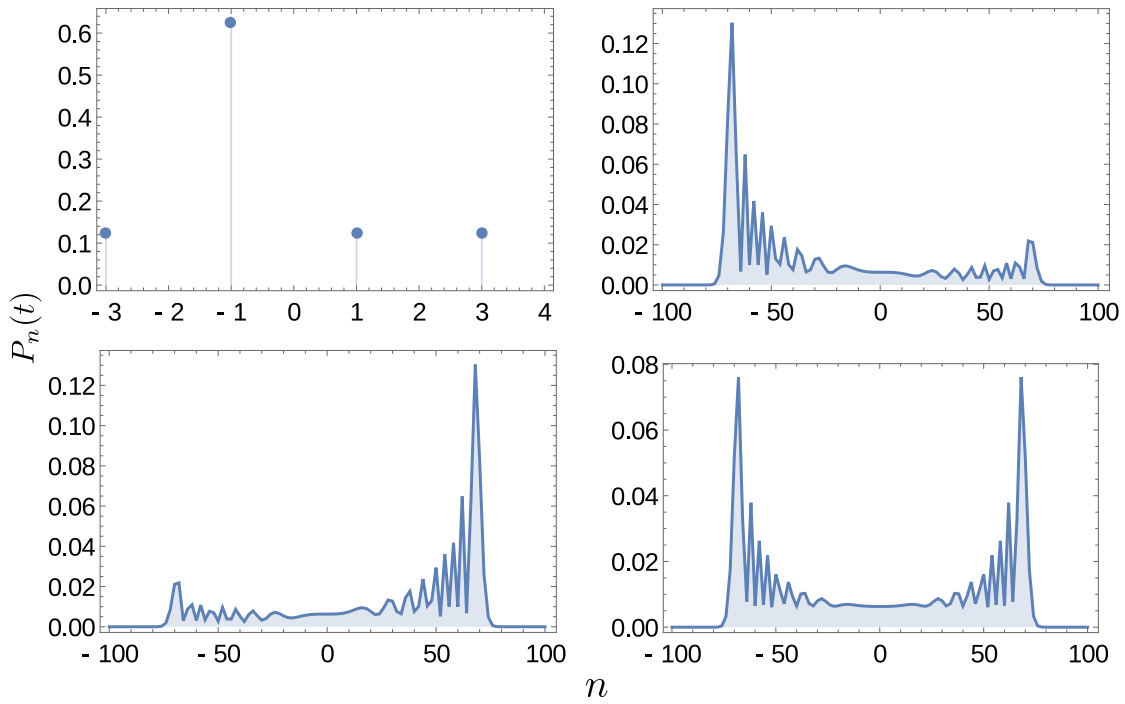
Figure 2.3: Probability distributions of the discrete-time quantum walk in the position space for different initial states and step numbers. (a) $t = 3$ and $|\Psi_0\rangle = |0,0\rangle$. In (b), (c) and (d) $t = 100$ and initial states are $|\Psi_0\rangle = |0,0\rangle$, $|\Psi_0\rangle = |1,0\rangle$ and $|\Psi_0\rangle = \frac{1}{\sqrt{2}}[|0\rangle + i|1\rangle] \otimes |0\rangle$, respectively. Here, only nonzero values of $P_n(t)$ are drawn.

Let us make a final comment on the randomness of discrete-time quantum walks. We have seen that a t-step quantum walk always results in the same final state for a given initial state. In this sense, the time evolution of quantum walks can be classified as deterministic. When it comes to measuring the position of the walker at the end of the walk, we obtain probabilistic results which is, indeed, a property that all quantum systems have in common. On the contrary, the final state of a classical random walk is a random position from a set of possible positions, and thus, completely probabilistic. Therefore, the time evolution of the quantum walk cannot be considered as random as in the case of the classical walk.

2.4.2 Recursion equations

The time evolution of the walk can equivalently be expressed by the recursion equations. In order to derive them, remember first that nonzero probabilities occur only at either odd or even labeled positions depending on the step number t. Therefore, nearly one half of these positions can be thought as receivers and the other half as transmitters to stand for the incoming and outgoing probability fluxes during a single step. Now, consider that position n is a transmitter at time t. The projection of the walker's state on $|n\rangle$ is, then,

$$(I \otimes |n\rangle\langle n|) |\Psi_t\rangle = |\Psi_t'\rangle = [\alpha_n(t)|0\rangle + \beta_n(t)|1\rangle] \otimes |n\rangle \neq 0. \tag{2.48}$$

19
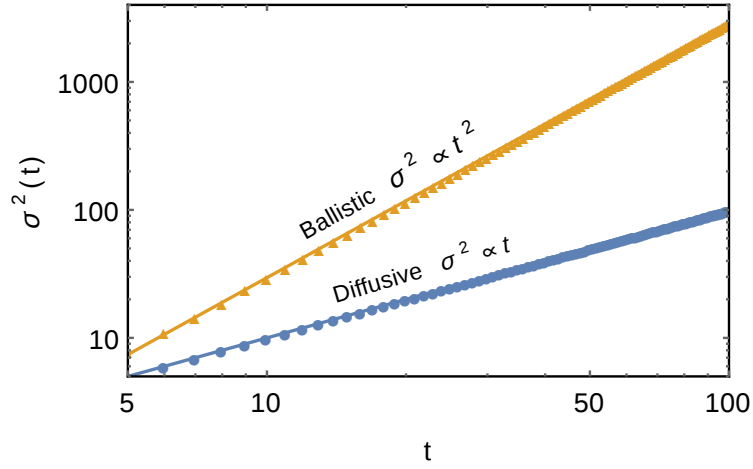
Figure 2.4: The variance of discrete-time quantum walk for the initial state (2.45) is proportional to the square of step number t, which is quadratically faster than that of the classical random walk. Similar results can be obtained for other initial states. The axes are drawn in logarithmic scale.

The coefficients in (2.46) are denoted by $a_{n,0} \equiv \alpha_n$ and $a_{n,1} \equiv \beta_n$ for clarity. Following the coin operation C_H, the state $|\Psi'_t\rangle$ transforms into

$$(C \otimes I)|\Psi'_t\rangle = \frac{1}{\sqrt{2}} \left[\overbrace{(\alpha_n(t) + \beta_n(t))}^{\text{left-going}} |0\rangle + \overbrace{(\alpha_n(t) - \beta_n(t))}^{\text{right-going}} |1\rangle \right] \otimes |n\rangle, \qquad (2.49)$$

indicating the outgoing amplitudes from position n once the shift operator is applied. It is clear that (2.49) is valid for all positions $\{n + 2k : k \in \mathbb{Z}\}$. Now, let us consider the scenario where n is a receiver this time at again, step number t. Along the step $t + 1$, the position n will receive the amplitude $\alpha_{n+1}(t) + \beta_{n+1}(t)$ from $n+1$ and $\alpha_{n-1}(t) - \beta_{n-1}(t)$ from $n - 1$ which results in

$$\alpha_n(t + 1) = \frac{1}{\sqrt{2}} \left[\alpha_{n+1}(t) + \beta_{n+1}(t) \right], \qquad (2.50)$$

$$\beta_n(t + 1) = \frac{1}{\sqrt{2}} \left[\alpha_{n-1}(t) - \beta_{n-1}(t) \right]. \qquad (2.51)$$

These are the recursion equations for C_H that connect the amplitudes between adjacent steps and are quite useful in numerical simulations in terms of simplicity and efficiency. Moreover, for the general coin operator in (2.43), recursion equations read as

$$a_{n,0}(t + 1) = a_{n+1,0}(t)\sqrt{\rho} + a_{n+1,1}(t)\sqrt{1 - \rho}e^{i\theta}, \qquad (2.52)$$

$$a_{n,1}(t + 1) = a_{n-1,0}(t)\sqrt{1 - \rho}e^{i\phi} - a_{n-1,1}(t)\sqrt{\rho}e^{i(\theta+\phi)}. \qquad (2.53)$$
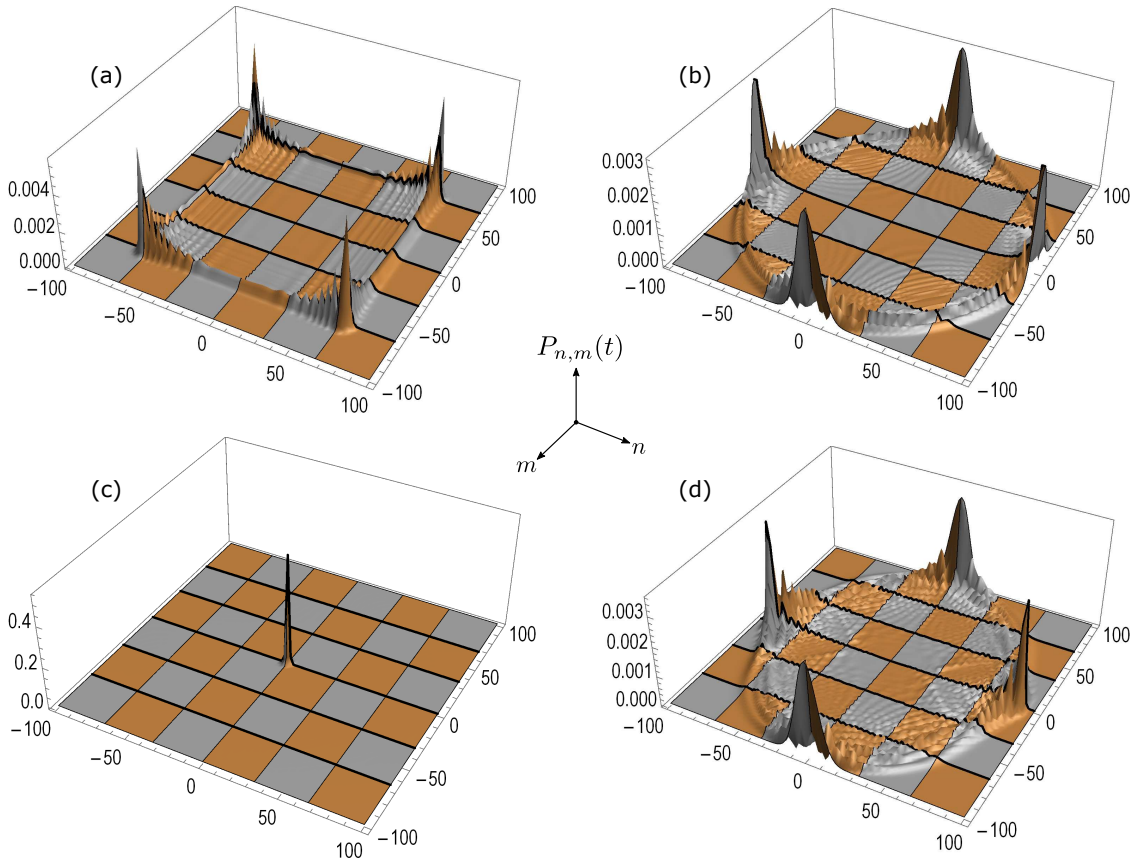
Figure 2.5: Probability distributions of (a) Hadamard walk with the initial state (2.57), (b) Grover walk with the initial state $|\Psi_0\rangle = |0\rangle \otimes |0,0\rangle$, (c) Grover walk with the initial state (2.58) and (d) DFT walk with the initial state (2.59) in two-dimensions.

2.4.3 Higher dimensions

The position space of the quantum walk we discussed in the previous section can obviously be interpreted as a line Cartesian space. Such walks are called 1-dimensional quantum walks. By definition, the dimension of the quantum walk is the number of degree of freedom in the position space. Therefore, a 1-dimensional quantum walk can be extended to higher dimensions by enlarging the coin and position spaces. For 2-dimensional quantum walk, for instance, the coin space can be chosen as four dimensional with the basis $\{|0,0\rangle, |0,1\rangle, |1,0\rangle, |1,1\rangle\} \equiv \{|0\rangle, |1\rangle, |2\rangle, |3\rangle\}$ while the position space is spanned by $\{|n,m\rangle \mid n, m \in \mathbb{Z}\}$. The coin can be interpreted as a single 4-level coin or two different 2-level coins. For both cases, the coin operator can be chosen as factorizable

$$C = C_H \otimes C_H = \frac{1}{2} \begin{bmatrix} 1 & 1 & 1 & 1 \\ 1 & -1 & 1 & -1 \\ 1 & 1 & -1 & -1 \\ 1 & -1 & -1 & 1 \end{bmatrix}, \tag{2.54}$$

or non-factorizable

$$C_G = \frac{1}{2} \begin{bmatrix} -1 & 1 & 1 & 1 \\ 1 & -1 & 1 & 1 \\ 1 & 1 & -1 & 1 \\ 1 & 1 & 1 & -1 \end{bmatrix}, \quad C_{DFT} = \begin{bmatrix} 1 & 1 & 1 & 1 \\ 1 & i & -1 & -i \\ 1 & -1 & 1 & -1 \\ 1 & -i & -1 & i \end{bmatrix}, \quad (2.55)$$

where C_G and C_{DFT} are the Grover coin and the discrete Fourier transform (DFT) coin [43], respectively. The quantum walks which use the Grover coin and the DFT coin as the coin operators are called the *Grover walk* and the *DFT walk*, respectively. When the position basis $|n, m\rangle$ corresponds to the sites of a square lattice, the shift operator is defined as a single operation that moves the walker in the left down, left up, right down and right up directions (i.e., towards corners) for respective coin states [44] as in

$$S = \sum_{n,m} |0\rangle\langle 0| \otimes |n-1, m-1\rangle\langle n, m| + |1\rangle\langle 1| \otimes |n-1, m+1\rangle\langle n, m|$$

$$+ |2\rangle\langle 2| \otimes |n+1, m-1\rangle\langle n, m| + |3\rangle\langle 3| \otimes |n+1, m+1\rangle\langle n, m|. \quad (2.56)$$

Let us discuss now some properties of 2-dimensional walks governed by these coin operators. In Fig. 2.5(a), we provide the probability distribution of a 2-dimensional Hadamard walk with the initial state

$$|\Psi_0\rangle = \frac{1}{2}(|0\rangle + i|1\rangle + i|2\rangle - |3\rangle) \otimes |0, 0\rangle. \quad (2.57)$$

which results in a symmetrical distribution. As discussed before, this symmetry is provided by the specific choice of the initial state here, i.e., the coefficients i prevent the cancellation of the terms going in opposite directions. The Grover walk is not able to spread unless we choose certain initial states such as

$$|\Psi_0\rangle = \frac{1}{2}(|0\rangle - |1\rangle - |2\rangle + |3\rangle) \otimes |0, 0\rangle \quad (2.58)$$

which gives the probability distribution in Fig. 2.5(b). Most of the other states that are initially localized at the origin with different coin states remain localized as the number of steps increases, which is demonstrated in Fig. 2.5(c). The probability distribution of the discrete Fourier coin can be seen in Fig. 2.5(d), where we started with the initial state

$$|\Psi_0\rangle = \frac{1}{2}\left(|0\rangle + \frac{1-i}{\sqrt{2}}|1\rangle + |2\rangle - \frac{1-i}{\sqrt{2}}|3\rangle\right) \otimes |0, 0\rangle \quad (2.59)$$

Consequently, by looking at Fig. 2.5, we can conclude that the spreading of Grover walk is the widest one among the others.

2.4.4 Entanglement

In this chapter, we will briefly introduce the concept of entanglement and one of its well known measures, von Neumann entropy, among many others recorded in the literature. Then, we will discuss the entanglement properties between the coin and position states of the discrete-time quantum walk. Detailed reviews of entanglement and its measures can be found in [45–50].

Consider a composite quantum system consisting of two parts, A and B. According to the postulates of quantum mechanics, the Hilbert space of the total system is spanned by the basis $\{|a_i, b_j\rangle\}$ where $\{|a_i\rangle\}$ and $\{|b_j\rangle\}$ are the orthonormal basis states of the Hilbert spaces of individual parts. A state of this composite system is written, in terms of the basis states, as

$$|\psi\rangle = \sum_{ij} c_{ij}|a_i b_j\rangle. \tag{2.60}$$

Now, assume that part A is initially prepared in the state $|\psi_A\rangle = \frac{1}{\sqrt{2}}(|0\rangle + |1\rangle)$ and B in the state $|\psi_B\rangle = \frac{1}{\sqrt{2}}(|0\rangle - |1\rangle)$. Thus, it is clear that the state of the composite system is

$$|\psi\rangle = |\psi_A\rangle \otimes |\psi_B\rangle = \frac{1}{2}(|0, 0\rangle - |0, 1\rangle + |1, 0\rangle - |1, 1\rangle), \tag{2.61}$$

where the coefficients in (2.60) are $c_{00} = 1/2$, $c_{01} = -1/2$, $c_{10} = 1/2$ and $c_{11} = -1/2$. These kinds of states, i.e., the states that can be written as the tensor product of individual systems, are called *seperable states*. However, the Hilbert space is huge; and there are also states which cannot be written as a simple tensor product. For example, the state

$$|\psi\rangle = \frac{1}{\sqrt{2}}(|0, 1\rangle + |1, 0\rangle) \tag{2.62}$$

is also an element of the Hilbert space of the composite system but there is no way of writing it in tensor product form. The states of this kind are called *entangled states*. At first glance, one may think there is something peculiar about it. A local measurement on system A instantaneously determines the state of B regardless of the distance between them. This situation contradicts the law that two bodies cannot interact faster than the speed of light so apparently, the state (2.62) cannot represent a real system. On the other hand, we know under the guidance of the words of the masters that [51], in a *complete physical theory*, *every element of the physical reality must have a counterpart*. Therefore, the state given in (2.62) should correspond to some physical reality. In fact, it does. Today, it has been shown by various experiments that entangled states do exist [52, 53]; however, they cannot be used to transfer any information faster than light [54, 55].

Up to now, we have discussed entanglement for pure quantum states. A density matrix ρ_{AB} which describes a mixed bipartite system is seperable if and only if it can be decomposed as [56],

$$\rho^{AB} = \sum_k p_k \rho_k^A \otimes \rho_k^B. \tag{2.63}$$

The ρ_k^A and ρ_k^B correspond to the density matrices of the systems A and B, respectively. The weights p_k are positive and satisfy $\sum_k p_k = 1$. In order to quantify the entanglement, there are several measures specific to the situation under consideration and we will be introducing one of them later on.

Shannon Entropy

Shannon entropy measures the information we have about a classical system [57]. From a different perspective, it quantifies the amount of source we should use in order to record the possible outcomes of this system. Think of a 4 sided dice whose sides are labeled by one of 1, 2, 3 or 4. Let us encode the results with binary numbers each time we throw the dice: $1 \rightarrow 00$, $2 \rightarrow 01$, $3 \rightarrow 10$ and $4 \rightarrow 11$. If the dice we have is fair, we have no idea of what the next outcome will be. Therefore, we need at least $\log_2 4 = 2$ binary numbers -or bits- to encode each outcome. Now, assume that we have a loaded dice instead of a fair one. After throwing the dice, say 1000 times, we will obtain a probability distribution for the possible outcomes. We will thus have some information about the system which can be used to encode the data more efficiently, e.g., the outcomes with higher probabilities can be encoded by 1 bit instead of 2 bits. In Fig. 2.6 we see such a procedure called *Huffman coding* which allows us to encode one outcome only with 1.4 bits on average. If, for example, we throw the dice 1000 times, we only need 1400 bits instead of 2000 while encoding the data. We see that the less amount of sources we need, the more information we have about the system; namely, the information we have increases the predictability of the system. For this reason, Shannon himself defines the unit of certainty in terms of bits. If we need 2 bits of data instead of 1.4 on average, it means that the system we are dealing with is more uncertain. In this sense, Shannon entropy can also be interpreted as a measure of randomness for a given system. For a classical system whose possible outcomes have probability distribution $p_1, \ldots, p_n$, the Shannon entropy (or, the uncertainty of the system) is defined as

$$H(p_1, \ldots, p_n) = - \sum_i p_i \log_2 p_i \tag{2.64}$$

24
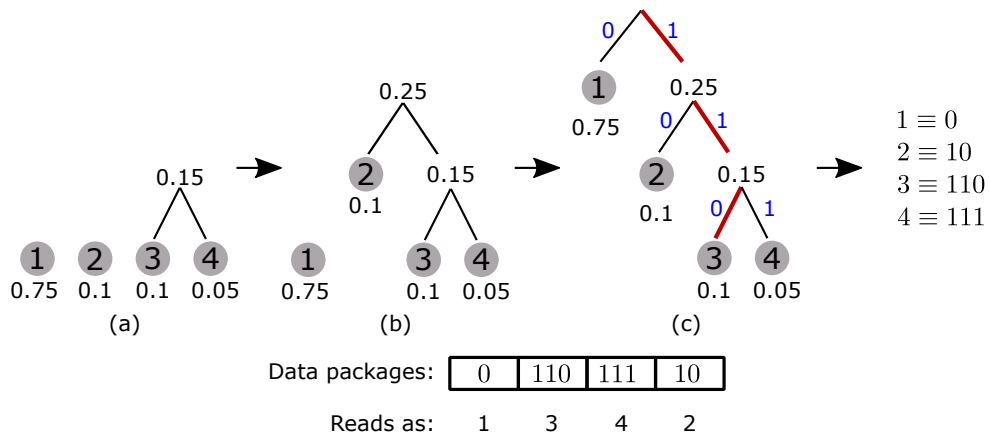
Figure 2.6: Huffman coding. There are 4 possible outcomes of a classical system labeled 1, 2, 3 and 4 and each time, the system returns one of these numbers as the result. Avoiding any loss of information, Huffman coding provides the most efficient method for encoding these outcomes in terms of classical bits implemented as follows: (a) Write down the possible outcomes with their corresponding probabilities as nodes. Select two least probable nodes, 3 and 4, and merge them into a single node with a branch. Then add the corresponding probabilities, $0.1 + 0.05 = 0.15$. (b) Repeat the same procedure for two least likely nodes again, $0.1 + 0.15 = 0.25$. (c) Stop the procedure after getting a single node at the top. Label each edge with 0 or 1 (in any order) for all the levels in the tree. The code (0,10,110 and 111) for each outcome is the path from the top to that given level. Therefore, the average number of bits to encode one outcome is $0.75 \times 1 + 0.1 \times 2 + 0.1 \times 3 + 0.05 \times 3 = 1.4$. Huffman coding is one of the widely used methods for lossless data compression in computer science.

where we assumed $0.\log_2 0 = 0$ since zero probability does not correspond to any outcome. In Fig. 2.7, we see the Shannon entropy of a coin, or any two-level system, with outcomes $\{H, T\}$ and corresponding probabilities $\{p, 1 - p\}$. At $p = 0.5$, the uncertainty about the system is maximum, meaning that we should have at least 1 bit to encode the outcomes. Moreover, the value $H(0.1) = 0.469$, for example, implies we need only 469 bits to encode the outcomes after tossing the coin for 1000 times.

Von Neumann Entropy

The quantum counterpart of Shannon entropy is the Von Neumann entropy which can be obtained by replacing the probability distributions with the density matrices:

$$S(\rho) = -\text{Tr}(\rho \ln \rho). \tag{2.65}$$

In order to get a better insight about the relationship between the Shannon and Von Neumann entropies, let us think of a system that can be found in an ensemble of states $\mathcal{A} = \{\rho_1, \ldots, \rho_r\}$ given by pure or mixed density matrices with probabilities $\{p_1 \ldots p_r\}$. The total state of this system can be written as a single density matrix

$$\rho = \sum_{i=1}^{r} p_i \rho_i. \tag{2.66}$$
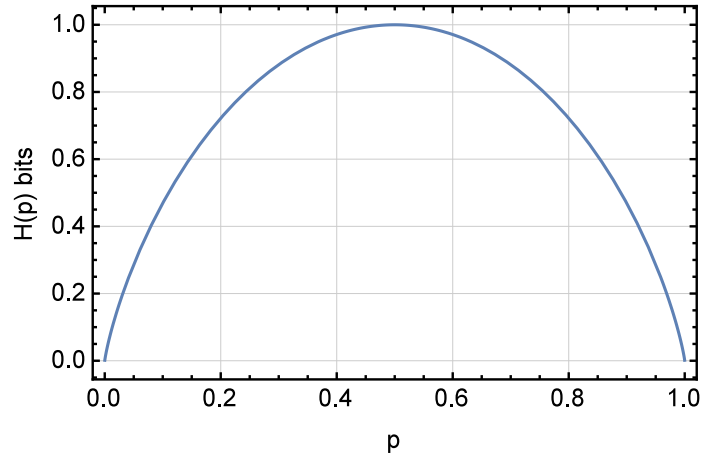
Figure 2.7: Shannon entropy of a classical system with two probable outcomes. The p is the probability of one of the possible outcomes taking place. The cases $p = 0$ or $p = 1$ imply that we know everything about the system since we can predict the next outcome exactly. If we want to encode the outcome in terms of classical bits, no bits are needed at all since there is no indeterminacy about the system, i.e., its entropy is zero $H(0) = 0$ bit. When $p = 0.5$, we have the chance of predicting the next outcome with probability 0.5. The indeterminacy about the system is maximum and we need at least one bit to encode each outcome, i.e., entropy is maximum $H(0.5) = 1$ bit.

By plugging (2.66) into (2.65) in terms of its eigenvectors $|i\rangle$ and eigenvalues λ_i, we obtain

$$
\begin{aligned}
S(\rho) &= -\sum_l \langle l| \left(\sum_j \lambda_j |j\rangle\langle j| \sum_k \ln\lambda_k |k\rangle\langle k| \right) |l\rangle, \\
&= -\sum_l \sum_{jk} \lambda_j \ln\lambda_k \langle l|j\rangle\langle j|k\rangle\langle k|l\rangle, \\
&= -\sum_l \lambda_l \ln\lambda_l.
\end{aligned}
\tag{2.67}
$$

Now let us assume an equivalent scenario in which Alice wants to send a message to Bob by using two quantum states $\mathcal{A} = \{|0'\rangle, |1'\rangle\}$ given as

$$
\begin{aligned}
|0'\rangle &= \cos\theta|0\rangle + \sin\theta|1\rangle, \\
|1'\rangle &= \sin\theta|0\rangle + \cos\theta|1\rangle,
\end{aligned}
\tag{2.68}
$$

where the states are created with probabilities $\{p, 1-p\}$. It is clear that for $\theta = 0$, these states correspond to orthogonal states and for $\theta = \pi/4$, they correspond to the identical state. The states $|0'\rangle$ and $|1'\rangle$ are get closer to each other while θ is increasing in the interval $0 \leqslant \theta \leqslant \pi/4$. Therefore, the density matrices of both states are written as

$$
\rho_{0'} \leftrightarrow \begin{bmatrix} \cos^2\theta & \cos\theta\sin\theta \\ \cos\theta\sin\theta & \sin^2\theta \end{bmatrix}, \quad \rho_{1'} \leftrightarrow \begin{bmatrix} \sin^2\theta & \cos\theta\sin\theta \\ \cos\theta\sin\theta & \cos^2\theta \end{bmatrix}.
\tag{2.69}
$$

26
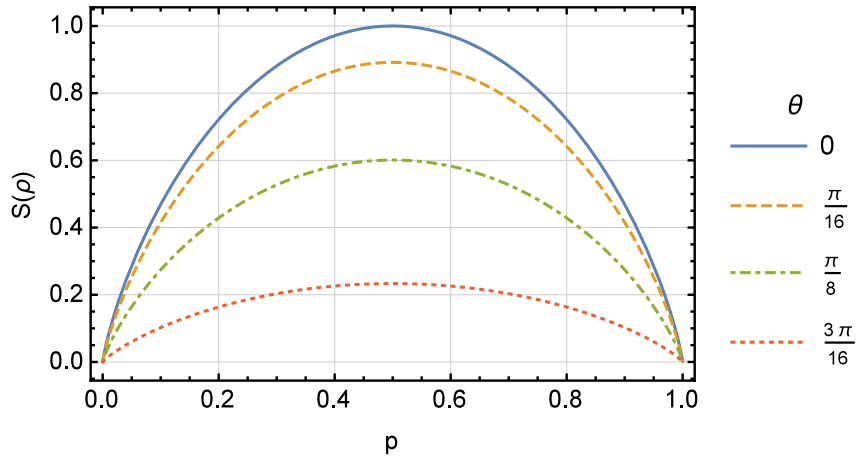
Figure 2.8: Von Neumann entropy of a quantum two-level system. The θ specifies the states $\{|0'\rangle, |1'\rangle\}$ in (2.68) which are non orthogonal if $\theta \neq 0$. Think of the scenario in which Alice prepares her qubit in one of the states $\{|0'\rangle, |1'\rangle\}$ with probabilities p and $1 - p$, respectively, and sends it to Bob. When $\theta = 0$, i.e., the states are orthogonal and $S(\rho)$ coincides with $H(p)$, and $p = 0.5$ Bob's lack of information about the system is maximum. He describes each qubit state sent by Alice by the density matrix $\rho = p|0\rangle\langle 0| + (1 - p)|1\rangle\langle 1|$ and needs at least $S(\rho) = 1$ qubit to encode this data. As θ gets larger, Bob manages to encode each qubit coming from Alice using less than one qubit ($S(\rho) < 1$) in average because he has more information about the system now.

Since Bob only knows that the states are selected from a probability distribution, he describes the system with a density matrix

$$\rho = p\rho_{0'} + (1 - p)\rho_{1'} = \begin{bmatrix} \sin^2\theta + p\cos 2\theta & \cos\theta \sin\theta \\ \cos\theta \sin\theta & \cos^2\theta - p\cos 2\theta \end{bmatrix}, \tag{2.70}$$

with the eigenvalues $\lambda_\pm = \frac{1}{2}\left(1 \pm \sqrt{1 + 4p(p-1)\cos^2 2\theta}\right)$. For different values of θ, Von Neumann entropy $S(\rho) = -\lambda_+\log_2\lambda_+ - \lambda_-\log\lambda_-$ is given in Fig. 2.8. For $\theta = 0$, Von Neumann entropy is the same as Shannon entropy. It can be seen that $S(\rho)$ decreases for less orthogonal states, i.e., the amount of information transferred from Alice to Bob decreases as the states $|0'\rangle$ and $|1'\rangle$ get more similar. If the two states coincide, it is obvious that no information is being transferred, and hence, the entropy is zero. Von Neumann entropy can also be used for pure bipartite systems in all dimensions [58, 59]. The *entropy of entanglement* for a pure bipartite state ρ_{AB} is defined as

$$E(\rho^{AB}) = S(\rho^A) = (\rho^B). \tag{2.71}$$

Here, the reduced density matrices ρ_A and ρ_B are obtained by calculating the partial traces over subsystems B and A, respectively. If ρ_{AB} is a separable state, then ρ_A and ρ_B are pure, which results in $E(\rho_{AB}) = 0$. However, the individual systems are mixed in general. For d-dimensional systems, the maximum value of $E(\rho_{AB})$ becomes $\log_2 d$.
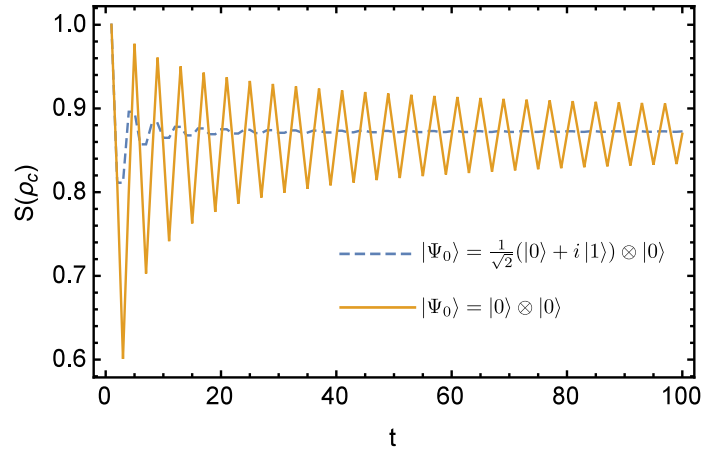
Figure 2.9: Coin-position entanglement of one-dimensional quantum walk for two different initial states.

Entanglement in discrete-time quantum walks

It is known that the shift operator entangles the coin and position spaces starting from the first step of the walk [60]. Since the step operator is unitary, the state of the total system $\rho_t = |\Psi_t\rangle\langle\Psi_t|$ remains pure while step number t is increasing. Therefore, we can use Von Neumann entropy to measure the entanglement between coin and position spaces. The entropy of entanglement at step number t becomes $E(\rho_t) = S(\rho_c)$ where $\rho_c = \text{Tr}_p(\rho_t)$. Here, the partial trace is taken over the position space. Looking at Fig. 2.9, we see that the position and coin spaces are maximally entangled in the first step. Later on, the entanglement fluctuates around an asymptote at 0.872. It has been analytically shown that this asymptotic value is independent of the initial state [61].

2.4.5 Decoherence

A system under *decoherence* loses its coherent properties in time due to its interaction with the environment. *Kraus representation* is one of the widely accepted methods in describing the dynamics of such systems [42]. In this method, the system (S) under consideration and its environment (E) are interpreted as different systems coupled to each other. The total system ($S + E$), however, is assumed to be an isolated one. Therefore, after evolving the system and its environment together, we trace out the environment to obtain the state of the system we consider . Mathematically,

$$\rho_s = \text{Tr}_e(U\rho U^\dagger) \tag{2.72}$$

where U is the unitary operator evolving the total system. Now, starting with a total initial state $\rho = \rho_{s,0} \otimes \rho_{e,0}$ where $\rho_{s,0}$ and $\rho_{e,0} = |\epsilon_0\rangle\langle\epsilon_0|$ are the initial states of the system and

its environment, (2.72) reads as

$$\rho_s = \sum_{n=0}^{m} \langle e_n|U|\epsilon_0\rangle \rho_{s,0} \langle \epsilon_0|U^\dagger|e_n\rangle = \sum_{n=0}^{m} E_n \rho_{s,0} E_n^\dagger \tag{2.73}$$

where $\{|e_n\rangle \mid n = 1, \ldots, m\}$ is the basis of the m-dimensional Hilbert space of the environment and $E_n = \langle e_n|U|\epsilon_0\rangle$ are the *Kraus operators*. They satisfy the condition $\sum_{n=0}^{m} E_n^\dagger E_n = I$. Choosing a separable initial state is a plausible assumption since all correlations between the system and its environment are destroyed during experimental preparation. Here, in order to obtain (2.73) we also assumed that the unitary operator can be decomposed in terms of linear operators X and Y as $U = \sum_i a_i X_i \otimes Y_i$. Moreover, we assumed that ρ_e is a pure state since we know it is possible to enlarge the environment until it becomes a pure state. This method will be used in this section also for describing the behavior of discrete-time quantum walks under decoherence [62].

For the discrete-time quantum walk, the total Hilbert space consists of three subspaces $\mathcal{H}_E \otimes \mathcal{H}_c \otimes \mathcal{H}_p$: the environment, position and coin spaces. In Kraus representation, a single step of the walk becomes

$$\rho(t+1) = \sum_{n=0}^{m} E_n \rho(t) E_n^\dagger. \tag{2.74}$$

In order to find out the Kraus operators, let us first discuss the interaction mechanism of the system S and its environment E. We know that if there were no decoherence effects in the environment, the system S would evolve with the unitary step operator $U' = S(C \otimes I)$ (see Sec. 2.4.1 for details). However, for the cases where the system interacts with its environment, we assume that U' changes due to the environmental effects in each step. Therefore, the operator U should affect the system S contingent upon the state of the environment. Before we introduce decoherence mechanisms for the quantum walk, let us assume that the environment exists in the state $|e_i\rangle$, and the operator A_i acts on the system S with probability p_i. We can, then represent the environment by an r-dimensional Hilbert space spanned by $\{|e_i\rangle\}$ where it is initially found in the state

$$|\epsilon_0\rangle = \sqrt{p_1}|e_1\rangle + \ldots + \sqrt{p_r}|e_r\rangle. \tag{2.75}$$

We note that in reality, the environment is the entire universe except the system we consider. However, we saw in (2.75) that we do not need to know the exact form of the environment. We only consider the part of it which effectively affects S. Therefore, there is no reason for $|\epsilon_0\rangle$ be normalized. We can now write the conditional unitary evolution

for the total system $(S + E)$ as

$$U = |e_1\rangle\langle e_1| \otimes A_1 + \ldots + |e_r\rangle\langle e_r| \otimes A_r, \tag{2.76}$$

where $|e_i\rangle\langle e_i|$ and A_i act on the environment E and the system S separately. It is clear that operators $|e_i\rangle\langle e_i|$ do not alter the environment, i.e., they are just a condition to apply the A_i properly. Thus, the Kraus operators and one step of the walk become

$$E_i = \langle e_i|U|\epsilon_0\rangle = \sqrt{p_i}A_i, \tag{2.77}$$

$$\rho(t + 1) = \sum_{i=1}^{r} E_i \rho E_i^\dagger = \sum_{i=1}^{r} p_i A_i \rho A_i^\dagger. \tag{2.78}$$

We may now discuss two types of decoherence taking place in quantum walks.

Coin decoherence

The distinctive properties of isolated quantum walks arise due to the coherent nature of the their unitary evolution. In other words, the system does not get measured between adjacent steps. Starting with the initial state $|\Psi(0)\rangle = \frac{1}{\sqrt{2}}(|0\rangle + |1\rangle)$, assume that we measure the coin state in each step in the basis $\{|0\rangle, |1\rangle\}$ before applying the shift operator. Following the measurement, we obtain either $|0\rangle$ or $|1\rangle$ with equal probabilities and the shift operator moves the walker to the either one of the two directions accordingly. It is obvious that this scenario is exactly the same as that of the classical random walk. As the number of realizations increase, the probability distribution converges to normal distribution. Now, the effect of environment on the quantum walk can be thought as the scenario we discussed here. Assume the environment 'measures' the coin state with some probability p or no measurement takes place at all with probability $(1 - p)$. Formally speaking, this corresponds to an orthonormal projection on the coin state performed with projection operators $D_1 = |0\rangle\langle 0|$ and $D_2 = |1\rangle\langle 1|$ with same probabilities $p_1 = p_2 = p/2$. We also demonstrate the null effect of the environment by $D_3 = I$ with probability $p_3 = (1 - p)$. Therefore, the state of the environment in (2.75) and Kraus operators in (2.77) become

$$|\epsilon_0\rangle = \sqrt{p}|e_1\rangle + \sqrt{p}|e_2\rangle + \sqrt{1 - p}|e_3\rangle, \tag{2.79}$$

$$E_i = \sqrt{p_i}A_i = \sqrt{p_i}S(C \otimes I)(D_i \otimes I). \tag{2.80}$$

The numerical results for the probability distribution of a quantum walk under coin decoherence is given in Fig. 2.10(a).
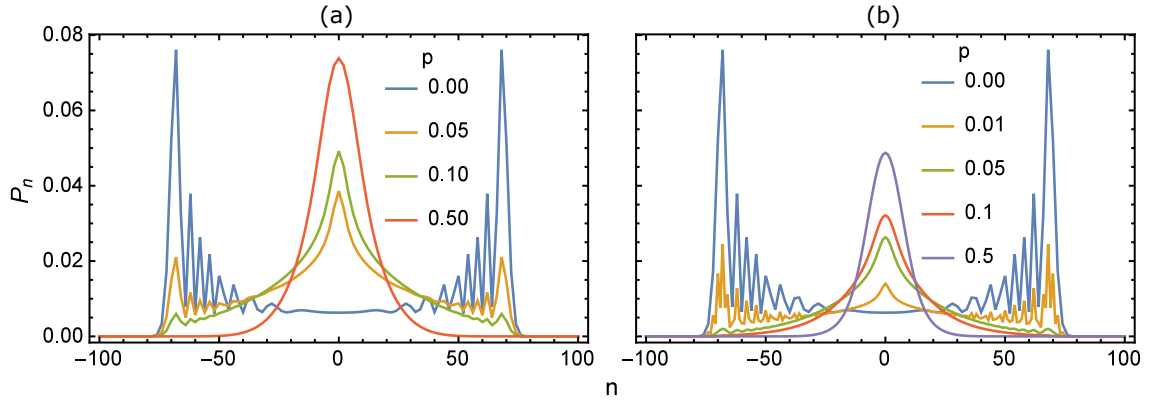
Figure 2.10: The probability distributions of discrete-time quantum walk under decoherence on the line after 100 steps. (a) The coin state is measured in each step with probability p (coin-decoherence). Only non-zero values of P_n are drawn (b) In each step, the connections between the nearest neighbors are redefined. The probability of a connection to exist is p. We see in both situations that a transition from quantum behavior to classical behavior takes place as we increase p as a decoherence parameter.

Coin-position decoherence

This decoherence scenario utilizes the imperfections in the lattice caused by missing connections between the positions where the walker may exist [63]. In each step, all connections in the lattice are reconfigured. Therefore, the walker may not be able to jump to any of the nearest possible positions with some probability p for a given step number. This probability is p^2, $p(1-p)$ and $(1-p)^2$ for the cases where both connections are broken, only one of them is broken and both exist, respectively. The environment state in (2.75) becomes

$$|\epsilon_0\rangle = (1-p)|e_1\rangle + \sqrt{p(1-p)}(|e_2\rangle + |e_3\rangle) + p|e_4\rangle. \tag{2.81}$$

Different than the coin decoherence which we have discussed in the previous section, we must redefine the shift operators by considering the broken connections for each environment basis state. The appropriate choices for the shift operators are

$$S_1 = \sum_n |0\rangle\langle 0| \otimes |n-1\rangle\langle n| + |1\rangle\langle 1| \otimes |n+1\rangle\langle n|,$$

$$S_2 = \sum_n -|1\rangle\langle 0| \otimes |n\rangle\langle n| + |1\rangle\langle 1| \otimes |n+1\rangle\langle n|,$$

$$S_3 = \sum_n |0\rangle\langle 0| \otimes |n-1\rangle\langle n| + |0\rangle\langle 1| \otimes |n\rangle\langle n|,$$

$$S_4 = \sum_n |1\rangle\langle 0| \otimes |n\rangle\langle n| + |0\rangle\langle 1| \otimes |n\rangle\langle n|.$$

Here, S_1 is the ordinary shift operator. The shift operator S_2 (S_3) is used when the left (right) connection is broken and we note that the walker is reflected to the opposite di-

31

rection if one of the connections are missing. However, if both connections are missing, the operator S_4 is used and the walker is not able to leave its current position. Once we write S_i, we may also write the operators $A_i = S_i(C \otimes I)$ which define the time evolution of the system. We provide numerical results for the probability distribution of a quantum walk under coin-position decoherence in Fig. 2.10(b).

2.5 Continuous-time quantum walks

The continuous-time quantum walk has first been suggested [5] as a quantum algorithm which reaches the nth level of a decision tree faster than a continuous-time Markov process. In this scheme of quantum walk, there is no coin space at all and the quantum state evolves with a unitary operator related with the transition matrix. Before we define the continuous-time quantum walk, it is helpful to start by introducing some basics of the graph theory.

In discrete mathematics, a graph $G = (V, E)$ is the representation of an object set V in which some pairs are connected by links E. The degree of any vertex $\deg(v)$ is the number of vertices incident to the vertex v. Geometrically, these objects and the links in between are represented by vertices (or sites) and edges (or bonds), respectively. There are various types of graphs some of which are displayed in Fig. 2.11. A graph G can be specified by the connectivity matrix A that keeps the information about the existence of bonds in between as follows:

$$
A_{ij} = \begin{cases} 1 & \text{if } i \neq j \text{ and } i, j \text{ connected}, \\ 0 & \text{otherwise}. \end{cases} \tag{2.82}
$$

An auxiliary matrix called the *Laplacian* also contains the degree information of each vertex in its corresponding diagonal elements:

$$
L_{ij} = \begin{cases} \deg(v_i) & \text{if } i = j, \\ -1 & \text{if } i \neq j \text{ and } i, j \text{ connected}, \\ 0 & \text{otherwise}. \end{cases} \tag{2.83}
$$

which is simply $L = A - D$, with D as the degree matrix $D_{ii} = \deg(v_i)$. Thus, L is a positive semi-definite matrix, i.e., its eigenvalues are non-negative. The Hamiltonian which governs the dynamics of the continuous-time quantum walk simply becomes $H = \gamma L$ which is also closely related with the tight-binding Hamiltonian in condensed matter physics. The value of γ represents the hopping rate between adjacent sites. A particle

localized on any site i is interpreted as being in the state $|i\rangle \leftrightarrow (0, \ldots, 0, 1, 0, \ldots, 0)^T$ and these states form a complete and orthonormal set over all sites, $\sum_{i \in \mathcal{N}} |i\rangle\langle i| = \mathbf{I}$. Therefore, starting from an initial state $|\Psi_0\rangle$, the time evolution is given by

$$|\Psi_t\rangle = e^{-iHt}|\Psi_0\rangle \tag{2.84}$$

where the time t is given in units of $[\hbar/H_{ij}]$. The probability of finding the particle at position m after some time t is given by

$$P_{n,m}(t) = |\langle m|e^{-iHt}|n\rangle|^2, \tag{2.85}$$

where n denotes the initial position of the particle. In order to define a continuous-time Markov process, we follow the same procedure as in that of the continuous-time quantum walk without any coherent properties. In other words, the state vector $|\Phi\rangle$ contains the probabilities instead of probability amplitudes and the evolution is given by

$$|\Phi_t\rangle = e^{Tt}|\Phi_0\rangle \tag{2.86}$$

where $T = -\gamma L$ is the transition matrix. The probabilities read as

$$P_{n,m}(t) = \langle m|e^{Tt}|n\rangle. \tag{2.87}$$

In Fig. 2.12, we see the probability distribution of one-dimensional continuous-time quantum walk and the corresponding Markov process for two different hopping rates. We will see in the following sections that the continuous-time quantum walks and Markov processes provide a simple but useful model for the coherent and incoherent transport processes, respectively.
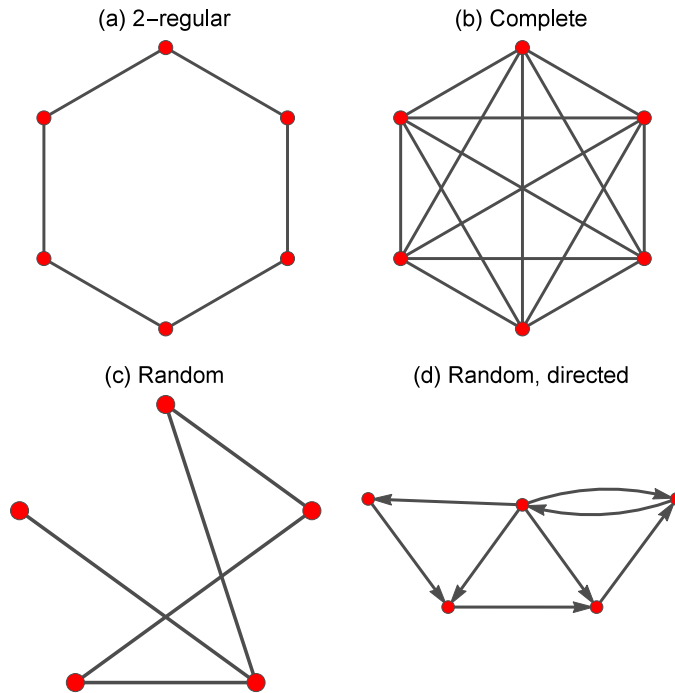
Figure 2.11: Various examples of graph structures in which a continuous-time quantum walk can take place. (a) In an *n-regular graph* each vertex has the same number of neighbors. (b) In a *complete graph* each pair of distinct vertices are connected by a unique edge. (c) A *random graph* can be constructed by placing edges randomly between vertices. (d) In a *directed graph*, all edges have a direction associated with them.
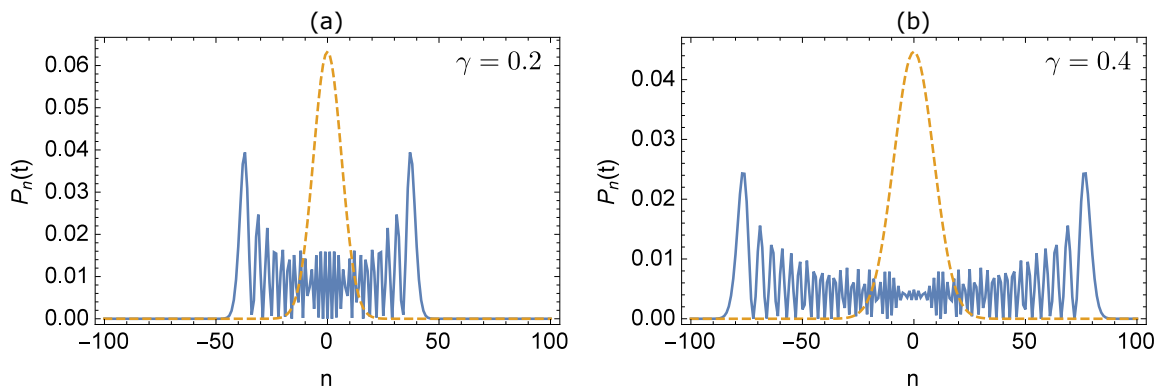
Figure 2.12: A comparison of the probability distributions of continuous-time quantum walk (solid) and continuous-time Markov process (dashed) for hopping rates (a) $\gamma = 0.2$ and (b) $\gamma = 0.4$.

Chapter 3

QUBIT STATE TRANSFER

Quantum state transfer from one location to another is a significant problem for quantum information processing systems. A quantum computer, which consists of different processing units, requires the quantum states to be transferred between its parts. Therefore, quantum state transfer will be an important part of quantum computer design. There are various ways of achieving this task depending on the technology at hand [64]. In this chapter, we consider two related fields of research, quantum state transfer and quantum walks on one-dimensional graphs.

Quantum communication through a spin chain was first considered by Bose [65] and since then it has been studied in depth [66–73]. This procedure consists of interacting spins on a chain, whose dynamics is governed by Heisenberg, XX or XY Hamiltonians. Perfect state transfer (PST) through a spin chain, in which adjacent spins are coupled by equal strength, can be achieved only over short distances [19, 20].

The time-evolution of qubit state transfer through a spin chain can be interpreted as a continuous-time quantum walk and PST is possible over a spin chain of any length with pre-engineered couplings [19, 20]. Furthermore, this interpretation can be extended to discrete-time quantum walk with a position-dependent coin operator [21]. PST in quantum walks on various graphs has been studied more specifically for the continuous-time model [22]. High fidelity transfer of specific quantum states on variants of cycles has been reported for the discrete-time quantum walk [23] without considering the internal coin state.

In this chapter, we show the perfect transfer of an unknown qubit state from one site (A) to another (B) on one-dimensional graphs in discrete-time quantum walk architecture. We treat the coin as our qubit whose state we aim to transfer. The coin is an internal degree of freedom of the walker, e.g. polarization, 2-energy levels, angular momenta or spin, which moves on discrete graph sites. At the end of the walk, we apply one more coin operator (*recovery operator*) to achieve PST. The recovery operator is independent of the initial coin state and it can be determined before the walk once a coin operator is

chosen. We study the periodicity of each case where PST occurs and show that for all PST cases the quantum walk is also periodic. Moreover, we show that redefinition of the shift operator which amounts a change in the directions in which the walker can move, may lead to PST with appropriate choices of the coin operator.

This chapter is organized as follows. In Sec. 3.1, we present quantum walks on finite graphs, namely N-lines and N-cycles, via defining two boundary conditions. We also introduce the spatial and local approaches to the definition of directions for the walker. In Sec. 3.2, we discuss the transfer of the walker between sites A and B without considering the coin state. In Sec. 3.3, we introduce the recovery operator and give a precise definition of PST for discrete-time quantum walks. In Sec. 3.4 and Sec. 3.5, we obtain the cases where PST occurs for N-lines and N-cycles

3.1 Quantum walk on finite graphs

The position Hilbert space of the quantum walk described in Sec. 2.4.1 does not necessarily be infinite and it can be restricted to a finite number of sites N by choosing appropriate conditions for boundaries. In this case, a different definition for the shift operator is required. In Fig. 3.1, two boundary conditions for the walk are presented and these are the ones that we will use throughout the article. In Fig. 3.1(a), the graph with N sites and reflecting boundaries (*N-line*) is represented. Self loops at the boundaries indicate that wave function is reflected after the shift operator is applied, similar to the approach used by Romanelli et al. for the broken links model [63]. The shift operator is of the form

$$S = |1\rangle\langle 0| \otimes |1\rangle\langle 1| + |0\rangle\langle 1| \otimes |N\rangle\langle N| +$$
$$|0\rangle\langle 0| \otimes \sum_{x=2}^{N} |x-1\rangle\langle x| + |1\rangle\langle 1| \otimes \sum_{x=1}^{N-1} |x+1\rangle\langle x|, \tag{3.1}$$

where the left (right)-going part at the first (last) site is diverted to the right (left)-going part at the same site to keep the flux conserved. Thus, the shift operator remains unitary. In Fig. 3.1(b), the graph with even N sites and periodic boundaries (*N-cycle*) is represented. Here, we simply connect the first and the last sites with one more edge.

For the walker, directions of motion can be defined in two ways. In the first one, which we shall call as *spatial approach*, the same coin state corresponds to the same spatial direction at every site. Without loss of generality, one can choose the $|0\rangle$ ($|1\rangle$) coin state to correspond the left (right) spatial direction or clockwise (anti-clockwise) rotation. In the second approach, which we shall call as *local approach*, we assign two orthogonal coin states to the two edges of every site in a self-consistent manner. The discussion here
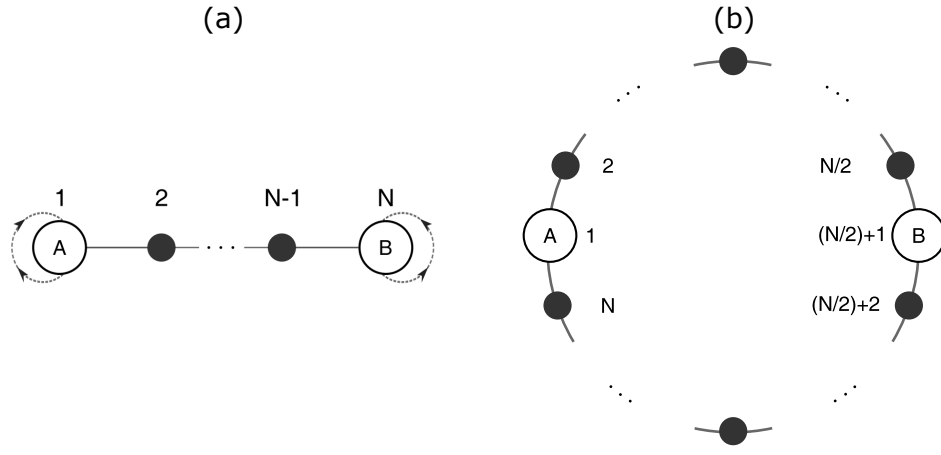
Figure 3.1: The position space where the quantum walk takes place with (a) reflecting boundary (N-line) and (b) periodic boundary (N-cycle) conditions (i.e., a 2-regular graph). Outermost sites are labeled with A and B. Site A is the initial position of the walker and site B is the position where we aim to transfer the coin state.
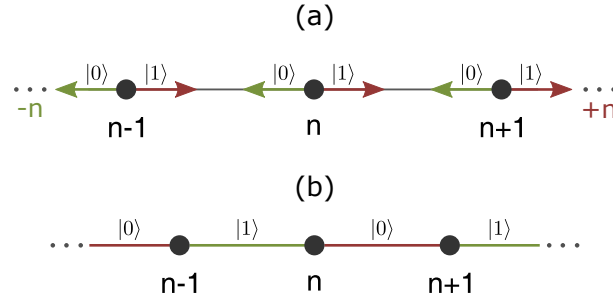
Figure 3.2: Two different approaches which specify the directions in the position space. (a) *Spatial approach*: $|0\rangle$ ($|1\rangle$) state corresponds to $-n$ ($+n$) direction for each site. (b) *Local approach*: Adjacent edges are labeled by different basis states of the coin space in a self-consistent manner. Thus, the walker found at site n takes a step towards $n+1$, and vice versa, if its coin state is $|0\rangle$.

could equivalently be done by redefining the shift operator as well. These approaches are summarized in Fig. 3.2.

A walk can start with any initial state. We will use only localized initial states of the form $|\Psi_0\rangle = |\psi_{0,n}\rangle \otimes |n\rangle$, where $|\psi_{0,n}\rangle = \alpha_{0,n}|0\rangle + \beta_{0,n}|1\rangle$ is the arbitrary initial coin state. The first and the second indices denote the number of steps and site, respectively. After t steps, the initially localized state disperses in the position space and the quantum state of the walker becomes

$$|\Psi_0\rangle \xrightarrow{U^t} |\Psi_t\rangle = \sum_x (\alpha_{t,n}|0\rangle + \beta_{t,n}|1\rangle) \otimes |n\rangle. \tag{3.2}$$

At the end of the walk, the probability of finding the walker at site n is given by summing the probabilities over the coin states

$$P_x(t) = |\alpha_{t,n}|^2 + |\beta_{t,n}|^2. \tag{3.3}$$

3.2 State revivals after limited number of steps

For classical random walks, *recurrence* is defined as the return of the walker to the origin and characterized by Pólya number [74]. In quantum walk case, the same definition is used and full-revival of the initial quantum state is not necessary [75, 76]. Here, we consider the transfer of the walker from site A to site B after limited number of steps without considering its coin state. In other words, we expect that the condition $P_B(t) = 1$ is fulfilled after t steps where t is an integer comparable with the number of graph sites.

In Fig. 3.3(a), for 4-cycle, we see that the walker appears recursively at site 3 with a period of 8 steps for 4-cycle. In Fig. 3.3(b), we also observe a recursive behaviour for 4-line but probability never reaches to 1. It means that it is impossible to transfer the walker from site 1 to 4 because $P_4(t)$ repeats itself in every 22 steps with 0.625 maxima. For 6-cycle (Fig. 3.3(c)) and 6-line (Fig. 3.3(d)), neither the walker can be transferred within the given time intervals, nor a recursive behaviour is observed. However, further analysis for long-time behaviour reveals repetitive patterns which display irregular periodicity [77]. In Fig. 3.3(e), we observe that peak values oscillate with quasi-periods of 2412 and 2698 steps. The maximum value is 0.57 and therefore transfer of the walker is impossible. In contrast, Fig. 3.3(f) demonstrates that it is quite probable (≈ 0.99) to find the walker at site 6 with quasi-periods of 6416 and 6016 steps. In this manuscript, we omit this kind of approximate transfers which appear after very large number of steps because of their unpredictability and experimental inconvenience. Instead, we consider the cases where exact transfer of the walker (e.g., Fig. 3.3(b)) is possible in a specific limited time. In Fig. 3.3, we consider the Hadamard walk only for initial coin state $|\psi_{0,A}\rangle = 1/\sqrt{2}[|0\rangle + i|1\rangle]$. For PST, we expect to obtain the same behavior for all initial coin states. Thus, we define our first criterion which we use in our numerical work for PST as follows: *For a given coin operator, the walker has to be transferred to the antipodal site of the graph after a specific number of steps for all initial coin states.* We examine coin operators whether they satisfy this criterion or not. Once this criterion is satisfied then we examine the final coin state for its similarity to the initial coin state. A precise definition for PST is given in the following section.

3.3 Recovery operator and perfect state transfer

The walker is initially localized at site A. We are interested in the perfect transfer of walker's coin state from site A to site B. For this purpose we define the *fidelity* at time t
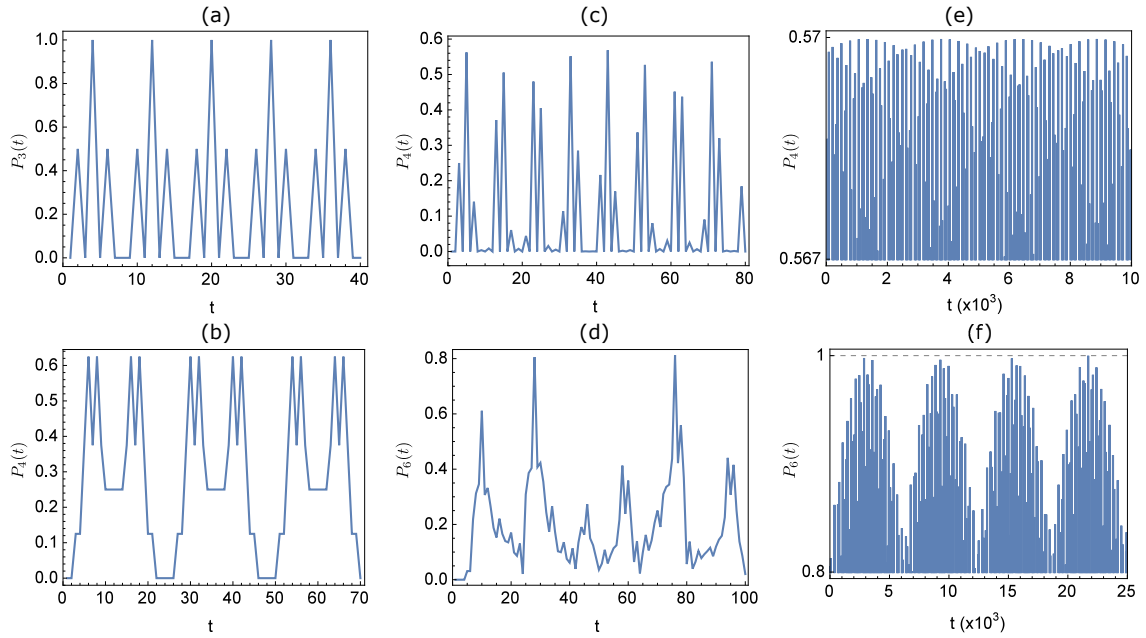
Figure 3.3: The probability of finding the walker at the antipodal site B on (a) 4-cycle, (b) 4-line, (c) 6-cycle and (d) 6-line for the Hadamard walk, $\rho = 1/2$. The initial coin state is chosen as $|\psi_{0,A}\rangle = (1/\sqrt{2})[|0\rangle + i|1\rangle]$ in each case. Long-time behaviors for (e) 6-cycle and (f) 6-line reveal the recursive behavior of the probability at site B. The lower parts of (e) and (f) are clipped.

and site B by

$$f_{t,B} = |\langle \Psi_B | \Psi_t \rangle|, \tag{3.4}$$

where $|\Psi_B\rangle = |\psi_{0,A}\rangle \otimes |B\rangle$ and $|\Psi_t\rangle$ is the quantum state of the walker at step number t. $|\psi_{0,A}\rangle$ is the coin state at $t = 0$ and site A. PST occurs if $f_{t,B} = 1$. Thus, we are looking for a class of time evolutions of the form [78]

$$|\psi_{0,A}\rangle \otimes |A\rangle \rightarrow |\psi_{0,A}\rangle \otimes |B\rangle. \tag{3.5}$$

Since we assume that our initial coin state is unknown, for a given coin operator, the required number of steps to transfer the coin state have to be the same for all $|\psi_{0,A}\rangle$'s (see the criterion in Sec. 3.2). The condition, $A = B$ and $f_{t,B} = 1$, implies that the walk is *periodic*, which means that the initial quantum state is completely recovered after t steps up to a phase constant. Periodicity has been first discussed by Travaglione and Milburn [79] for 4-cycle. They have shown the full-revival of the initial quantum state $|\Psi_0\rangle = |0\rangle \otimes |0\rangle$ after 8 steps with Hadamard coin. Later, Treggenna et al. have extended this result by showing that, except 7-cycle, all N-cycles with $N < 11$ manifest periodicity with appropriate choices of (ρ, θ, ϕ) in (2.43) for every initial coin state [43]. Dukes has analysed the periodicity of N-cycles in detail and presented the general conditions for periodicity [80]. Here, although our main aim is to achieve PST, we will also study the
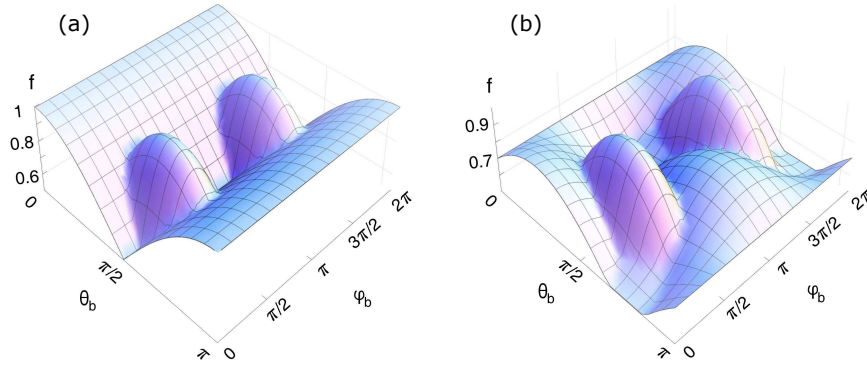
Figure 3.4: Fidelities of the initial coin states on 2-line. 1st and 2nd sites are chosen as A and B, respectively. The (θ_b, ϕ_b) plane represents the initial coin states on Bloch sphere (Fig. 2.1) and f is the maximum fidelity over time. (a) Identity coin operator is used. Independent of ϕ_b, the coin states $\theta_b = 0$ and $\theta_b = \pi$ are transferred perfectly. (b) Hadamard coin operator is used and no PST is observed within a limited time interval.

periodicity for each case under consideration. We consider a quantum walk to be periodic, if it is periodic for all initial coin states as in [43].

As we have discussed in Sec. 3.2, for a given number of steps, the walker may appear at B with probability 1. However, its coin state $(|\psi_{t,B}\rangle)$ can be different from the initial one $(|\psi_{0,A}\rangle)$. Since (2.43) includes all possible rotations for a two-dimensional coin, one can transform $|\psi_{t,B}\rangle$ to $|\psi_{0,A}\rangle$ with suitable parameters, (ρ',θ',ϕ'). Let us denote this coin operator with primed parameters as $C_R = C' \otimes I$ (*recovery operator*) to distinguish it from the one which governs the walk. Since the initial coin state is unknown, recovery operator have to be independent of the initial coin state. We define this condition as our second criterion for PST as follows: *For a given coin operator and graph, there should be only one recovery operator which transforms the final coin state to the initial coin state.* In Sec. 3.4 and 3.5, we show that all cases which satisfy the first criterion (in Sec. 3.2) also satisfy the second one. Thus, once we decide on the coin operator which we will use for the walk, we can also determine the recovery operator which will be applied at the end of the walk to achieve PST. This PST scheme can be summarized as

$$|\psi_{0,A}\rangle \otimes |A\rangle \xrightarrow{U^t} |\psi_{t,B}\rangle \otimes |B\rangle \xrightarrow{C_R} |\psi_{0,A}\rangle \otimes |B\rangle. \tag{3.6}$$

In our calculations, A and B are chosen as the outermost sites on the graph. These are 1st and Nth sites for the N-line, 1st and $(\frac{N}{2} + 1)$th sites for the N-cycle with even N, respectively. We do not analyse N-cycles with odd N for PST, since we cannot assign a unique A and B pair. First we have numerically determined all cases where the walker is found with probability 1 at B for all coin states (the first criterion) by scanning whole Bloch sphere shown in Fig. 2.1. We have restricted the graph size to $N < 11$ if $\rho \neq 1$. Without loss of generality, we have also restricted the coin operator to $\phi = 0$ [43]. Then,

Table 3.1: For the 2-line, these are the cases where the walker is found with probability 1. The other parameters of the coin operator are chosen as $\theta = \phi = 0$.

ρ	Steps (t)	Site (n)	Coin state
$\frac{1}{4}$	6	2	$-\beta|0\rangle + \alpha|1\rangle$
	12	1	$|\psi_{0,1}\rangle$
$\frac{1}{2}$	4	2	$-\beta|0\rangle + \alpha|1\rangle$
	8	1	$|\psi_{0,1}\rangle$
$\frac{3}{4}$	6	1	$|\psi_{0,1}\rangle$

we have analytically studied these cases for their aptness to periodicity and PST (the second criterion), by using (2.53).

For PST, without any knowledge about the initial coin state, one should be able to transfer all coin states with $f_{t,B} = 1$. However, an arbitrary coin operator and an arbitrary graph do not provide quantum walks which allow PST in general. In Fig. 3.4, two specific examples are demonstrated. These are the numerical analyses of fidelity distributions over initial coin states for 2-line. In Fig. 3.4(a), it can be seen that only limited number of initial coin states are transferred perfectly for identity coin operator. In Fig. 3.4(b), Hadamard coin is used and there is no PST at all. Further analysis for the other coin operators and graphs give similar results except the 4-cycle which will be explained in Sec. 3.5.

3.4 Perfect state transfer on N-lines

Case: $\rho \neq 1$

In Table 3.1, the cases where the walker is found with probability 1 on the 2-line are given. The cases with coin state $|\psi_{0,1}\rangle$ manifest periodicity. To achieve a PST, we consider the other cases where the total state is

$$|\Psi_t\rangle = [-\beta|0\rangle + \alpha|1\rangle] \otimes |2\rangle. \tag{3.7}$$

After t steps, we apply appropriate recovery operator, $(\rho', \theta', \phi') = (0, 0, -\pi)$, on (3.7). In this way, we obtain the initial coin state and hence PST. Overall process can be written as

$$|\psi_{0,1}\rangle \otimes |1\rangle \xrightarrow{\mathbf{C}_R \mathbf{U}^t} |\psi_{0,1}\rangle \otimes |2\rangle. \tag{3.8}$$

Thus, any coin state can be transferred on 2-line perfectly with appropriate (ρ, t) values given in Table 3.1. We note that recovery operator is constant for a given coin operator and it provides PST for all initial coin states. In each PST case, the quantum walk is periodic. For example, after 4 steps of the walk with $\rho = 1/2$, if the walker proceeds 4 more steps, the initial quantum state is recovered. There is also a case with $\rho = 3/4$, where 2-line is periodic but it does not lead to PST. PST requires the total state to localize more than one sites in turn and this process naturally gives rise to periodicity.

After applying the recovery operator, we initialize the walker with the initial coin state at a different site. For example, when $\rho = 1/2$, if the walker is acted on by sequence of operations, such as $C_R U^4 C_R U^4$, it will be initialized on sites 1 and 2 alternatingly. The sequence of initializations which keeps the initial coin state unchanged, suggest us to define a new classification for discrete-time quantum walks which we call *n-periodicity*. We can define one step of the walk for the example above as $U' = C_R U^4$. Then, after each step, coin state will be conserved and the only change will occur in the position space. In other words, U' is same as that of $I \otimes (|2\rangle\langle 1| + |1\rangle\langle 2|)$. Since the walker is localized on two sites in an alternating manner, the quantum walk under consideration becomes 2-periodic. In general, the number n gives the total number of sites where initial coin state is localized during the time evolution. If quantum walk is periodic, we will call it 1-periodic, i.e., well-known periodicity concept becomes a member of the general n-periodicity class. Thus, N-line or N-cycle allow maximum N-periodicity. This definition is useful because it generalizes the periodicity definition so that it includes the PST too.

For $\rho \neq 1$, reflecting boundaries ensure that there will always be a non-zero probability for finding the walker at A, independent of t, if there is no destructive interference. However, the dimension of the position space for 2-line allows the wave function to vanish at A and gives rise to the cases given in Table 3.1.

Case: $\rho = 1$

When we restrict the coin operators to $\rho = 1$, independent of the initial coin state, the walker is transferred from A to B and B to A at intervals of N steps for all N-lines. In general, the walker is at the position B or A if $t = N(2l - 1)$ or $t = 2Nl$ steps are taken, respectively. Here, $l \in \mathcal{Z}^+$ specifies the number of "one-way trips" of the walker within the graph. In order to find the coin state of the walker at t, we have derived the total quantum states

$$|\Psi_{N(2l-1)}\rangle = e^{i(l-1)\Theta}[-\beta e^{i(\theta+\phi)}|0\rangle + \alpha|1\rangle] \otimes |N\rangle, \qquad (3.9)$$

$$|\Psi_{2Nl}\rangle = e^{il\Theta}[\alpha|0\rangle + \beta|1\rangle] \otimes |1\rangle, \tag{3.10}$$

where $\Theta(\theta, \phi, N) = (\theta + \phi)N + \mu\pi$ and θ, ϕ are the parameters of the coin operator. Here, μ is a function which adds the phase π for odd N and it can be defined as $\mu(N) = [1-(-1)^N]/2$. It is shown in (3.10) that the total state is periodically localized at opposite sites which agrees with the numerical results. Furthermore, the walk is periodic with a period of $2Nl$ steps up to an overall phase. After N steps, we apply recovery operator $(\rho', \theta', \phi') = (0, 0, -\theta - \phi - \pi)$ for PST. Recovery operator is a function of θ and ϕ which means that for all coin operators with $\rho = 1$, there is always a corresponding recovery operator. Hence, step operator $U' = C_R U^N$ makes N-line 2-periodic for $\rho = 1$.

3.5 Perfect state transfer on N-cycles

Case: $\rho \neq 1$

For 2-cycle, full evolution can simply be written in matrix form as

$$\mathbf{U}^t \leftrightarrow \begin{pmatrix} \sqrt{\rho} & \sqrt{1-\rho}e^{i\theta} \\ \sqrt{1-\rho}e^{i\phi} & -\sqrt{\rho}e^{i(\theta+\phi)} \end{pmatrix}^t \otimes \begin{pmatrix} 0 & 1 \\ 1 & 0 \end{pmatrix}^t. \tag{3.11}$$

In (3.11), we see that, shift operator swaps the position of the walker independent of its coin state. At $t = 1$, the total state becomes

$$|\Psi_1\rangle = \left[(\alpha\sqrt{\rho} + \beta\sqrt{1-\rho}e^{i\theta})|0\rangle + (\alpha\sqrt{1-\rho}e^{i\phi} - \beta\sqrt{\rho}e^{i(\theta+\phi)})|1\rangle\right] \otimes |2\rangle \tag{3.12}$$

Since the coin operator is unitary, $C_R = C^\dagger \otimes I$ leads to PST after first step. If we define one-step as $U' = (C^\dagger \otimes I)S(C \otimes I)$, quantum walk becomes 2-periodic and it keeps the initial coin state unchanged. In other words, the initial coin state bounces back and forth between two sites. In contrast to 2-line, 2-cycle allows PST for all coin operators with the aid of appropriate recovery operators. We note that, if we choose $\theta = \phi = 0$, without any recovery operator, the walk is naturally periodic with a period of 2 steps for $\rho \in [0, 1]$ which generalizes the $\rho = 1/2$ condition in Ref. [43].

A special case for PST on circles is the 4-cycle. In this case, we achieve PST by using well-known Hadamard coin operator (in 4 steps) or the biased coin operator $\rho = 1/4$ (in 6 steps) without any recovery operators. These results are given in table 3.2 and Fig. 3.5. We see that for each PST case the walk is also periodic. In Ref. [43], it has been already shown that 4-cycle has a period of 8 steps for $\rho = 1/2$. We extend this result by showing

Table 3.2: For the 4-cycle, these are the cases where the walker is found with probability 1. The other parameters of coin operator are chosen as $\theta = \phi = 0$. The overall phase $e^{i\pi}$ for $\rho = 1/2$ appears if $\theta = \pi$.

ρ	Steps (t)	Site (n)	Coin state
$\frac{1}{4}$	6	3	$\lvert\psi_{0,1}\rangle$
	12	1	$\lvert\psi_{0,1}\rangle$
$\frac{1}{2}$	4	3	$(e^{i\pi})\lvert\psi_{0,1}\rangle$
	8	1	$\lvert\psi_{0,1}\rangle$
$\frac{3}{4}$	6	1	$\lvert\psi_{0,1}\rangle$

that it also has a period of 12 steps for $\rho = 1/4$ and period of 6 steps for $\rho = 3/4$.

$(\alpha\lvert0\rangle + \beta\lvert1\rangle) \otimes \lvert1\rangle$ $(\alpha\lvert0\rangle + \beta\lvert1\rangle) \otimes \lvert3\rangle$
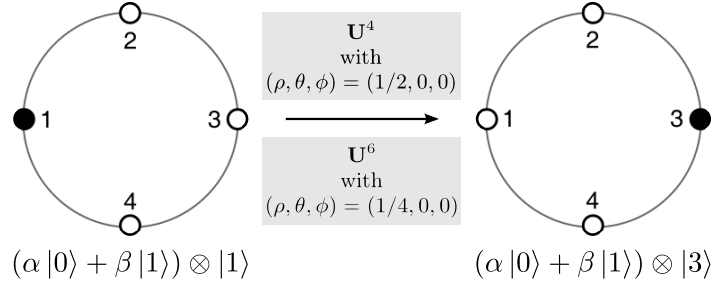
Figure 3.5: PST on 4-cycle. This is the only case where discrete-time quantum walk allows PST with Hadamard coin operator or with a biased coin, $\rho = 1/4$, without any recovery operators. Black and hollow dots indicate $P_n(t) = 1$ and $P_n(t) = 0$, respectively.

Case: $\rho = 1$

Now, we consider the N-cycles with even N and $\theta, \phi \neq 0$. Since the coin operator is diagonal, $\lvert0\rangle$ and $\lvert1\rangle$ terms do not mix, and generate propagations in opposite directions. After $N/2$ steps, we find the walker at B with probability 1. We note that the coin operator adds the phase $e^{i(\theta+\phi+\pi)}$ to the coefficient of $\lvert1\rangle$ in each step. Thus, after $N/2$ steps, the total state becomes

$$\lvert\Psi_{N/2}\rangle = (\alpha\lvert0\rangle + \beta e^{i\frac{N\Theta}{2}}\lvert1\rangle) \otimes \lvert\tfrac{N}{2}+1\rangle, \tag{3.13}$$

where $\Theta = \theta + \phi + \pi$. Without loss of generality, one can choose $\theta' = 0$ and use the recovery operator $(\rho', \theta', \phi') = (1, 0, -[N\Theta/2] + \pi)$ to achieve PST. The step operator $U' = C_R U^{N/2}$ makes the walk 2-periodic. If N is odd, wave function does not localize at any site except the initial one. The total state after N steps is

$$\lvert\Psi_N\rangle = (\alpha\lvert0\rangle + \beta e^{iN\Theta}\lvert1\rangle) \otimes \lvert1\rangle. \tag{3.14}$$

Appropriate choice for the recovery operator can be given as $(\rho', \theta', \phi') = (1, 0, -N\Theta + \pi)$ at $t = N$. The step operator $U' = C_R U^N$ makes the walk 1-periodic.

We have shown that the coin operator which is restricted to $\rho = 1$ allows PST on N-cycles. Although, it has not been indicated in the discussion about N-cycles above, spatial approach has been used intrinsically, i.e., clockwise rotations correspond to $|1\rangle$. If the walk is driven by the coin operator $(\rho, \theta, \phi) = (0, 0, 0)$ (the flip coin operator), we define the directions with the local approach for PST (see Fig. 3.2). When N is odd, N-cycle is ill-defined since we have to label at least two edges with the same basis state. Therefore, we consider N-cycles with even N only. If we label all edges as in Fig. 3.2(b), after $N/2$ steps, the total state becomes

$$L_{ij} = \begin{cases} |\psi_{0,in}\rangle \otimes |\frac{N}{2} + 1\rangle & \text{for even } N/2, \\ \alpha e^{i\phi}|0\rangle + \beta e^{i\theta}|1\rangle) \otimes |\frac{N}{2} + 1\rangle & \text{for odd } N/2. \end{cases} \quad (3.15)$$

Both case have the overall phase $e^{i\lfloor N/4 \rfloor(\theta + \phi)}$ where $\lfloor \rfloor$ is the floor function. The first case shows that PST is achieved after $N/2$ steps. Also, it is clear that we can use $(\rho', \theta', \phi') = (0, -\phi, -\theta)$ to recover the second case and make the walk periodic. However, N-lines do not have the same property, i.e., PST is not possible if we use flip coin operator with local approach. We can demonstrate this fact by evaluating the first two steps as follows:

$$|\Psi_0\rangle = \alpha|0, 1\rangle + \beta|1, 1\rangle \xrightarrow{\mathbf{U}} \alpha|0, 1\rangle + \beta|1, 2\rangle \xrightarrow{\mathbf{U}} \alpha|0, 1\rangle + \beta|1, 3\rangle \xrightarrow{\mathbf{U}} \cdots \quad (3.16)$$

where U involves the flip coin operator. We see that after each step, the first term in the summation is stuck at site 1 because of the reflecting boundary. For an N-line, after N steps, the second term will be stuck at site N as well. Thus, neither PST nor periodicity is possible.

Chapter 4

COHERENT TRANSPORT OVER EXPLOSIVE PERCOLATION LATTICES

Coherent transport over complex networks has been a topic of much interest in the recent years [81]. Such processes are often related with the dynamics of excitations over networks modeled by quantum walks and studied for both variants, namely the discrete-[3, 82–88] and the continuous-time [89–96] quantum walks. Although the original proposals [2, 5] of either models are mainly aimed to outperform their classical counterparts in terms of spreading rates, it has been shown later that quantum walks are useful tools also for developing new quantum algorithms [6], quantum simulations [12–14, 97, 98] and the universal quantum computation [11]. In the context of coherent transport, they provide simple models to describe quite significant physical phenomena such as the excitonic energy transfer through the photosynthetic light-harvesting complexes [17] or breakdown of an electron system driven by strong electric fields [16].

It is possible to introduce a disorder to a network using the standard percolation model [99] in which the bonds between sites are either present or missing with some probability p. A group of connected sites is called a cluster and its size is defined by the number of these sites in total. For an infinite network, if p is smaller than some critical value p_c (the percolation threshold), there exist small and discrete clusters. However, if $p > p_c$, small clusters start merging into larger ones and eventually form a single large cluster comparable to the network in size. This kind of disorder constitutes a source of decoherence for quantum walks and appears in two variants: the static and dynamic percolations. In the former, the network configuration does not change during propagation, whereas in the latter, connections between sites do alter in time. Both variants have extensively been studied so far in the context of transport and spreading properties for discrete- and continuous-time quantum walks [63, 100–108].

Achlioptas *et al.* proposed a new percolation model for network construction by slightly changing the standard one [109]. According to this model, two bond candidates

are randomly selected each time a new bond is intended to be added. Then, the one leading to a smaller cluster size is placed as a new bond and the other one is eliminated. This simple selection rule suppresses the growth of the largest cluster but eventually results in the abrupt (or so-called *explosive*) growth of the largest cluster. In contrast with the standard percolation, the network configuration for a given p depends on the total previous occupation history. In this sense, the disorder due to explosive percolation cannot be considered as a fully random process but rather a correlated one.

In this chapter, we are interested in the transport of an excitation along a certain direction over a square lattice where the bond configuration is determined by explosive percolation statically. We therefore introduce the sites on the left edge of the lattice as sources and the ones on the right as sinks, where an excitation is created and absorbed, respectively [105]. In this way, we monitor the survival probability over the lattice in the long time limit to find out the transport efficiency after starting with an initial state localized on the source sites. In modeling the transport, we use the continuous-time quantum walk which is also closely related with the tight-binding models in solid state physics. We compare the transport efficiencies with increasing bond fraction for standard and explosive percolation models to find out whether any model has supremacy over the other.

This chapter is organized as follows. In Sec. 4.1, we overview coherent and incoherent transport over dissipative lattices along with the description of percolation models to be used. In Sec. 4.2.1, we compare the efficiencies of transport models in case of standard and explosive percolation disorders. In Sec. 4.2.2, we investigate the spreading of eigenstates.

4.1 Methods

4.1.1 Coherent and incoherent transport

We consider a square lattice of N sites, which we will denote by $L = \sqrt{N}$, as the environment where the transport process takes place. The sites are labeled by positive integers $\mathcal{N} = \{1, 2, \ldots, N\}$. The information about the existence of bonds in between is held by the Laplacian matrix L where the non-diagonal elements L_{ij} are -1 if site i and site j are connected and zero otherwise. The diagonal elements L_{ii} hold the total number of bonds that belong to the site i. Thus, L is a positive semi-definite matrix, i.e., its eigenvalues are non-negative. An excitation localized on any site i is interpreted as being in the state $|i\rangle$ and these states form an orthonormal and complete set over all sites, i.e., $\langle k|j\rangle = \delta_{kj}$ and $\sum_{i \in \mathcal{N}} |i\rangle\langle i| = I$. A coherent (incoherent) transport is modeled by continuous-time

quantum (random) walk which is described by the Hamiltonian (transfer matrix) $H_0 = L$ ($T_0 = -L$) [5, 81]. Here, we assume that transition rates are identical and equal to 1 for all sites. The transition probability from the initial state $|\psi_j\rangle$ at $t = 0$ to the state $|\psi_k\rangle$ is $p_{kj}(t) = \langle\psi_k| \exp(T_0 t)|\psi_j\rangle$ for the incoherent and $\pi_{kj}(t) = |\langle\psi_k| \exp(-iH_0 t)|\psi_j\rangle|^2$ for the coherent transport, where we assumed $\hbar = 1$.

Once an excitation covers the lattice from one side to another, we understand that it did get transported over the lattice. In order to keep track of this process, we define the sites at the left (right) edge of the lattice as the sources (sinks) as in Fig. 4.1 [105]. We will denote the set of all source and sink sites by $\mathcal{S}$ and $\mathcal{S}'$, respectively. Sources are the only sites where an excitation can initially be localized and the sinks are abstract representations of absorption or trapping processes. Thus, a 'leak' taking place on the right edge implies that an excitation, originally localized on the left edge, has been transported along the lattice. This process can be introduced by a projection operator $\Gamma = \sum_{k\in\mathcal{S}'} |k\rangle\langle k|$ perturbing the Hamiltonian $H = H_0 - i\Gamma$ or the transfer matrix $T = T_0 - \Gamma$ where we choose the leaking rates to be the same and equal to 1 for all sink sites. In the limit $t \to \infty$ and for the initial state $|\psi_j\rangle$, the total probability of finding the excitation on the lattice, namely the survival probabilities for coherent and incoherent transports are given as,

$$\Pi_j^\infty = \sum_l |\langle\psi_j|\Phi_l^R\rangle|^2, \quad P_j^\infty = \sum_{k\in\mathcal{N}}\sum_l \langle k|\phi_l^0\rangle\langle\phi_l^0|\psi_j\rangle, \tag{4.1}$$

where $|\Phi_l^R\rangle$ and $|\phi_l^0\rangle$ are the eigenstates of H and T with real and zero eigenvalues, respectively. The initial state $|\psi_j\rangle$ may involve sites only from the set $\mathcal{S}$. In this chapter, we will denote the complement of survival probabilities by μ which can equally be interpreted as the transport efficiency [110] or the percolation probability [86]. By calculating μ, we will monitor how much information may escape from the lattice.

4.1.2 Calculation of survival probabilities

We calculate the survival probability after starting with the initial state $|\psi_j\rangle$ by summing the transition probabilities over all lattice sites as

$$\Pi_j = \sum_{k\in\mathcal{N}} \pi_{kj}(t) = \sum_{k\in\mathcal{N}} \langle\psi_j|e^{iH^\dagger t}|k\rangle\langle k|e^{-iHt}|\psi_j\rangle$$
$$= \langle\psi_j|e^{iH^\dagger t}e^{-iHt}|\psi_j\rangle. \tag{4.2}$$

The Hamiltonian $H = H_0 - i\Gamma$ is non-Hermitian and it has N complex eigenvalues $E_l = \epsilon_l - i\gamma_l$ and $E_l^* = \epsilon_l + i\gamma_l$ with respective left $|\Phi_l\rangle$ and right $\langle\tilde{\Phi}_l|$ eigenstates. These eigenstates can be taken as biorthonormal [111] $\langle\tilde{\Phi}_l|\Phi_{l'}\rangle = \delta_{ll'}$ and complete

$\sum_{l=1}^{N} |\Phi_l\rangle\langle\tilde{\Phi}_l| = I$. Also, they satisfy $\langle k|\Phi_l\rangle^* = \langle\tilde{\Phi}_l|k\rangle$. Therefore, Eq. (4.2) becomes,

$$\Pi_j = \sum_{ll'=1}^{N} \langle\psi_j|\Phi_l\rangle\langle\tilde{\Phi}_l|e^{iH^\dagger t}e^{-iHt}|\Phi_{l'}\rangle\langle\tilde{\Phi}_{l'}|\psi_j\rangle. \tag{4.3}$$

By using the following identities,

$$e^{-iHt}|\Phi_{l'}\rangle = e^{-i\epsilon_{l'}t}e^{-\gamma_{l'}t}|\Phi_{l'}\rangle,$$
$$\langle\tilde{\Phi}_l|e^{iH^\dagger t} = \langle\tilde{\Phi}_l|e^{i\epsilon_l t}e^{-\gamma_l t}, \tag{4.4}$$

Eq. (4.3) becomes,

$$\Pi_j = \sum_{ll'=1}^{N} \langle\psi_j|\Phi_l\rangle\langle\tilde{\Phi}_l|\Phi_{l'}\rangle\langle\tilde{\Phi}_{l'}|\psi_j\rangle e^{i\epsilon_l t}e^{-\gamma_l t}e^{-i\epsilon_{l'}t}e^{-\gamma_{l'}t}$$
$$= \sum_{l=1}^{N} e^{-2\gamma_l t}\langle\psi_j|\Phi_l\rangle\langle\tilde{\Phi}_l|\psi_j\rangle = \sum_{l=1}^{N} e^{-2\gamma_l t}|\langle\psi_j|\Phi_l\rangle|^2 \tag{4.5}$$

This provides information on how an excitation decays over the lattice in time. In the limit $t \to \infty$, we expect Π_j to decay exponentially because of the imaginary parts γ_l if the lattice is fully connected. However, when some bonds in the lattice are broken, there exist non imaginary eigenvalues which results in $\lim_{t\to\infty} \Pi_j(t) \neq 0$. Therefore, in Eq. 4.5 only the terms with $\gamma_l = 0$ may remain and we obtain,

$$\Pi_j^\infty = \lim_{t\to\infty} \Pi_j(t) = \sum_{\{l|E_l\in\mathbb{R}\}} |\langle\psi_j|\Phi_l\rangle|^2. \tag{4.6}$$

If we choose an initial state $|\psi_j\rangle = \frac{1}{\sqrt{L}}\sum_{i\in S} |i\rangle$ which is a superposition of L sites from the set S, Eq. (4.6) becomes,

$$\Pi_S^\infty = \frac{1}{L} \sum_{\{l|E_l\in\mathbb{R}\}} \left|\sum_{i\in S} \langle i|\Phi_l\rangle\right|^2 \tag{4.7}$$

Similarly, we can calculate the survival probability for the incoherent transport as

$$P_j = \sum_{k\in\mathcal{N}} \langle k|e^{Tt}|\psi_j\rangle = \sum_l \sum_{k\in\mathcal{N}} e^{-\lambda_l t}\langle k|\phi_l\rangle\langle\phi_l|\psi_j\rangle. \tag{4.8}$$

where $-\lambda_l$ and $|\phi_l\rangle$ are the eigenvalues and the corresponding eigenstates of the transfer matrix $T = T_0 - \Gamma$. In the $t \to \infty$ limit, only the terms with $\lambda_l = 0$ survive. Therefore, Eq. (4.8) becomes

$$P_j^\infty = \sum_{\{l|\lambda_l=0\}} \sum_{k\in\mathcal{N}} \langle k|\phi_l\rangle\langle\phi_l|\psi_j\rangle \tag{4.9}$$
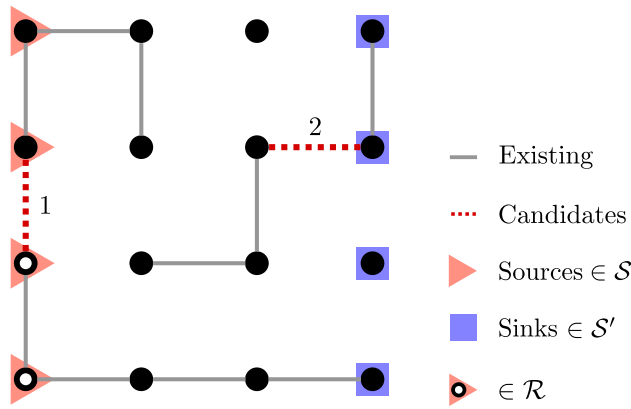
Figure 4.1: An example of a bond percolation lattice for $L = 4$. Left (right) edge contains source (sink) sites where an excitation occurs (is absorbed). Dashed lines represent two randomly selected bond candidates labeled by 1 and 2 with corresponding weights $w_1 = 4 \times 5 = 20$ and $w_2 = 2 \times 3 = 6$. According to the best-of-two rule, bond 2 will be selected and bond 1 discarded for $w_2 < w_1$. A wrapping cluster is defined to be the one connecting the left edge to the right edge. For this example, it lies along the bottom edge of the lattice and occupies two source sites.

Then, the initial state $|\psi_j\rangle = \frac{1}{L} \sum_{i \in \mathcal{S}} |i\rangle$ yields,

$$P_{\mathcal{S}}^{\infty} = \frac{1}{L} \sum_{\{l | \lambda_l = 0\}} \sum_{k \in \mathcal{N}} \langle k | \phi_l \rangle \left(\sum_{i \in \mathcal{S}} \langle \phi_l | i \rangle \right). \tag{4.10}$$

4.1.3 Explosive percolation

The standard bond percolation is implemented on a square lattice by first removing all bonds between the sites and then, randomly adding them one after another. This process results in random growth of discrete clusters. For infinite lattices, the opposite borders get connected to each other through one large wrapping cluster after reaching a critical fraction of bonds $p_c = 0.5$ [112] called the percolation threshold. Here, the bond fraction p is defined as the ratio of the number of bonds present in lattice to the number of total possible bonds, $p = n/(2L^2 - L)$.

In explosive percolation, a similar implementation procedure is followed with slight modification. Now, in order to add a bond, m random bond candidates are chosen and a weight is assigned to each of them equal to the product of cluster sizes they may potentially merge. Then, the bond with smallest weight is occupied and the others are discarded (see Fig. 4.1). In case a bond connects two sites within the same cluster, the corresponding weight becomes the square of the cluster size. We will see later that this complementary rule has drastic effects on the results we obtain. This selection rule here, called the *best-of-m product rule* [113, 114], systematically suppresses the merging of small discrete

clusters and consequently avoids the formation of a giant cluster up to some percolation threshold p_c dependent on m [115, 116]. Once the threshold is exceeded, finite discrete clusters start joining each other much faster than in standard percolation ($m = 1$) and finally, this results in an explosive behavior in the growth of the largest cluster. In particular, $m = 2$ corresponds to the Achlioptas *et al.* model [109].

For $m > 1$, discrete clusters cannot grow in a completely random manner as in standard percolation case. The shape and size of a given cluster becomes somewhat correlated with those of other clusters during the growth process. In this context, we interpret m as the correlation strength since it specifies the number of discrete clusters taken into account while deciding to add a new bond. We examine the behavior of transport processes for lattices built by using different m values.

Lastly, we note that a transport process can only take place after a wrapping cluster is formed. In infinite lattices, this happens just after $p = p_c$. In finite lattices, however, there is still a chance of having no wrapping clusters when $p > p_c$ and, indeed, having one for $p < p_c$. Consequently, the efficiency of the transport inevitably gets affected by these finite-size effects.

4.2 Numerical results

We numerically determined all eigenvalues and corresponding eigenvectors of H and T for each lattice realization to calculate Π_j^∞ and P_j^∞ in Eq. (4.1). It is clear that these quantities depend sensitively on the total number of real and zero eigenvalues. For this reason, we carefully compared numerical eigenvalues with the exact ones for different lattice sizes and concluded that $L = 7$ is the optimal one where there is one-to-one correspondence between the exact and numerical results provided that numerical values smaller than 1.0×10^{-14} are set to zero. In order to obtain notable quantities for the above mentioned static percolation models, we averaged our results over 4×10^3 lattice realizations for each p. From now on, $\langle \ldots \rangle$ will be used to indicate the ensemble averaged quantities we have obtained.

4.2.1 Transport efficiency

We choose an initial state which is equiprobably distributed over the source sites as $|\psi_j\rangle \equiv |\Psi_\mathcal{S}\rangle = \kappa \sum_{i \in \mathcal{S}} |i\rangle$ where $\kappa = L^{-1/2}$ for the coherent transport and $\kappa = L^{-1}$ for the incoherent transport. This state represents our lack of knowledge about the exact position of the excitation at $t = 0$. In the limit $t \to \infty$, we define the average transport efficiencies
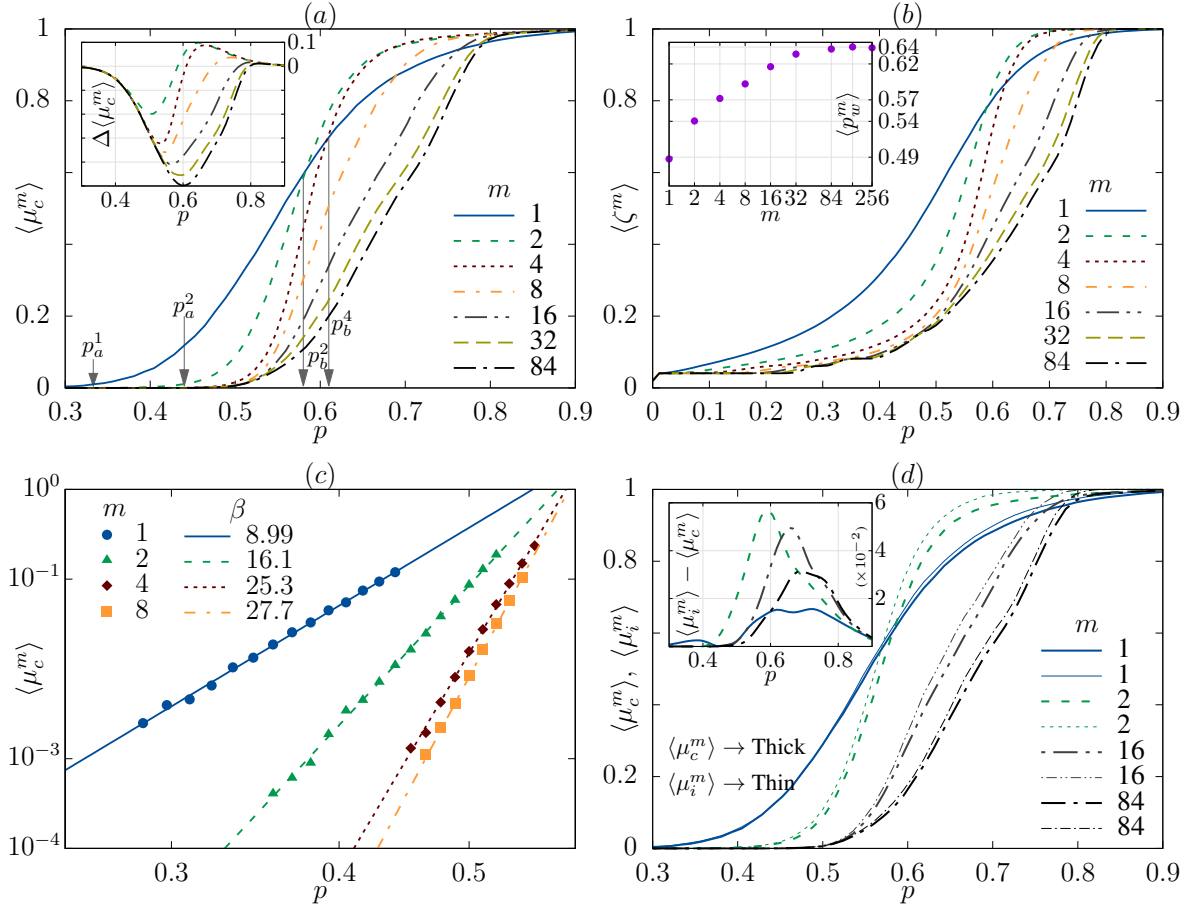
Figure 4.2: (a) The average transport efficiency of coherent transport $\langle \mu_c^m \rangle = 1 - \langle \Pi_{\mathcal{S}}^{\infty,m} \rangle$ vs. bond fraction p for different correlation strengths m after starting with the initial state $|\psi_{\mathcal{S}}\rangle$. The standard percolation and Achlioptas *et al.* models [109] correspond to $m = 1$ and $m = 2$, respectively. The inset represents the comparison of $m = 1$ and $m > 1$, namely $\Delta \langle \mu_c^m \rangle = \langle \mu_c^1 \rangle - \langle \mu_c^{m>1} \rangle$. (b) The average ratio of number of sites in the largest cluster to total number of sites $\langle \zeta^m \rangle$. The inset represents the average bond fraction of having a wrapping cluster $\langle p_w^m \rangle$ for different m values, which are also represented in Table 4.1. The m axis is drawn in the logarithmic scale. (c) The initial growth rate of $\langle \mu_c^m \rangle$ which obeys a power law such that $\langle \mu_c^m \rangle = 10^\alpha |p - p_s^m|^\beta$ for $m \leqslant 8$. The axes are drawn in logarithmic scale. (d) Comparison of the transport efficiencies of coherent and incoherent transports. The inset shows the differences between the efficiencies of incoherent and coherent transports.
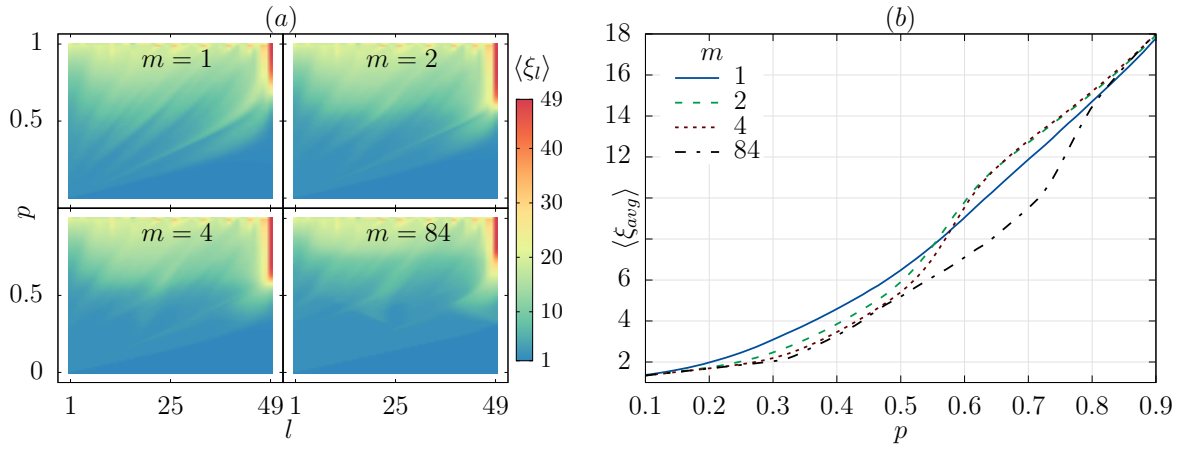
Figure 4.3: (a) The participation ratios $\xi_l(p)$ of each eigenstate $|\Phi_l^0\rangle$ of the Hamiltonian H_0 with respect to the fraction of bonds p in the lattice. (b) The participation ratios averaged over different eigenstates for a given p.

for a given bond fraction p and correlation strength m as

$$\langle \mu_c^m(p) \rangle \equiv 1 - \langle \Pi_{\mathcal{S}}^{\infty,m}(p) \rangle, \quad \langle \mu_i^m(p) \rangle \equiv 1 - \langle P_{\mathcal{S}}^{\infty,m}(p) \rangle, \tag{4.11}$$

for coherent and incoherent transports, respectively. These quantities are the average probabilities for the excitation to be trapped in the limit $t \to \infty$. We will use the superscript m for labeling purposes through the rest of this chapter. Let us also define p_a^m here as the minimum bond percentage which satisfies $\langle \mu_c^m \rangle \geqslant 0.01$ [86] in order to determine the effective starting point of the coherent transport.

In Fig. 4.2(a) the change in $\langle \mu_c^m \rangle$ is plotted with respect to p. The differences $\Delta \langle \mu_c^m \rangle \equiv \langle \mu_c^1 \rangle - \langle \mu_c^{m>1} \rangle$ between the efficiency of the case $m = 1$ and the efficiencies of the cases with larger m are given in its inset. We see that when $m > 1$, we obtain transports with partially higher efficiencies than that of the $m = 1$ once p exceeds certain values denoted by p_b^m. Additionally, p_a^m increases and gets fixed for $m \geqslant 8$ (see Table 4.1). The case $m = 2$ starts to overcome $m = 1$ at $p_b^2 = 0.58$ and the maximum peak occurs at $p = 0.64$ where $\Delta \langle p_c^m \rangle \approx 0.1$. Actually, this is the extreme case among the

Table 4.1: Numerical values of some important parameters related to m.

m	p_a^m	p_b^m	$\langle \mu_c(p_b^m) \rangle$	α^m	β^m	$\langle p_w^m \rangle$
1	0.33	n/a	n/a	2.3	9.0	0.49
2	0.44	0.58	0.61	3.8	16	0.54
4	0.50	0.61	0.69	5.8	25	0.57
8	0.51	0.69	0.87	6.3	28	0.59
16	0.51	0.76	0.94	n/a	n/a	0.62
32	0.51	0.80	0.96	n/a	n/a	0.63
84	0.51	0.81	0.97	n/a	n/a	0.64

others, i.e., a two-by-two correlation between discrete clusters contributes the most to the transport efficiency here unlike the rest of the cases. For increasing values of m following $m = 2$, the positive peak of $\Delta\langle\mu_c\rangle$ decreases in contrast with its increasing negative peak and p_b^m shifts towards higher bond percentages. When $m = 84$, there is almost no contribution to the transport efficiency: $\langle\mu_c^{84}\rangle$ can barely exceed the $\langle\mu_c^1\rangle$ after $p_b^{84} = 0.809$. It is therefore evident that higher correlation strengths are increasingly inhibiting the transport process.

In Fig. 4.2(b), size of the largest cluster $\langle\zeta^m\rangle$ with respect to p is given. The inset shows the bond fractions $\langle p_w^m\rangle$ where a wrapping cluster is formed on average. When $p < 0.5$, although $\langle\zeta^m\rangle$ reduces with increasing m, it tends to remain almost the same for $m > 8$ where there is no significant change also in $\langle p_w^m\rangle$. This result actually explains the behavior of p_m^a in Fig. 4.2(a): The bond fractions p_a^m where coherent transport effectively starts are directly related with the size of the largest cluster and average wrapping probability at p_a^m. When $p > 0.5$, the ζ^m decreases for higher m values which is very similar with the behavior of μ_c^m. Also, the p_b^m appear to be very close to the bond fractions where $\langle\zeta^{m>2} \approx \zeta^1\rangle$. Therefore, the comparison of Fig. 4.2(a) and (b) strongly suggests that independent of m, the transport efficiency is determined by the size of the largest cluster.

Our choice of $m = 84$ as an upper limit for this chapter is intentional. There can be maximum 84 bonds in the lattice in total, and hence, all discrete clusters most probably get correlated with each other as the lattice gets filled with bonds. We have done the calculations also for $m > 84$ and obtained quite similar results with the $m = 84$ case. Therefore, it can be considered as an upper limit and the transport properties do not change thereafter.

When we again look at Fig. 4.2(a), we see that the behavior of each $\langle\mu_c^m\rangle$ can be examined in three successive regions: (i) An initial power-law-like growth in the vicinity of p_a^m, (ii) an approximately linear behavior and (iii) saturation. In order to quantify the growth rate in region (i), let us assume that transport process starts at some $p = p_s^m$ on average where $p_s^m \lesssim p_a^m$. In Fig. 4.2(c), we see that $\langle\mu_c^m\rangle$ obeys a power law such that $\langle\mu_c^m\rangle = 10^\alpha(p - p_s^m)^\beta$ for $p > p_s^m$. The α^m and β^m can be found in Table 4.1 for different m values. We see that the exponent β^2 for the Achlioptas *et al.* model is approximately twice as large as β^1 which is the exponent for the standard percolation model. The exponent β^m keeps increasing with m up to $m = 8$ with a reducing rate. We find out that the power law behavior disappears for $m > 8$ since the linear behavior in region (ii) starts to gradually dominate the behavior in region (i) as can be seen in Fig. 4.2(a). The reason for this is the suppressed growth of the largest cluster even just after p_a^m for $m \geqslant 8$.

We see that the increasing correlation strength tries to prevent the largest cluster from growing further. Consequently, transport processes become inefficient and the power law behavior near p_m^a disappears. In order to understand the mechanism behind this, let us note that when there exists many discrete clusters in the lattice, adding new bonds joining two discrete clusters is generally favored over adding others that would join the sites of a single cluster (see Sec. 4.1.3). For example, think of a U-shaped cluster with 4 connected sites. Let us choose two bond candidates where one of them converts this U-shaped cluster into a unit square with weight $4 \times 4 = 16$ and the other connects two discrete clusters of sizes 3 and 4 with weight 12. Obviously, the one with weight 12 will be occupied even though the total size of the cluster it forms will be greater than that of the unit square. Therefore, the rules we have defined for the growth of lattices support the merging of isolated clusters to form larger ones instead of just 'feeding' the present discrete clusters. This fact, of course, suppresses the wrapping probability but later on, leads to an abrupt growth of the largest cluster seen in Fig. 4.2(a) and (b) for $m = 2$ and $m = 4$. However, as discrete clusters get more correlated with each other, they are forced to grow in a more specific way, i.e., they grow as homogeneous as possible in size along the lattice as we add the bonds are added one by one. There will not be any discrimination among discrete clusters for becoming the largest one, so, all discrete clusters will remain as large as possible during the growth of the lattice which eventually results in the suppression of the explosive behavior. Therefore, in order to obtain the most efficient transports, m should be kept at an optimal value and in our case, it is $m = 2$ where discrete clusters are 'slightly aware' of each other.

In case of an incoherent transport, the excitation can be interpreted as a classical random walker transported with unit efficiency in the limit $t \to \infty$, provided that it is initially localized on one of the sites from the set $\mathcal{R}$ (see Fig. 4.1). The reason for this is that the walker has enough time to find a correct path towards sink sites within the wrapping cluster. However, in the coherent transport case, the walker may not be able to cross the lattice even if it is initially localized on one of the sites that belong to $\mathcal{R}$. This result originates from the localization effects due to the random scatterings within the disordered structure of the wrapping cluster, namely the Anderson localization [117]. In two-dimensions, although the finite size scaling theory suggests that all eigenstates of the system should be exponentially localized independent of disorder strength in thermodynamic limit [118], it is an ongoing debate whether there are some delocalized states or not due to the different nature of disorder in the percolation model [119–121]. For our case, since different m values provide different growth mechanisms, there are structural differences between the clusters they form. This may lead to different localization effects which directly affect the

transport efficiency, especially in finite lattices.

We see in Fig. 4.2(d) that coherent transport is slightly inefficient than incoherent transport for all m values even though their behaviors with respect to p are almost completely the same, i.e., most of the eigenstates with large localization lengths in coherent transport are able to reach the opposite site and get trapped as they do in incoherent case in the limit $t \to \infty$. Yet, it is interesting to see that there exist some localized eigenstates on average for coherent transport which leads to a decrease in transport efficiency even for $L = 7$. The differences between their efficiencies are depicted in the inset of Fig. 4.2(d). The excitations are obliged proceed in zigzag paths along the wrapping clusters which results in destructive interferences, and hence, a decrease in the efficiency. As we expect, the difference is higher for bond fractions where the lattice is highly disordered for each m. When $p < 0.4$ or $p > 0.8$, the difference disappears for the lattice transforms into an ordered structure. The cases where the most and the least differences occur are $m = 1$ and $m = 2$, respectively. This result suggests that, the wrapping clusters formed by choosing $m = 2$ are the 'most zigzaggy ones' that eventually prevent the excitations from reaching the sink sites coherently even in the infinite time limit. As we mentioned earlier, this zigzag pattern of clusters is highly supported by the $m = 2$ case since the selection rule itself favors connecting discrete clusters over placing bonds within a single cluster. Therefore, at a certain bond fraction, the total number of bonds per cluster size in a given wrapping cluster is the least for $m = 2$. For $m > 2$, the difference depicted in the inset of Fig. 4.2(d) starts to reduce since the probability of connecting two discrete clusters gets more equal to the probability of adding a bond to an existing cluster. These results may imply that the amount of correlation between discrete clusters can affect the localization length of eigenstates of coherent transport.

4.2.2   Localization of eigenstates

In order to gain better insight into the localization effects of coherent transport, we can examine each eigenstate of H_0 to find out whether they are localized or not. Here we will ignore the trap sites and consider only how disorder affects the eigenstates. Let $|\Phi_l^0(p)\rangle$ be the lth eigenstate of H_0 for bond fraction p. Then, $|\langle i|\Phi_l^0(p)\rangle|^2$ gives the probability distribution of the lth state over the sites $i \in \mathcal{N}$. The participation ratio provides information about how much a given probability distribution is spread over the lattice and for our case it can be defined as

$$\xi_l(p) = \left(\sum_i^N |\langle i|\Phi_l^0(p)\rangle|^4 \right)^{-1}. \tag{4.12}$$

It estimates the number of sites over which the lth eigenstate is distributed, i.e., for $\xi_l = 1$ the distribution is localized on a single site whereas $\xi = N$ indicates a homogeneous distribution over N sites.

In Fig. 4.3(a), $\langle \xi_l(p) \rangle$ is given for $m = 1, 2, 4$ and 84. Obviously, when $\langle \xi_l(p) \rangle < L$, there is no way for an eigenstate to cover the lattice thoroughly. Moreover, it is rather unlikely to have an eigenstate satisfying $\langle \xi_l(p) \rangle = L$ since it would require a straight line-shaped wrapping cluster stretching between the source and trap sites. We have found for $L = 7$ that regardless of m, there is a 95% probability of having a cluster sized greater than 10 in the ensemble average. Therefore, let us safely assume that the eigenstates start delocalizing effectively and contribute to transport for $\langle \xi_l(p) \rangle > 10$. It can be seen in general that all eigenstates are localized for $p < 0.2$. Some eigenstates for $m = 1$ and $m = 2$ start delocalizing after $p = 0.25$ and $p = 0.4$, respectively, which also goes along with the results of Fig. 4.2(a) (see p_a^1 and p_a^2). While m is increasing, we observe that the delocalized states get accumulated above $p = 0.5$ and support our findings in Fig. 4.2(a) where the transport efficiency starts increasing effectively for $p > 0.5$. We also note that there are some highly delocalized states near $l = 49$. They appear between nearly $p \in [0.75, 1]$ for $m = 1$ and $m = 84$ whereas the same interval becomes $p \in [0.5, 1]$ for $m = 2$ and $m = 4$. For $m = 2, 4$ and 84, the sharp transition to these highly delocalized states with increasing p suggests that the wrapping cluster is most likely to reach almost all the sites of the lattice as soon as it is formed (see Table 4.1). We can further deduce that for $m = 1$, the wrapping cluster does not instantly cover the whole lattice when it first appears since the average wrapping probability of $m = 1$ is smaller than others. We need to keep adding bonds until $p = 0.75$ to make the wrapping cluster cover the lattice. This is one of the main consequences of correlation effects on the transport efficiency.

Lastly, let us examine the average participation ratio of all eigenstates which we define as $\xi_{\text{avg}}(p) = \frac{1}{N} \sum_{l=1}^{N} \xi_l(p)$ shown in Fig. 4.3(b). We see that ξ_{avg} increases smoothly for $m = 1$ whereas it is suppressed up to $p = 0.5$ for $m = 1, 2$ and up to $p = 0.7$ for $m = 84$, i.e., the greater the value of m, the more suppressed is ξ_{avg}. This result also clears up the decrease in efficiency for increasing m values in Fig. 4.2(a). The eigenstates abruptly delocalize following this suppression and get distributed in the lattice over larger regions than the ones in the $m = 1$ case. We finally note that the minimum bond fractions satisfying $\langle \xi_{\text{avg}}^{m>1} \rangle > \langle \xi_{\text{avg}}^{m=1} \rangle$ are almost the same with p_b^m.

Chapter 5

SPREADING UNDER AN ARTIFICIAL MAGNETIC FIELD

A quantum computer was envisioned by Feynman as a device overcoming the difficulty of simulating quantum mechanical systems with classical computers [122]. Today, ultracold atomic systems are of great interest for implementing highly controllable analogues of quantum systems under consideration [123, 124]. One way of creating and controlling such systems is trapping ultracold neutral atoms in periodic potentials of optical lattices formed by a laser. Since the atoms are neutral, external electric or magnetic fields, which are essential for quantum phenomena such as the quantum Hall effect and topological phases, have no effect on their trajectories. On the other hand, analogous effects can be implemented into optical lattices artificially to extend their simulation abilities. There are several proposals [125, 126] and experiments [127–130] focusing on the creation of tunable artificial gauge fields for ultracold neutral atoms in optical lattices by using atom-light interaction.

We will consider the discrete-time quantum walk here, which was originally proposed by Aharonov *et al.* as a quantum counterpart of the classical random walk, where the quantum walk leads to ballistic spread of the walker rather than the diffusive one observed in the classical case [2]. As we have discussed in previous chapters that quantum walks are useful for developing new quantum algorithms [6], they provide a model for universal quantum computation [11] and they also supply a fertile framework for simulating various quantum systems [12–16, 18]. Today, quantum walks can be realized experimentally in various physical systems including ultracold atoms in optical lattices [18, 24–29]. More-over, recent experimental studies on optical lattices can allow the realization of quantum walks under artificial gauge fields. For example, it has been experimentally shown that the effect of an electric field on a charged particle can be mimicked by quantum walks in a one-dimensional optical lattice [98]. Also, the proposal by Boada *et al.* utilizes photonic circuits for the realization of quantum walks under an artificial magnetic field [131].

In this chapter we investigate the dynamics of two-dimensional quantum walks on a square lattice in the presence of an artificial magnetic field. For this purpose, we introduce position- and direction- dependent phases corresponding to the Peierls phases of the hopping terms between neighboring sites in the Hamiltonian representing a charged particle under a uniform magnetic field. We can control the propagation of the walker by changing the magnetic flux Φ through the unit cell. Depending on Φ, we show that ballistic behavior can be suppressed within a time interval or can be completely broken. It is known that, classical diffusive behavior in quantum walks is observed when quantum coherence is removed in some way, e.g., by decohering the coin and/or the position [35]. We show that quantum walk is also diffusive at long times if the magnetic flux ratio $\alpha = \Phi/\Phi_0$ (Φ_0 being the flux quantum) is an irrational number and the walker remains highly localized at the origin throughout the walk. Moreover, we demonstrate that when α is chosen properly the walk stops to propagate and propagates back towards the origin during a limited time interval. We also analyze the entanglement between the coin and the position of the walker and show that the well-known asymptotic behavior vanishes when $\alpha \neq 0$. We observe that the coin and the position become maximally entangled at specific steps under the effect of the artificial magnetic field on a long time scale.

This chapter is organized as follows. In Sec. 5.1 we give a very brief overview of quantum walks and introduce the Peierls model to the formalism. In Sec. 5.2 we compare the behavior of the quantum walk under rational and irrational α's and we demonstrate the localization of the walker. In Sec. 5.3 we examine the effect of the magnetic field on coin-position entanglement.

5.1   Peierls model in quantum walks

In analogy to the classical random walk, the master equation for the discrete-time quantum walk is given by $|\Psi_{t+1}\rangle = U|\Psi_t\rangle$ (see Sec. 2.4.1), where U is a unitary transformation describing the time evolution of the state vector $|\Psi_t\rangle$ in discrete bipartite coin-position Hilbert space $H_c \otimes H_p$ spanned by $\{|0\rangle, |1\rangle\}$ and $\{|n\rangle \mid n \in \mathbb{Z}\}$, respectively. The operator $U = S(C \otimes I)$ is called a step of the walk and it is composed of a shift operator S and a coin operator C. The coin operator acts only on the coin space and it can be any unitary operation in SU(2). In the first proposal of the quantum walk [2], C was chosen as the Hadamard gate

$$\mathcal{C}_H = \frac{1}{\sqrt{2}}(|0\rangle\langle 0| + |0\rangle\langle 1| + |1\rangle\langle 0| - |1\rangle\langle 1|), \tag{5.1}$$

which is the one we use throughout this chapter. The conditional shift operator on a line is

$$S = \sum_{n=-\infty}^{+\infty} (|0\rangle\langle 0| \otimes |n-1\rangle\langle n| + |1\rangle\langle 1| \otimes |n+1\rangle\langle n|), \qquad (5.2)$$

which acts on both spaces (coin and position) and it moves the walker to the left (right) when the coin component is in the state $|0\rangle$ ($|1\rangle$). If the walk starts with the initial state $|\Psi_0\rangle$, after t steps, the final state becomes

$$|\Psi_t\rangle = U^t|\Psi_0\rangle = \sum_{c,n} a_{n,c}(t)|c,n\rangle \qquad (5.3)$$

where $a_{n,c}(t)$ are the site amplitudes and $c \in \{0,1\}$. The probability of being found at any position $P_n(t) = \sum_c |a_{n,c}(t)|^2$ is calculated by summing over the probabilities in the coin space.

In Sec. 2.4.3 we have seen that quantum walks on a line can be extended to higher dimensions by enlarging the coin and the position spaces. For a two-dimensional quantum walk, the coin and position spaces are spanned by $\{|0\rangle, |1\rangle, |2\rangle, |3\rangle\}$ and $\{|n,m\rangle_p \mid n,m \in \mathbb{Z}\}$, respectively. When the position basis $|n,m\rangle$ corresponds to the position eigenstates of the walker on a square lattice, the shift operator is defined as a single operation that moves the walker in the left down, left up, right down and right up directions (i.e., towards corners) for respective coin states [44]. On the other hand, experimentally, the walker can step to the nearest neighbors rather than the corners. Therefore, if we want the walker to be found at the corners in one step, we have to implement the shift operator as two separate operations, i.e., a shift along one axis followed by a second shift along the other axis. An alternative method for realization of two-dimensional quantum walks is to use a single two-level coin instead of a four-level coin [132, 133]. In this scheme, a step is defined as $U = S_y(C \otimes I)S_x(C \otimes I)$, where the walker is first shifted along the x direction followed by a shift along y direction. The Hadamard operator in Eq. (5.1) is chosen as the coin operator and it is applied before each shift. It has been shown that, with this scheme, the probability distribution of the Grover walk can be mimicked. This alternate scheme has advantages over a walk with a four-level coin when experimental aspects for square lattices are considered. Therefore, in this chapter, we use this alternate scheme.

We consider quantum walks on a square optical lattice with a tunable artificial gauge field. We label the space coordinates as $x = na$ and $y = ma$, where a is the lattice constant. We choose the symmetrical initial state $|\Psi_0^s\rangle = |\psi\rangle \otimes |0,0\rangle$, where both n and m are defined as zero and $|\psi\rangle = \frac{1}{\sqrt{2}}(|0\rangle + i|1\rangle)$. We introduce the shift operator in the y
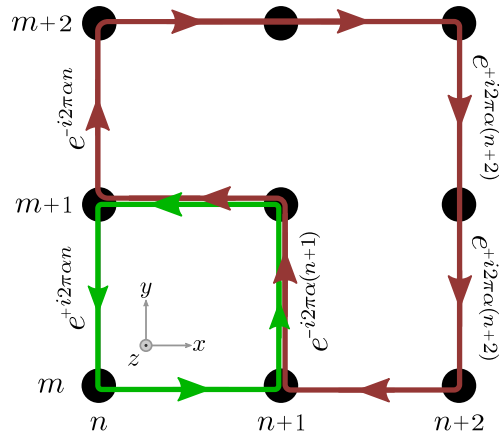
Figure 5.1: Phases gained by the walker while hopping between neighboring sites in the y direction. These phases are analogous to those acquired by a charged particle subjected to a constant external magnetic field in the z direction, in the Landau gauge. Black circles denote the sites of the square lattice labeled by the integer pairs (n, m). The arrows show two possible trajectories. The walker gains a total phase of $e^{-i2\pi\alpha}$ along the smaller paths and $e^{-i2\pi(3\alpha)}$ along the larger paths. In general, for an arbitrary closed path, the coefficient of α gives the number of unit cells enclosed. No phase is gained along the x direction.

direction as

$$
\begin{aligned}
S_y = & |0\rangle\langle 0| \otimes \sum_{n,m} e^{+i2\pi\alpha n} |n, m-1\rangle\langle n, m| \\
& + |1\rangle\langle 1| \otimes \sum_{n,m} e^{-i2\pi\alpha n} |n, m+1\rangle\langle n, m|
\end{aligned}
\tag{5.4}
$$

where $\alpha \in [0, 1]$ is the tuning parameter and $e^{\pm i2\pi\alpha n}$ are both site and direction-dependent phases of hopping terms between neighboring lattice sites. At this point our approach differs from [98] and [134], where only site-dependent phases on a one-dimensional lattice are used. When we consider the motion of a charged particle on a square lattice under a uniform magnetic field $\mathbf{B} = B_0\hat{\mathbf{z}}$, the appropriate Peierls substitution is given by [135, 136]

$$
t \longrightarrow t \exp\left(-i\frac{2\pi}{\Phi_0} \int_{\mathbf{r_1}}^{\mathbf{r_2}} \mathbf{A}.d\mathbf{l}\right)
\tag{5.5}
$$

where t is the nearest-neighbor hopping amplitude and $\Phi_0 = h/e \approx 4.14 \times 10^{-15}$ Wb is the flux quantum (h and e being the Planck constant and elementary charge, respectively). Here $\mathbf{r_1}$ and $\mathbf{r_2}$ denote the initial and final positions of the particle, respectively, and the integral is evaluated along the line connecting these points. If the vector potential is chosen as $\mathbf{A} = B_0 x\hat{\mathbf{y}}$ (Landau gauge), the transition amplitude along the x direction remains unaffected while along the y direction it gains a factor of

$$
\exp\left(\pm i2\pi\frac{\Phi}{\Phi_0}n\right)
\tag{5.6}
$$

61
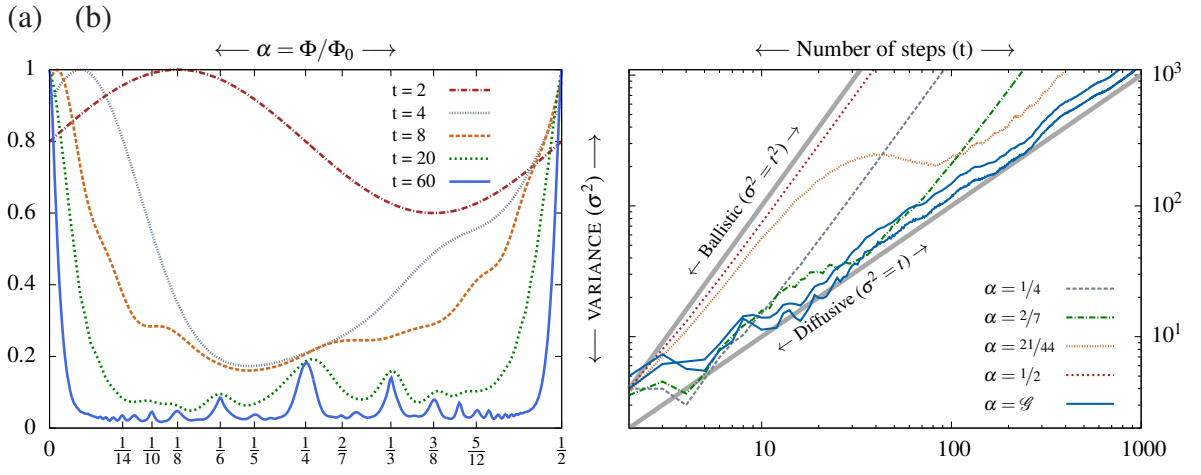
Figure 5.2: (a) Spreading of the walk after a different number of steps t with respect to the magnetic flux Φ in units of flux quantum Φ_0. The symmetrical initial state $|\Psi_0^s\rangle$ is used. Only one period of variances is drawn within the interval $[0, 1]$. The vertical axis is rescaled with the maximum value of the variance for each t. For the rational values of α, sharp peaks become apparent when the number of steps is increased. (b) Spreading of the walk with respect to the number of steps for different values of α. When α is the golden ratio G, we used two different initial conditions. The lower solid line corresponds to the symmetric case used for the other α values and the upper one is $|\Psi_0\rangle = |0\rangle \otimes |0, 0\rangle$.

when hopping from site m to $m \pm 1$. Here $\Phi = B_0 a^2$ is the magnetic flux through the unit cell. Therefore, we interpret the phases in Eq. (5.4) as artificial Peierls phases shown in Fig. 5.1. In this chapter, we consider both rational and irrational flux ratios $\alpha = \Phi/\Phi_0$ to find out the effects of the magnetic field on the characteristics of quantum walks such as the variance, participation ratio, and coin-position entanglement.

5.2 Rational vs irrational flux ratios

We consider the variance σ_t^2 of the probability distribution,

$$\sigma_t^2 = \sum_{n,m} (n^2 + m^2) P_{(n,m)}(t), \tag{5.7}$$

as a measure of the spreading. Here, $P_{(n,m)}(t)$ is the probability of the walker being found at site (n, m) after t steps and we look for how the variance behaves under rational and irrational magnetic fields. When the flux ratio α is an integer, the original translational symmetry of the lattice is preserved. Similarly, when it is a rational number such as p/q, where both p and q are coprime integers, translational symmetry is preserved only if the unit cell is considered q times as large. However, for irrational α values, the number of unit cells enclosed by the walker (see Fig. 5.1) is incommensurable with the parameter α. Therefore, we cannot exploit a rescaling as we did in the rational case. In Fig. 5.2(a), we show the change of the variance with respect to α for different step numbers. Although the
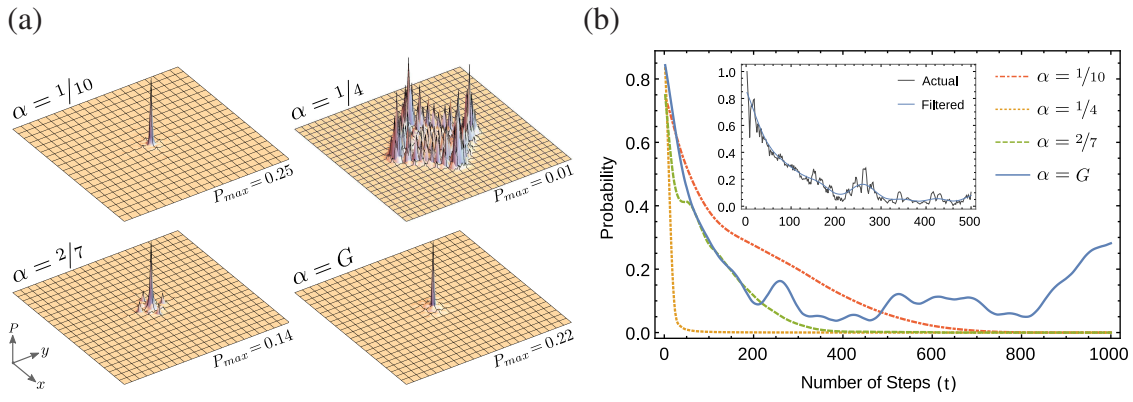
Figure 5.3: (a) Probability distribution of the walk after 100 steps for different flux ratios. Here G is the golden ratio. (b) Probability of finding the walker in the vicinity of the origin after t steps: the sum of the probabilities at sites (n, m), where $n, m \in \{-2, 0, 2\}$ with respect to the number of steps. Since an odd number of steps gives vanishing probability, the probabilities for only an even number of steps are shown. Data are smoothed out via Gaussian filtering for simplicity. The inset shows a comparison of the actual data with the filtered data for $\alpha = G$.

variance is meaningful for the walks with a large number of steps, we intentionally present the results for a small number of steps to demonstrate an interesting effect of magnetic fields on quantum walks. Note that since the variance repeats itself with a period of $1/2$ within the interval $[0, 1]$, only one period is drawn for each case. When $t = 2, 4$, or 8, for each case there are two maxima at non-zero α values. While the number of steps is increasing, the maxima move to the left and their positions converge to $\alpha = 0$ and $\alpha = 1/2$. For example, the analytic expression of the variance for two steps is

$$\sigma_2^2 = 3 + 2\cos^2(2\pi\alpha - \frac{\pi}{4}). \tag{5.8}$$

It is clear that the maximum value of Eq. (5.8) occurs at $\alpha = 1/8$ and $5/8$. It is also notable that in this case the probability at the origin,

$$P_{(0,0)}(2) = \frac{1}{2}\cos^2(2\pi\alpha + \frac{\pi}{4}), \tag{5.9}$$

becomes zero because of the destructive interference of the incoming amplitudes. In other words, the walker avoids stepping into the center at the second step as a result of the applied field. Similarly, maxima for four and eight steps occur at $\alpha = 3/100$ and $\alpha = 3/400$, respectively. Hence, with an appropriate choice of the α, the walk spreads faster than the case where there is no applied field for a small number of steps. For 20 and 60 steps, spreading of the walk is dramatically reduced by the non zero values of α except $1/2$. However, some peaks occur at the rational values of α and more peaks become apparent when the number of steps is larger. This happens because the more steps taken, the more routes that satisfy translational symmetry corresponding to different

63
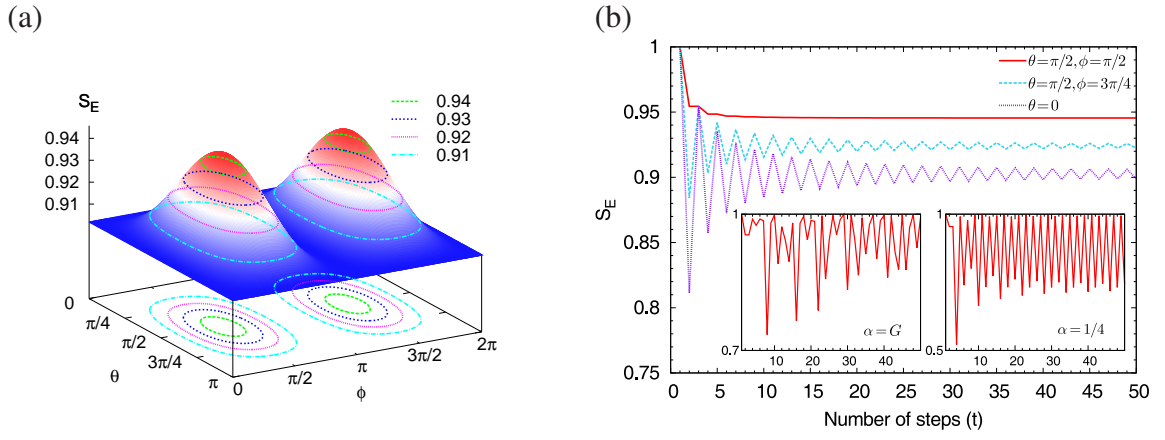
Figure 5.4: (a) Asymptotic values of coin-position entanglement of a quantum walk on a square lattice with two-level initial coin states $|\psi\rangle_c = \cos\frac{\theta}{2}|0\rangle + e^{i\phi}\sin\frac{\theta}{2}|1\rangle$ for $\alpha = 0$. The figure is symmetrical about $\phi = \pi$ and varies between its maximum $\simeq 0.903$ and minimum $\simeq 0.945$. The maximum value is attained for symmetrical initial coin states $(\theta, \phi) = (\pi/2, \pi/2)$ and $(\pi/2, 3\pi/2)$. (b) Time dependence of the entanglement for specific values of the initial coin state. The asymptotic behavior can be observed explicitly. The insets show that when $\alpha \neq 0$, the asymptotic behavior vanishes. For $\alpha = G$ (left inset) and for $\alpha = 1/4$ (right inset), after the fourth step, the coin and the position become almost maximally entangled ($S_E \simeq 0.99$) every two steps.

α values can be followed. Translational symmetry due to any rational number α requires the walker to take at least a number of steps that is enough to follow a closed path covering the unit cell rescaled by α appropriately. Therefore, we increase the α resolution of the walk by increasing the step number and thus the walk becomes more sensitive to the α values. By counting the number of peaks in Fig. 5.2(a) roughly, we see that while the system is able to resolve 4 of those symmetries at 20 steps, it can resolve more than 20 if we increase the step number to 60.

In Fig. 5.2(a) we see that if $\alpha = 1/2$, the variance is the same as the case where there is no magnetic flux $\alpha = 0$ for a large number of steps. Actually, the walk has exactly the same dynamics for this two case and the same probability distribution is obtained after each step. The reason is that in the second and each succeeding step, translational symmetry is preserved, i.e., in each step the gained phases cancel each other after following a closed path that covers two unit cells. Hence, there is no net effect of magnetic flux $\alpha = 1/2$ on the walk. Note that no components of the wave function interfere with each other at the first step, i.e., the wave function only spreads towards the nearest corners. Therefore, the possible effects of the magnetic field occur after the first step for each walk under our consideration.

In Fig. 5.2(b) we demonstrate that, for two different initial states, the walk spreads diffusively in a long time range if α is an irrational number and the golden ratio ($G = \frac{\sqrt{5}-1}{2}$), due to the broken translational symmetry of the lattice. In this case, there is no

rescaled unit cell that is commensurable with the original one to obtain a translational symmetry. In contrast, if α is rational, after few steps, spreading of the walk returns to its usual ballistic behavior. A remarkable case in which the spreading is nearly stopped and reversed during steps 35-50 and 50-85, respectively, occurs for $\alpha = 21/44$. Also, further simulations show that similar effects as in $\alpha = 21/44$ can be observed if α is chosen sufficiently close to 0 or $1/2$. In general, we can conjecture that when α is a rational number, even if the spreading of the walk fluctuates at the beginning, it will revert to its original ballistic behavior after a finite number of steps. Only irrational α values permanently suppress the spreading and result in a diffusive behavior.

Figure 5.3(a) demonstrates that whether α is a rational or an irrational number, the walker tends to be localized around the origin. However, some values of α cause stronger localization. In Fig. 5.3(b) the sum of probabilities of the walker being found at the origin and some nearby sites with respect to the number of steps is given. When α is a rational number, even though the robustness of the localization against step number changes for different α's, the probability of finding the particle around the origin converges to zero while the number of steps is increasing. In contrast, when $\alpha = G$, the probability does not converge to zero within the interval $[0, 1000]$ and moreover it increases to approximately 0.3 when $t = 1000$. Although we examine the sum of probabilities at several sites around the origin, Fig. 5.3(a) ensures that the significant contribution to this sum comes from the origin. Therefore, an irrational flux ratio guarantees that the probability is the highest at the origin in the range up to 1000 steps.

Although our results include only one irrational number (the golden ratio), further simulations for $1/\pi$, $1/e$, $1/\sqrt{2}$, and $1/\zeta(3)$ show that all of them exhibit diffusive behavior on average. As we have mentioned above, the reason is the incommensurability of the number of unit cells enclosed by the walker and the magnetic flux ratio for each case. Note that, as shown in Fig. 5.2(b), the walk can exhibit higher spreading rates temporarily, e.g., between $t = 250$ and 600 for $\alpha = G$, but on average, spreading fluctuates around the diffusive trend. However, these temporary deviations from the diffusive spreading can extend over relatively large time intervals for some irrational numbers. Among our simulations, the only example is $\alpha = 1/\pi$, where we observe such a deviation over the interval from $t = 100$ to 2000. A possible explanation of this behavior can be given by answering the question of how well an irrational number can be approximated by the rationals. It is known that the best rational approximations to an irrational number are found in its convergents of continued fraction which are represented by $c_i = [a_0, a_1, \cdots, a_i] = p_i/q_i$ [137]. By adding more terms, we obtain better approximations. Since the Peierls phases can be written as $e^{i2\pi c_i} e^{\pm i2\pi \alpha_{\text{err},i}}$ where $\alpha_{\text{err},i} = |c_i - \alpha|$, the phases $e^{i2\pi c_i}$ allow vari-

ous translational symmetries determined by q_i. We also know that if $\alpha_{\text{err},i}$ is sufficiently close to 0 or $1/2$, the effects result from $e^{\pm i2\pi\alpha_{\text{err},i}}$ cannot be observed for a while (see $\alpha = 21/44$ in Fig. 5.2 and $\alpha = 1/500$ in Fig. 5.5). While the number of steps increases, the walk continuously tries to catch different translational symmetries required by the convergents but due to the accumulation of $e^{\pm i2\pi\alpha_{\text{err},i}}$ phases, this can never be done completely, which thereby results in temporary higher spreading rates. Therefore, if the α_{err}'s are sufficiently small for a given irrational α, we can expect to observe higher spreading rates extending over relatively long time intervals. What makes $1/\pi$ special is that its convergents have the minimal errors when we compare it with the other irrational numbers we used. It has the best rational approximations among the others and this can be the reason for the deviations in long ranges. A detailed analysis including a careful comparison of the convergents of different irrational numbers and the corresponding errors is left to future research.

5.3 Effect of magnetic fields on entanglement

The shift operator generates entanglement between the coin and the position degrees of freedom [60, 61, 100] (see Sec. 2.4.4). Since the step operator U is unitary, the density matrix $\rho_t = |\Psi_t\rangle\langle\Psi_t|$ at any step t will be a pure state. Therefore, it is convenient to use the von Neumann entropy as a measure of the coin-position entanglement

$$S_E = -\sum_i \lambda_i \log_2 \lambda_i, \tag{5.10}$$

where the λ_i's are the eigenvalues of the reduced density matrix $\rho_c = \text{Tr}_p(\rho_t)$ obtained by tracing out the position degree of freedom (see Sec. 2.1.2 for the details). The asymptotic behavior of the entanglement in quantum walks on a line and two-dimensional quantum walks with a four-level coin is already known [60, 61]. Here we demonstrate that a two-dimensional quantum walk with a two-level coin also exhibits the same behavior for all initial coin states for $\alpha = 0$. In Fig. 5.4(a) the dependence of the asymptotic values of coin-position entanglement on initial coin states is given. It can be seen that entanglement varies between a maximum of 0.945 and a minimum of 0.903. The maximum value occurs for the symmetrical initial state $|\Psi_0^s\rangle$. In Fig. 5.4(b) time dependence of coin-position entanglement for three specific initial coin states is given. For all cases, entanglement decays to an asymptotic value.

The inset in Fig. 5.4(b) shows the change in coin-position entanglement in the presence of a magnetic field (for $\alpha \neq 0$ and $\alpha \neq 1/2$). For both $\alpha = 1/4$ and $\alpha = G$, the
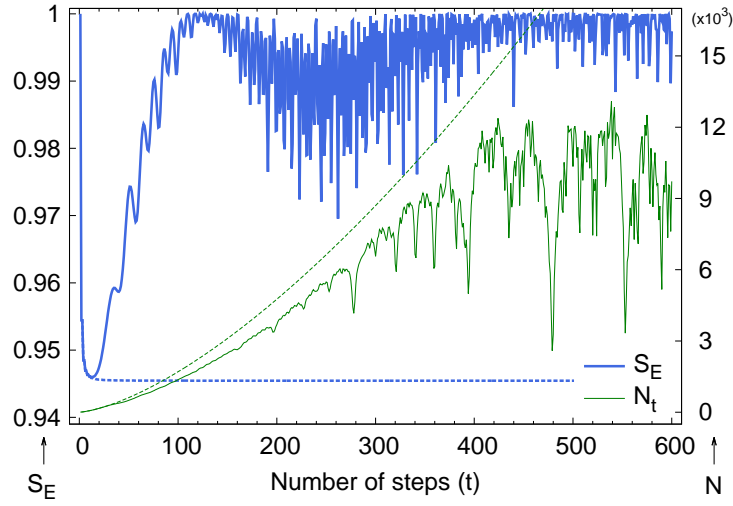
Figure 5.5: Comparison between coin-position entanglement (thick) S_E and participation ratio (thin) N when $\alpha = 1/500$. Dashed lines represent the behavior of each case when $\alpha = 0$.

asymptotic behavior disappears completely. Although we show only two cases for simplicity, we observe similar behaviors for the other α values. When $\alpha = 1/4$, the value $S_E \simeq 0.99$ indicates that the coin and the position are almost maximally entangled in every odd step after the fourth step. When $\alpha = G$, we obtain almost maximally entangled states in a quasi-periodic manner in a long time range again. To gain insight into the cause of the large values of entanglement, we consider the participation ratio at step number t,

$$N = \left(\sum_{n,m} P_{n,m}^2(t) \right)^{-1}, \tag{5.11}$$

which can be interpreted as an estimate for the number of sites over which the walker is distributed. While $N = 1$ indicates that the walker is completely localized at only one site, $N = d$ indicates a uniform spreading over d sites. In Fig. 5.5 we compare the coin-position entanglement and the participation ratio for a small magnetic field. During the first 10 steps, we see that the entanglement is exactly the same for $\alpha = 0$ and $\alpha = 1/500$. Further simulations for smaller values of α show that the entanglement is the same as the $\alpha = 0$ case even for a larger number of steps. This observation suggests that the effects of the magnetic field start to appear after a sufficient amount of phases has accumulated. After about 400 steps, the participation ratio starts to oscillate strongly and we also observe quasi periodic oscillations in S_E, which results in almost maximally entangled states as in the insets of Fig. 5.4(b). Since strong oscillations in the participation ratio imply the tendency of the walker to return to the origin, we can conclude that localization of the walker plays an important role in the large values of coin-position entanglement in the presence of a magnetic field.

Chapter 6

CONCLUSION

In this thesis, we have focused on two closely related subjects, namely the spreading and transport properties of quantum walks for various graph structures and decoherence models. The main results given in chapters three, four and five are compiled from our three articles [138–140].

In the third chapter, we have proposed a perfect state transfer scheme for qubit states by introducing recovery operators in discrete-time quantum walk architecture on N-lines and N-cycles. We have shown that by using identity or flip coin operator, an unknown qubit state can be transferred to an arbitrary distance perfectly with the aid of appropriate recovery operator. The 2-cycle is the only lattice which allows PST for all coin operators up to N=10. Also, the Hadamard coin and biased coin $\rho = 1/4$ allow PST on 2-line. We have shown that the 4-cycle is a special case where PST occurs if the walk is driven by the Hadamard coin operator or the biased coin operator $\rho = 1/4$, without any recovery operators. Moreover, we have introduced new periodic discrete-time QWs on N-lines and also extended periodicity cases which has already been known for 2-cycle and 4-cycle [43]. We have shown the strong relation between the periodicity and PST. Since recovery operators are just additional coin operators and PST occurs after small number of steps (which is comparable with the lattice size), it seems that the experimental realization of our scheme is quite feasible with today's technology.

In the fourth chapter, we have studied the coherent and incoherent transports between opposite edges of a finite square lattice where the existence of bonds between sites are determined by either standard or explosive percolation models. Since the explosive percolation model provides a disorder source enabling discrete clusters to grow in correlation with each other, we managed to investigate the possible effects of this correlated disorder on the transport efficiency. We have shown that the least possible correlation is the most contributing to the transport efficiency after 58% of bonds are present in the lattice. We have obtained more efficient transports than that of the standard percolation case with smaller correlation. As we increased the correlation strength, the transport efficiency

gradually decreased and reduced below that of the standard percolation case. We have demonstrated that the effective starting point and the efficiency of any transport process is directly related to the size of the largest cluster for a given bond fraction. Moreover, we compared our results with the incoherent transport to see possible localization effects. We have shown that more correlation causes less localization. Therefore, the least correlation provides the most efficient transport despite inducing localization the most. We have explained the possible mechanism behind these localization effects. Lastly, we supported our findings by explicitly examining the average participation ratio of the eigenstates of the system, which allows us to decide whether an eigenstate is localized or delocalized over the lattice. Depending on our results we conjecture that the localization length of the eigenstates in case of an explosive percolation may be altered by making a change in the correlation strength between clusters. This conjecture, of course, requires careful analysis of the localization properties of eigenstates for larger lattices, which we leave as a topic of further research.

In the fifth chapter, we have studied the spreading properties and coin-position entanglement for the QW on a square lattice under an artificial magnetic field. We have demonstrated that the presence of such fields increases the spreading for a small number of steps. Moreover, irrational flux ratios cause a diffusive spreading rather than a ballistic one even in the long time range because of the broken translational symmetry. This also causes the probability at the origin to be the highest even for a large number of steps. For rational flux ratios, ballistic spreading can be suppressed within a limited time range. However, the walk returns to the original ballistic behavior after a finite number of steps. We have demonstrated that the coin-position entanglement in a QW on a square lattice with a single two-level coin exhibits an asymptotic behavior as in the four-level case. We have also shown that this behavior changes in the presence of an artificial gauge field and it is possible to keep the coin and the position maximally entangled in a long time range if the field is chosen appropriately. However, we have not observed any distinguishing property of irrational or rational magnetic flux ratios while examining the coin-position entanglement. Finally, we note that our scheme may be realized with today's technology and some of our results, especially the ones that require only a few number of steps, may be verified. We believe that our work can provide a further step towards simulating many-body quantum systems in gauge fields by engineering the interactions of ultracold atoms with light.

Bibliography

[1] S. S. Schweber, "Feynman and the visualization of space-time processes," *Reviews of Modern Physics Letters*, vol. 58, pp. 449–508, 1986.

[2] Y. Aharonov, L. Davidovich, and N. Zagury, "Quantum random walks," *Physical Review A*, vol. 48, pp. 1687–1690, 1993.

[3] A. Ambainis, E. Bach, A. Nayak, A. Vishwanath, and J. Watrous, "One-dimensional quantum walks," in *Proceedings of the Thirty-third Annual ACM Symposium on Theory of Computing*, STOC '01, (New York, NY, USA), pp. 37–49, ACM, 2001.

[4] J. Kempe, "Quantum random walks: an introductory overview," *Contemporary Physics*, vol. 44, no. 4, pp. 307–327, 2003.

[5] E. Farhi and S. Gutmann, "Quantum computation and decision trees," *Physical Review A*, vol. 58, pp. 915–928, 1998.

[6] A. Ambainis, "Quantum walks and their algorithmic applications," *International Journal of Quantum Information*, vol. 01, no. 04, pp. 507–518, 2003.

[7] A. Ambainis, "Quantum walk algorithm for element distinctness," *SIAM Journal of Computing*, vol. 37, no. 1, pp. 210–239, 2007.

[8] N. Shenvi, J. Kempe, and K. B. Whaley, "Quantum random-walk search algorithm," *Physical Review A*, vol. 67, p. 052307, 2003.

[9] J. Kempe, "Discrete quantum walks hit exponentially faster," *Probability Theory and Related Fields*, vol. 133, no. 2, pp. 215–235, 2005.

[10] A. M. Childs, "Universal computation by quantum walk," *Physical Review Letters*, vol. 102, p. 180501, 2009.

[11] N. B. Lovett, S. Cooper, M. Everitt, M. Trevers, and V. Kendon, "Universal quantum computation using the discrete-time quantum walk," *Physical Review A*, vol. 81, p. 042330, 2010.

[12] T. Kitagawa, M. S. Rudner, E. Berg, and E. Demler, "Exploring topological phases with quantum walks," *Physical Review A*, vol. 82, p. 033429, 2010.

[13] A. Crespi, R. Osellame, R. Ramponi, V. Giovannetti, R. Fazio, L. Sansoni, F. De Nicola, F. Sciarrino, and P. Mataloni, "Anderson localization of entangled photons in an integrated quantum walk," *Nature Photonics*, vol. 7, pp. 322–328, 2013.

[14] J. Ghosh, "Simulating Anderson localization via a quantum walk on a one-dimensional lattice of superconducting qubits," *Physical Review A*, vol. 89, p. 022309, 2014.

[15] O. Buerschaper and K. Burnett, "Stroboscopic quantum walks," arXiv:quant-ph/0406039v2.

[16] T. Oka, N. Konno, R. Arita, and H. Aoki, "Breakdown of an electric-field driven system: A mapping to a quantum walk," *Physical Review Letters*, vol. 94, p. 100602, 2005.

[17] M. Mohseni, P. Rebentrost, S. Lloyd, and A. Aspuru-Guzik, "Environment-assisted quantum walks in photosynthetic energy transfer," *The Journal of Chemical Physics*, vol. 129, no. 17, 2008.

[18] A. Schreiber, A. Gábris, P. P. Rohde, K. Laiho, M. Štefaňák, V. Potoček, C. Hamilton, I. Jex, and C. Silberhorn, "A 2d quantum walk simulation of two-particle dynamics," *Science*, vol. 336, no. 6077, pp. 55–58, 2012.

[19] M. Christandl, N. Datta, A. Ekert, and A. J. Landahl, "Perfect state transfer in quantum spin networks," *Physical Review Letters*, vol. 92, p. 187902, 2004.

[20] M. Christandl, N. Datta, T. C. Dorlas, A. Ekert, A. Kay, and A. J. Landahl, "Perfect transfer of arbitrary states in quantum spin networks," *Physical Review A*, vol. 71, p. 032312, 2005.

[21] P. Kurzyński and A. Wójcik, "Discrete-time quantum walk approach to state transfer," *Physical Review A*, vol. 83, p. 062315, 2011.

[22] V. M. Kendon and C. Tamon, "Perfect state transfer in quantum walks on graphs," *Journal of Computational and Theoretical Nanoscience*, vol. 8, pp. 422–433, 2011.

[23] K. Barr, T. Proctor, D. Allen, and V. Kendon, "Periodicity and perfect state transfer in quantum walks on variants of cycles," *Quantum Information and Computation*, vol. 14, pp. 417–438, 2014.

[24] H. B. Perets, Y. Lahini, F. Pozzi, M. Sorel, R. Morandotti, and Y. Silberberg, "Realization of quantum walks with negligible decoherence in waveguide lattices," *Physical Review Letters*, vol. 100, p. 170506, 2008.

[25] M. Karski, L. Förster, J.-M. Choi, A. Steffen, W. Alt, D. Meschede, and A. Widera, "Quantum walk in position space with single optically trapped atoms," *Science*, vol. 325, no. 5937, pp. 174–177, 2009.

[26] F. Zähringer, G. Kirchmair, R. Gerritsma, E. Solano, R. Blatt, and C. F. Roos, "Realization of a quantum walk with one and two trapped ions," *Physical Review Letters*, vol. 104, p. 100503, 2010.

[27] M. A. Broome, A. Fedrizzi, B. P. Lanyon, I. Kassal, A. Aspuru-Guzik, and A. G. White, "Discrete single-photon quantum walks with tunable decoherence," *Physical Review Letters*, vol. 104, p. 153602, 2010.

[28] A. Peruzzo, M. Lobino, J. C. F. Matthews, N. Matsuda, A. Politi, K. Poulios, X.-Q. Zhou, Y. Lahini, N. Ismail, K. Wörhoff, Y. Bromberg, Y. Silberberg, M. G. Thompson, and J. L. OBrien, "Quantum walks of correlated photons," *Science*, vol. 329, no. 5998, pp. 1500–1503, 2010.

[29] L. Sansoni, F. Sciarrino, G. Vallone, P. Mataloni, A. Crespi, R. Ramponi, and R. Osellame, "Two-particle bosonic-fermionic quantum walk via integrated photonics," *Physical Review Letters*, vol. 108, p. 010502, 2012.

[30] G. Benenti, G. Casati, and G. Strini, *Principles of quantum computation and information: basic concepts*. World Scientific, 2004.

[31] G. Benenti, G. Casati, and G. Strini, *Principles of quantum computation and information: basic tools and special topics*. World Scientific, 2007.

[32] M. Nielsen and I. Chuang, *Quantum computation and quantum information*. Cambridge University Press, 2000.

[33] L. Diósi, *A short course in quantum information theory: an approach from theoretical physics*. Springer, 2007.

[34] S. E. Venegas-Andraca, "Quantum walks: a comprehensive review," *Quantum Information Processing*, vol. 11, no. 5, pp. 1015–1106, 2012.

[35] V. Kendon, "Decoherence in quantum walks — a review," *Mathematical Structures in Computer Science*, vol. 17, pp. 1169–1220, 2007.

[36] P. A. M. Dirac, *The principles of quantum mechanics*. No. 27, Oxford University Press, 1981.

[37] J. Sakurai and J. Napolitano, *Modern quantum mechanics*. Addison-Wesley, 2010.

[38] R. Shankar, *Principles of quantum mechanics*. Springer, 1994.

[39] D. Griffiths, *Introduction to quantum mechanics*. Pearson Prentice Hall, 2005.

[40] K. Gottfried and T. Yan, *Quantum mechanics: fundamentals*. Springer, 2003.

[41] A. Peres, *Quantum theory: concepts and methods*. Springer, 1995.

[42] K. Kraus, *States, effects, and operations: fundamental notions of quantum theory*. Springer-Verlag, 1983.

[43] B. Tregenna, W. Flanagan, R. Maile, and V. Kendon, "Controlling discrete quantum walks: coins and initial states," *New Journal of Physics*, vol. 5, no. 1, p. 83, 2003.

[44] T. D. Mackay, S. D. Bartlett, L. T. Stephenson, and B. C. Sanders, "Quantum walks in higher dimensions," *Journal of Physics A: Mathematical and General*, vol. 35, no. 12, p. 2745, 2002.

[45] S. Hill and W. K. Wootters, "Entanglement of a pair of quantum bits," *Physical Review Letters*, vol. 78, pp. 5022–5025, 1997.

[46] W. K. Wootters, "Entanglement of formation of an arbitrary state of two qubits," *Physical Review Letters*, vol. 80, pp. 2245–2248, 1998.

[47] G. Vidal and R. F. Werner, "Computable measure of entanglement," *Physical Review A*, vol. 65, p. 032314, 2002.

[48] M. Horodecki, "Entanglement measures," *Quantum Information and Computation*, vol. 1, pp. 3–26, 2001.

[49] M. B. Plenio and S. Virmani, "An introduction to entanglement measures," *Quantum Information and Computation*, vol. 7, pp. 1–51, 2007.

[50] R. Horodecki, P. Horodecki, M. Horodecki, and K. Horodecki, "Quantum entanglement," *Reviews of Modern Physics*, vol. 81, pp. 865–942, 2009.

[51] A. Einstein, B. Podolsky, and N. Rosen, "Can quantum-mechanical description of physical reality be considered complete?," *Physical Review*, vol. 47, pp. 777–780, 1935.

[52] A. Aspect, P. Grangier, and G. Roger, "Experimental tests of realistic local theories via bell's theorem," *Physical Review Letters*, vol. 47, pp. 460–463, 1981.

[53] M. A. Rowe, D. Kielpinski, V. Meyer, C. A. Sackett, W. M. Itano, C. Monroe, and D. J. Wineland, "Experimental violation of a Bell's inequality with efficient detection," *Nature*, vol. 409, no. 6822, pp. 791–794, 2001.

[54] A. Peres and D. R. Terno, "Quantum information and relativity theory," *Reviews of Modern Physics*, vol. 76, pp. 93–123, 2004.

[55] W. K. Wootters and W. H. Zurek, "A single quantum cannot be cloned," *Nature*, vol. 299, no. 5886, pp. 802–803, 1982.

[56] R. F. Werner, "Quantum states with Einstein-Podolsky-Rosen correlations admitting a hidden-variable model," *Physical Review A*, vol. 40, pp. 4277–4281, 1989.

[57] C. Shannon, "A mathematical theory of communication," *The Bell System Technical Journal*, vol. 27, pp. 379–423,623–656, 1948.

[58] C. H. Bennett, H. J. Bernstein, S. Popescu, and B. Schumacher, "Concentrating partial entanglement by local operations," *Physical Review A*, vol. 53, pp. 2046–2052, 1996.

[59] S. Popescu and D. Rohrlich, "Thermodynamics and the measure of entanglement," *Physical Review A*, vol. 56, pp. R3319–R3321, 1997.

[60] I. Carneiro, M. Loo, X. Xu, M. Girerd, V. Kendon, and P. L. Knight, "Entanglement in coined quantum walks on regular graphs," *New Journal of Physics*, vol. 7, no. 1, p. 156, 2005.

[61] G. Abal, R. Siri, A. Romanelli, and R. Donangelo, "Quantum walk on the line: Entanglement and nonlocal initial conditions," *Physical Review A*, vol. 73, p. 042302, 2006.

[62] M. Annabestani, S. J. Akhtarshenas, and M. R. Abolhassani, "Decoherence in a one-dimensional quantum walk," *Physical Review A*, vol. 81, p. 032321, 2010.

[63] A. Romanelli, R. Siri, G. Abal, A. Auyuanet, and R. Donangelo, "Decoherence in the quantum walk on the line," *Physica A: Statistical Mechanics and its Applications*, vol. 347, no. 0, pp. 137 – 152, 2005.

[64] G. M. Nikolopoulos and I. Jex, *Quantum State Transfer and Network Engineering*. Springer, Berlin, 2014.

[65] S. Bose, "Quantum communication through an unmodulated spin chain," *Physical Review Letters*, vol. 91, p. 207901, 2003.

[66] V. Subrahmanyam, "Entanglement dynamics and quantum-state transport in spin chains," *Physical Review A*, vol. 69, p. 034304, 2004.

[67] A. Wójcik, T. Ł uczak, P. Kurzyński, A. Grudka, T. Gdala, and M. Bednarska, "Multiuser quantum communication networks," *Physical Review A*, vol. 75, p. 022330, 2007.

[68] C. Di Franco, M. Paternostro, and M. S. Kim, "Perfect state transfer on a spin chain without state initialization," *Physical Review Letters*, vol. 101, p. 230502, 2008.

[69] C. Chudzicki and F. W. Strauch, "Parallel state transfer and efficient quantum routing on quantum networks," *Physical Review Letters*, vol. 105, p. 260501, 2010.

[70] K. Lemr, K. Bartkiewicz, A. Černoch, and J. Soubusta, "Resource-efficient linear-optical quantum router," *Physical Review A*, vol. 87, p. 062333, 2013.

[71] S. Paganelli, S. Lorenzo, T. J. G. Apollaro, F. Plastina, and G. L. Giorgi, "Routing quantum information in spin chains," *Physical Review A*, vol. 87, p. 062309, 2013.

[72] A. Zwick, G. A. Álvarez, J. Stolze, and O. Osenda, "Robustness of spin-coupling distributions for perfect quantum state transfer," *Physical Review A*, vol. 84, p. 022311, 2011.

[73] A. Zwick, G. A. Álvarez, J. Stolze, and O. Osenda, "Spin chains for robust state transfer: Modified boundary couplings versus completely engineered chains," *Physical Review A*, vol. 85, p. 012318, 2012.

[74] G. Pólya, "Über eine aufgabe der wahrscheinlichkeitsrechnung betreffend die irrfahrt im straßennetz," *Mathematische Annalen*, vol. 84, pp. 149–160, 1921.

[75] M. Štefaňák, I. Jex, and T. Kiss, "Recurrence and pólya number of quantum walks," *Physical Review Letters*, vol. 100, p. 020501, 2008.

[76] M. Štefaňák, T. Kiss, and I. Jex, "Recurrence of biased quantum walks on a line," *New Journal of Physics*, vol. 11, no. 4, p. 043027, 2009.

[77] P. P. Rohde, A. Fedrizzi, and T. C. Ralph, "Entanglement dynamics and quasi-periodicity in discrete quantum walks," *Journal of Modern Optics*, vol. 59, no. 8, pp. 710–720, 2012.

[78] X. Zhan, H. Qin, Z.-h. Bian, J. Li, and P. Xue, "Perfect state transfer and efficient quantum routing: A discrete-time quantum-walk approach," *Physical Review A*, vol. 90, p. 012331, 2014.

[79] B. C. Travaglione and G. J. Milburn, "Implementing the quantum random walk," *Physical Review A*, vol. 65, p. 032310, 2002.

[80] P. R. Dukes, "Quantum state revivals in quantum walks on cycles," *Results in Physics*, vol. 4, pp. 189–197, 2014.

[81] O. Mülken and A. Blumen, "Continuous-time quantum walks: Models for coherent transport on complex networks," *Physics Reports*, vol. 502, pp. 37 – 87, 2011.

[82] N. Konno, T. Namiki, T. Soshi, and A. Sudbury, "Absorption problems for quantum walks in one dimension," *Journal of Physics A: Mathematical and Theoretical*, vol. 36, no. 1, p. 241, 2003.

[83] E. Bach, S. Coppersmith, M. P. Goldschen, R. Joynt, and J. Watrous, "One-dimensional quantum walks with absorbing boundaries," *Journal of Computer and System Sciences*, vol. 69, no. 4, pp. 562 – 592, 2004.

[84] T. Yamasaki, H. Kobayashi, and H. Imai, "Analysis of absorbing times of quantum walks," *Physical Review A*, vol. 68, p. 012302, 2003.

[85] L. C. Kwek and Setiawan, "One-dimensional quantum walk with a moving boundary," *Physical Review A*, vol. 84, p. 032319, 2011.

[86] C. Chandrashekar and T. Busch, "Quantum percolation and transition point of a directed discrete-time quantum walk," *Scientific reports*, vol. 4, 2014.

[87] J. K. Asboth and J. M. Edge, "Edge-state-enhanced transport in a two-dimensional quantum walk," *Physical Review A*, vol. 91, p. 022324, 2015.

[88] M. Gönülol, E. Aydıner, Y. Shikano, and O. E. Müstecaplıoğlu, "Survival probability in a one-dimensional quantum walk on a trapped lattice," *New Journal of Physics*, vol. 13, no. 3, p. 033037, 2011.

[89] O. Mülken and A. Blumen, "Slow transport by continuous time quantum walks," *Physical Review E*, vol. 71, p. 016101, 2005.

[90] O. Mülken and A. Blumen, "Spacetime structures of continuous-time quantum walks," *Physical Review E*, vol. 71, p. 036128, 2005.

[91] O. Mülken and A. Blumen, "Efficiency of quantum and classical transport on graphs," *Physical Review E*, vol. 73, p. 066117, 2006.

[92] O. Mülken, V. Bierbaum, and A. Blumen, "Coherent exciton transport in dendrimers and continuous-time quantum walks," *Journal Chemical Physics*, vol. 124, no. 12, 2006.

[93] P. Krapivsky, J. Luck, and K. Mallick, "Survival of classical and quantum particles in the presence of traps," *Journal of Statistical Physics*, vol. 154, no. 6, pp. 1430–1460, 2014.

[94] O. Mülken, A. Blumen, T. Amthor, C. Giese, M. Reetz-Lamour, and M. Weidemüller, "Survival probabilities in coherent exciton transfer with trapping," *Physical Review Letters*, vol. 99, p. 090601, 2007.

[95] A. Blumen, V. Bierbaum, and O. Mülken, "Coherent dynamics on hierarchical systems," *Physica A*, vol. 371, no. 1, pp. 10 – 15, 2006.

[96] A. Volta, O. Mülken, and A. Blumen, "Quantum transport on two-dimensional regular graphs," *Journal of Physics A: Mathematical and General*, vol. 39, no. 48, p. 14997, 2006.

[97] A. Schreiber, A. Gábris, P. P. Rohde, K. Laiho, M. Štefaňák, V. Potoček, C. Hamilton, I. Jex, and C. Silberhorn, "A 2d quantum walk simulation of two-particle dynamics," *Science*, vol. 336, no. 6077, pp. 55–58, 2012.

[98] M. Genske, W. Alt, A. Steffen, A. H. Werner, R. F. Werner, D. Meschede, and A. Alberti, "Electric quantum walks with individual atoms," *Physical Review Letters*, vol. 110, p. 190601, 2013.

[99] N. G. Van Kampen, *Percolation*. Springer, Berlin, 1999.

[100] M. Annabestani, M. R. Abolhasani, and G. Abal, "Asymptotic entanglement in 2d quantum walks," *Journal of Physics A: Mathematical and Theoretical*, vol. 43, no. 7, p. 075301, 2010.

[101] G. Leung, P. Knott, J. Bailey, and V. Kendon, "Coined quantum walks on percolation graphs," *New Journal of Physics*, vol. 12, no. 12, p. 123018, 2010.

[102] P. Schijven, J. Kohlberger, A. Blumen, and O. Mülken, "Modeling the quantum to classical crossover in topologically disordered networks," *Journal of Physics A: Mathematical and Theoretical*, vol. 45, no. 21, p. 215003, 2012.

[103] B. Kollár, T. Kiss, J. Novotný, and I. Jex, "Asymptotic dynamics of coined quantum walks on percolation graphs," *Physical Review Letters*, vol. 108, p. 230505, 2012.

[104] O. Mülken, V. Pernice, and A. Blumen, "Quantum transport on small-world networks: A continuous-time quantum walk approach," *Physical Review E*, vol. 76, p. 051125, 2007.

[105] A. Anishchenko, A. Blumen, and O. Mülken, "Geometrical aspects of quantum walks on random two-dimensional structures," *Physical Review E*, vol. 88, p. 062126, 2013.

[106] Z. Darázs and T. Kiss, "Time evolution of continuous-time quantum walks on dynamical percolation graphs," *Journal of Physics A: Mathematical and Theoretical*, vol. 46, no. 37, p. 375305, 2013.

[107] Z. Darázs, A. Anishchenko, T. Kiss, A. Blumen, and O. Mülken, "Transport properties of continuous-time quantum walks on sierpinski fractals," *Physical Review E*, vol. 90, p. 032113, 2014.

[108] F. Elster, S. Barkhofen, T. Nitsche, J. Novotný, A. Gábris, I. Jex, and C. Silberhorn, "Quantum walk coherences on a dynamical percolation graph," *Scientific reports*, vol. 5, 2015.

[109] D. Achlioptas, R. M. D'Souza, and J. Spencer, "Explosive percolation in random networks," *Science*, vol. 323, no. 5920, pp. 1453–1455, 2009.

[110] M. Štefaňák, J. Novotný, and I. Jex, "Percolation assisted excitation transport in discrete-time quantum walks," *New Journal of Physics*, vol. 18, no. 2, p. 023040, 2016.

[111] M. M. Sternheim and J. F. Walker, "Non-hermitian hamiltonians, decaying states, and perturbation theory," *Physical Review C*, vol. 6, pp. 114–121, 1972.

[112] J. W. Essam, "Percolation and cluster size," in *Phase transitions and critical phenomena* (C. Domb, M. S. Greene, and J. L. Lebowtiz, eds.), vol. 2, p. 197, Academic, London, 1972.

[113] J. S. Andrade, H. J. Herrmann, A. A. Moreira, and C. L. N. Oliveira, "Transport on exploding percolation clusters," *Physical Review E*, vol. 83, p. 031133, 2011.

[114] R. A. da Costa, S. N. Dorogovtsev, A. V. Goltsev, and J. F. F. Mendes, "Explosive percolation transition is actually continuous," *Physical Review Letters*, vol. 105, p. 255701, 2010.

[115] F. Radicchi and S. Fortunato, "Explosive percolation: A numerical analysis," *Physical Review E*, vol. 81, no. 3, p. 036110, 2010.

[116] R. M. Ziff, "Scaling behavior of explosive percolation on the square lattice," *Physical Review E*, vol. 82, no. 5, p. 051105, 2010.

[117] P. W. Anderson, "Absence of diffusion in certain random lattices," *Physical Review*, vol. 109, pp. 1492–1505, 1958.

[118] E. Abrahams, P. W. Anderson, D. C. Licciardello, and T. V. Ramakrishnan, "Scaling theory of localization: Absence of quantum diffusion in two dimensions," *Physical Review Letters*, vol. 42, pp. 673–676, 1979.

[119] Y. Meir, A. Aharony, and A. B. Harris, "Delocalization transition in two-dimensional quantum percolation," *Europhysics Letters*, vol. 10, no. 3, p. 275, 1989.

[120] C. M. Soukoulis and G. S. Grest, "Localization in two-dimensional quantum percolation," *Physical Review B*, vol. 44, pp. 4685–4688, 1991.

[121] S. B. Dillon and H. Nakanishi, "Localization phase diagram of two-dimensional quantum percolation," *European Physics Journal B*, vol. 87, no. 12, pp. 1–9, 2014.

[122] R. Feynman, "Simulating physics with computers," *International Journal of Theoretical Physics*, vol. 21, no. 6-7, pp. 467–488, 1982.

[123] I. Bloch, J. Dalibard, and W. Zwerger, "Many-body physics with ultracold gases," *Reviews of Modern Physics Letters*, vol. 80, pp. 885–964, 2008.

[124] I. Buluta and F. Nori, "Quantum simulators," *Science*, vol. 326, no. 5949, pp. 108–111, 2009.

[125] D. Jaksch and P. Zoller, "Creation of effective magnetic fields in optical lattices: the hofstadter butterfly for cold neutral atoms," *New Journal of Physics*, vol. 5, no. 1, p. 56, 2003.

[126] J. Dalibard, F. Gerbier, G. Juzeliūnas, and P. Öhberg, "*Colloquium* : Artificial gauge potentials for neutral atoms," *Reviews of Modern Physics Letters*, vol. 83, pp. 1523–1543, 2011.

[127] J. Struck, C. Ölschläger, M. Weinberg, P. Hauke, J. Simonet, A. Eckardt, M. Lewenstein, K. Sengstock, and P. Windpassinger, "Tunable gauge potential for neutral and spinless particles in driven optical lattices," *Physical Review Letters*, vol. 108, p. 225304, 2012.

[128] Y. J. Lin, R. L. Compton, K. Jiménez-García, J. V. Porto, and I. B. Spielman, "Synthetic magnetic fields for ultracold neutral atoms," *Nature*, vol. 462, pp. 628–632, 2009.

[129] M. Aidelsburger, M. Atala, S. Nascimbène, S. Trotzky, Y.-A. Chen, and I. Bloch, "Experimental realization of strong effective magnetic fields in an optical lattice," *Physical Review Letters*, vol. 107, p. 255301, 2011.

[130] K. Jiménez-García, L. J. LeBlanc, R. A. Williams, M. C. Beeler, A. R. Perry, and I. B. Spielman, "Peierls substitution in an engineered lattice potential," *Physical Review Letters*, vol. 108, p. 225303, 2012.

[131] O. Boada, L. Novo, F. Sciarrino, and Y. Omar, "Quantum walks in synthetic gauge fields with 3d integrated photonics," arXiv:1503.07172v2 [quant-ph].

[132] A. Ambainis, K. Julia, and A. Rivosh, "Coins make quantum walks faster," (Philadelphia, PA, USA), pp. 1099–1108, Society for Industrial and Applied Mathematics, 2005.

[133] C. Di Franco, M. Mc Gettrick, and T. Busch, "Mimicking the probability distribution of a two-dimensional grover walk with a single-qubit coin," *Physical Review Letters*, vol. 106, p. 080502, 2011.

[134] C. Cedzich, T. Rybár, A. H. Werner, A. Alberti, M. Genske, and R. F. Werner, "Propagation of quantum walks in electric fields," *Physical Review Letters*, vol. 111, p. 160601, 2013.

[135] R. E. Peierls, "On the theory of diamagnetism of conduction electrons," *Zeitschrift für Physik*, vol. 80, pp. 763–791, 1933.

[136] D. R. Hofstadter, "Energy levels and wave functions of bloch electrons in rational and irrational magnetic fields," *Physical Review B*, vol. 14, pp. 2239–2249, 1976.

[137] A. Rockett and P. Szüsz, *Continued fractions*. World Scientific, Singapore, 1992.

[138] İ. Yalçınkaya and Z. Gedik, "Qubit state transfer via discrete-time quantum walks," *Journal of Physics A: Mathematical and Theoretical*, vol. 48, no. 22, p. 225302, 2015.

[139] İ. Yalçınkaya and Z. Gedik, "Two-dimensional quantum walk under artificial magnetic field," *Physical Review A*, vol. 92, p. 042324, 2015.

[140] İ. Yalçınkaya and Z. Gedik, "Coherent transport over an explosive percolation lattice," arXiv:1608.03936 [quant-ph].